Un modèle multi-échelle de la magnétorésistance anisotrope

Andras Bartok

NNT : 2015SACLS094

THESE DE DOCTORAT
DE L'UNIVERSITE PARIS-SACLAY,
préparée à l'Université Paris-Sud

ÉCOLE DOCTORALE N°575
EOBE(Electrical, optical, bio-physics and engineering)

Spécialité de doctorat : Physique

Par

M Andras Bartok

A multiscale model for anisotropic magnetoresistance

Thèse présentée et soutenue à Gif-sur-Yvette, le 3 décembre 2015 :

Composition du Jury :

M Frédéric Mazaleyrat	Professeur, ENS de Cachan	Président du Jury
M Stéphane Flament	Professeur, ENSICAEN	Rapporteur
M Olivier Hubert	Professeur, ENS de Cachan	Rapporteur
M Christophe Coillot	Ingénieur de recherche HDR, Laboratoire Charles Coulomb	Examinateur
M Adel Razek	Directeur de recherche émérite, CNRS	Directeur de thèse
M Laurent Daniel	Maître de conférences, Université Paris-Saclay	Co-directeur de thèse

"La simplicité est la chose la plus difficile à obtenir dans ce monde, c'est la dernière limite de l'expérience et le dernier effort du génie."

George Sand.

A ma fille, Lilla.

Remerciements

Les travaux de recherche présentés dans ce mémoire de thèse ont été réalisés au Laboratoire GeePs (ex-LGEP, Laboratoire de Génie Électrique de Paris) au sein de l'équipe ICHAMS (Interaction Champs-Matériaux et Structures) du département MOCOSEM (Modélisation et Contrôle de Systèmes Électromagnétiques). Cette thèse est le fruit de l'engagement de plusieurs personnes qui m'ont accompagné tout au long de ce parcours, c'est pourquoi je profite de cet espace pour leur exprimer toute ma considération.

Je remercie en premier lieu **M. Frédéric BOUILLAULT** et **M. Claude MARCHAND**, Professeurs à l'Université Paris-Sud et directeurs du LGEP, pour m'avoir accueilli au laboratoire. Je remercie **M. Lionel PICHON**, Directeur de Recherche au CNRS et responsable de l'équipe ICHAMS pour m'avoir accueilli dans son équipe du laboratoire.

Je remercie également **M. Frédéric MAZALEYRAT**, Professeur à l'École Normale Supérieur de Cachan, d'avoir accepté de présider le jury de ma thèse. Je remercie également **M. Stéphane FLAMENT**, Professeur à l'École Nationale Supérieure d'Ingénieurs de Caen et **M. Olivier HUBERT**, Professeur à l'École Normale Supérieur de Cachan, pour m'avoir fait l'honneur d'être les rapporteurs de mon manuscrit de thèse, ainsi pour leur apports scientifiques en ayant enrichi ces travaux de leur remarques précieuses.
Je tiens aussi à remercier **M. Christophe COILLOT**, Ingénieur de Recherche au CNRS, pour avoir participé en tant qu'examinateur au jury de ma thèse et qui a lui aussi pris la peine d'apporter ses remarques précieuses au manuscrit.

J'exprime ma profonde gratitude à mon directeur de thèse **M. Adel RAZEK**, Directeur de Recherche émérite au CNRS et à mon encadrant **M. Laurent DANIEL**, Maître de conférences à l'Université Paris-Sud, pour leur soutien durant ces longues années de thèse. Je les remercie notamment pour leur grande qualité humaine, leur confiance et leur patience, et surtout parce qu'ils ont toujours cru en moi - jusqu'à la fin. Sans ces qualités, ces travaux n'auraient pas abouti.

Le déroulement de ce travail doit aussi beaucoup aux personnels administratifs et techniques du LGEP que je remercie pour leur compétence.

Ces années m'ont également permis de rencontrer des personnes qui m'ont toujours soutenu, ont été d'une aide précieuse et avec lesquelles j'ai passé de très bons moments et j'espère en passer encore d'autres, aussi bien sur le plan professionnel que personnel. Je voudrais pour cela dire un grand merci à mes anciens doctorants-collègues du LGEP : **Trang**, **Laid**, **Valentin, Mehdi** et **Romain**.

Enfin je souhaite remercier toute ma famille et notamment ma femme, **Agnes**, notre petite **Lilla**, mes parents, **Ildiko** *(anya)* et **Janos** *(apa)*, ainsi que mon frère, **Daniel** pour leur soutien de tous les jours et à qui je dois beaucoup.

Contents

List of Figures

List of Tables

Notations

W^p	Potential energy.
W^{ex}	Exchange energy.
W^K	Magnetocrystalline anisotropy energy.
W^H	Magneto-static energy.
W^σ	Elastic energy.
W^z	Zeeman energy.
W^s	Surface energy.
$\mathbf{H}_0$	External magnetic field.
$\mathbf{M}$	Magnetization.
$\boldsymbol{\alpha}$	Direction cosines of the magnetization.
$\boldsymbol{\beta}$	Direction cosines of the current.
$\mathbf{H}_d$	Demagnetizing field.
$\boldsymbol{\varepsilon}^e$	Elastic strain.
$\boldsymbol{\varepsilon}^{\boldsymbol{\mu}}$	Magnetostriction strain.
$\boldsymbol{\sigma}$	Stress.
$\bar{\mathbf{I}}$	Current.
$\tilde{\varsigma}$	Conductivity.
$\tilde{\delta\rho}$	Variation of the resistivity.
f_α	Volume fraction of domains with orientation $\boldsymbol{\alpha}$.
$\mathcal{B}_\sigma$	Stress concentration tensor.
$\mathcal{A}_\sigma$	Strain localization tensor.
$\mathcal{L}^{\text{inc}}$	Tensor accounting for elastic incompatibilities due to magnetostriction.
$\mathcal{S}^E$	Eshelby tensor.
$\mathcal{I}$	Fourth order identity tensor.
S	Sensor sensitivity.
H_{max}	Sensor range of measurement.

Material constants

μ_0	Vacuum permeability.
M_s	Saturation magnetization.
χ_0	Initial anhysteretic susceptibility.
K_1, K_2	First- and second order anisotropy constants.
λ_{100}, λ_{111}	Magnetostrictive constants of the single crystal.
k_1,k_2,k_3,k_4,k_5	Material constants of Döring model.
$\mathcal{C}_g$	Single crystal stiffness tensor.
ρ_0	Initial resistivity.
A_s	Adjustable parameter of our model.
N_s	Demagnetizing factor.

Introduction

Small magnetic sensors are widely used integrated in vehicles, mobile phones and medical devices. The most common type of sensors today are the AMR (anisotropic magnetoresistance), GMR (giant magnetoresistance), Fluxgate and Hall sensors. The newest types of silicon based magnetic sensors, both AMR and GMR sensors, are being implemented in a variety of new applications thus posing a challenge for traditional Hall devices.

Magnetic sensors offer several key advantages, such as non-contact measurements (electrical currents or mechanical quantities like angle of rotation and angular speed), robust and inexpensive to manufacture. One of their biggest market today is automotive applications. In advanced motors where load changes and knowledge of torque is needed, Hall or anisotropic magnetoresistive (AMR) sensors are used in order to measure the motor position of the shaft.

As presented in Figure 1., the magnetic sensor market was expected to show an increase of nearly 30% until 2016. Particularly the digital compass (mostly AMR sensors) is becoming ubiquitous as a standard feature of smartphones, tablets, cameras and other consumer devices. The use of AMR in automotive applications will also increase in the next five years. An example is for the tachometer motors used to indicate speed and RPM (revolution per minute) instruments, for reasons of motor quietness [Dixon, 2011].

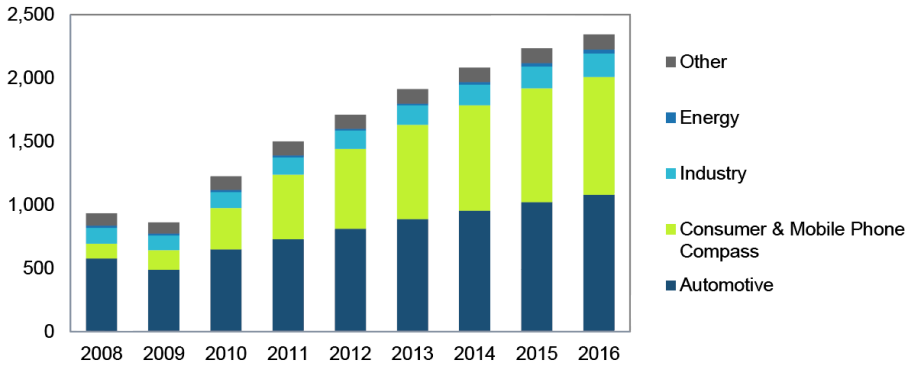

Figure 1: Magnetic sensor market between 2008-2012 and forecast until 2016 (Millions of USD) [Bouchaud, 2012]

AMR sensor is one of the most widely deployed magnetic field sensor. In contrast to other silicon based sensors, which require complex multilayer systems, the AMR sensor is characterized by its simplicity. AMR sensors can be bulk manufactured on silicon wafers and mounted in commercial IC packages, permitting automated assembly with other circuit. AMR sensors offer low production cost, high sensitivity, small size, and immunity to noise.

The AMR effect, discovered in 1857 by William Thomson (Lord Kelvin), consists in the change of electrical resistance in a magnetic material as a response of a variation in the environmental magnetic field. This effect is strongly dependent on the local magnetization in the material. An AMR sensor has two main parts, a magnetoresistive sensor element and a comparator circuit prepared on one chip. These sensor elements are mostly made of strongly textured ferromagnetic thin films. The application of a magnetic field changes the magnetization of the film, and the corresponding change in resistivity is measured through the electronic circuit.

The distribution of magnetization within a ferromagnetic film is very heterogeneous. From the modeling point of view, this is the reason why numerical models for AMR effect are mostly based on micromagnetic calculations. In these approaches the number of degrees of freedom and interactions are growing quickly with the number of magnetic moments, so that these simulations can only address small volumes corresponding to a limited number of domains.

On the other hand, a large part of phenomenological models for the AMR effect are based on the hypothesis that the material is at magnetic saturation so that it can be described as a one-domain particle. This is however a strong simplification due to the complex magnetic domain structure of the magnetoresistive element.

An alternative is the use of a micro-macro (or multiscale) approach that incorporates statistical view of the microstructure to define the effective properties of ferromagnetic materials. In this thesis a micro-macro model is proposed which offers an opportunity to investigate optimal material composition, crystallographic texture, film thickness or bias field level for specific applications of AMR sensors. The effect of stress on the sensing properties of these sensors can be also estimated.

This thesis is composed of four chapters.

The first one gives an overview of magnetic field sensing technologies. This chapter introduces also the phenomena related to magnetoresistance effects and magnetoelastic behavior of ferromagnetic materials and gives a literature review of different models of anisotropic magnetoresistance effect.

At the beginning of the second chapter a multiscale approach for stress-dependent anisotropic magnetoresistance is presented. Then the meso-micro scale transition rules are discussed and the magnetoelastic and magnetoresistive properties of some ferromagnetic single crystals are investigated.

The third chapter presents the extension of the multiscale modeling strategy to polycrystals. The macro-meso scale transition rules are introduced and the model is validated on isotropic ferromagnetic polycrystals. At the end of the chapter the effect of stress and crystallographic texture are investigated.

The last chapter proposes an application of this micro-macro model. Surface effect and textured film properties are introduced and thin film AMR sensor properties are investigated. The effect of bias magnetic field and the effect of stress on the properties of AMR sensor is discussed.

Chapter 1

Magnetoresistance effects and magnetoelastic behavior of ferromagnetic materials

Contents

In this chapter the basis of magnetic field sensing technologies using magnetoresistive elements is summarized. Next, the phenomena related to magnetoresistance effects and magnetoelastic behavior of ferromagnetic materials is introduced. A review of different models of AMR (anisotropic magnetoresistance) is also presented in order to define the state of the art in this field. Finally it is shown that an adequate computation tool is needed to achieve an accurate and rigorous model of magnetoresistance and magnetoelastic coupling.

1.1 Magnetoresistive elements for magnetic field sensing

1.1.1 Hall sensors

Hall Effect sensors dominated today the magnetic field sensor market with more than 70% of market share, while newer technologies such as AMR and GMR sensors are gradually gaining visibility [Dixon, 2011].

The Hall effect is the production of an electric charge difference (the Hall voltage) across an electrical conductor, transverse to an electric current in the conductor and a magnetic field perpendicular to the current. It was discovered by Edwin Hall in 1879 [Chikazumi and Graham, 1997].

The Hall effect is due to the nature of the current in a conductor. Current consists of the movement of many small charge carriers, typically electrons, holes, ions or all three. When a magnetic field is present that is not parallel to the direction of motion of moving charges, these charges experience a force, called the Lorentz force ($\overrightarrow{F}$):

$$\overrightarrow{F} = q(\overrightarrow{E} + \overrightarrow{v} \wedge \overrightarrow{B}) \tag{1.1}$$

where q is the charge, $\overrightarrow{v}$ its velocity and $\overrightarrow{E}$ and $\overrightarrow{B}$ the electric and magnetic fields.

When there is no magnetic field, the charges follow approximately straight lines parallel to the electric field. However, when a magnetic field with a perpendicular component is applied, their paths between collisions are curved so that moving charges accumulate on one face of the material. This leaves equal and opposite charges exposed on the other face, where there is a scarcity of mobile charges.

The result is an asymmetric distribution of charge density across the Hall element that is perpendicular to both the path and the applied magnetic field (Fig. 1.1). The separation of charge establishes an electric field that opposes the migration of further charge, so a steady electrical potential is established for as long as the charge is flowing. This dissymmetry in electrical charges can be measured through a voltage measurement (in the direction perpendicular to the flowing current).

Hall probes are often used as magnetometers, i.e. to measure magnetic fields, or inspect materials (such as tubing or pipelines) using the principles of magnetic flux

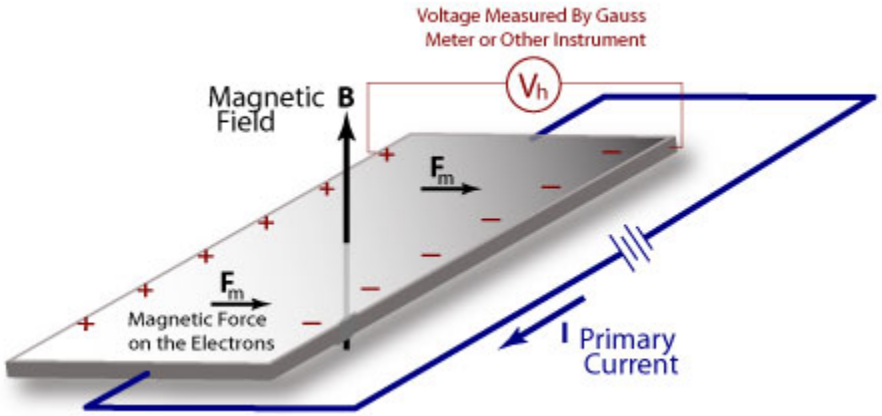

Figure 1.1: Representation of the Hall effect (image from [NDT-Inc., 2015])

leakage.

Hall effect devices produce a very low signal level and thus require amplification. While suitable for laboratory instruments, the vacuum tube amplifiers available in the first half of the 20th century were too expensive, power consuming, and unreliable for everyday applications. It was only with the development of the low cost integrated circuit that the Hall effect sensor became suitable for mass application. Many devices now sold as Hall effect sensors in fact contain both the sensor as described above plus a high gain integrated circuit (IC) amplifier in a single package.

The main suppliers of Hall Effect sensors are Allegro, Micronas, Melexis, Austria Microsystems, and AKM.

1.1.2 Anisotropic Magnetoresistance (AMR) based sensors

The anisotropic magneto-resistive effect, abbreviated AMR effect, was already discovered in 1857 by William Thomson. Thomson found out that magnetic field can influence the electric resistance of ferromagnetic materials (change of 1-2%). Finally, 120 years later and by applying the thin-film technology, this knowledge was first used for a technological product - the MR sensor.

Thomson's experiments are an example of AMR, property of a material in which a dependence of electrical resistance on the angle between the direction of electric current and direction of magnetization is observed [Bozorth, 1993]. The physical origin of the magnetoresistance effect lies in spin orbit coupling. The electron cloud about each nucleus deforms slightly as the direction of the magnetization rotates, and this deformation changes the amount of scattering undergone by the conduction electrons when traversing the lattice. A heuristic explanation is that the magnetization direction rotates the closed orbit orientation with respect to the current direction. If the field and magnetization are oriented transverse to the current, then the electronic orbits are in the plane of the current, and there is a small cross-section for scattering, giving a low resistance state. Conversely for fields applied parallel to

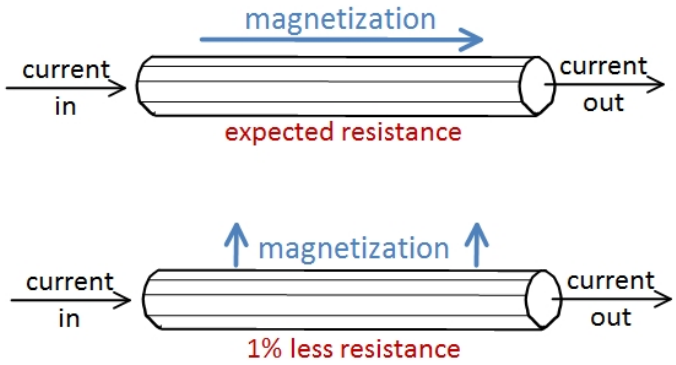

Figure 1.2: Schematic representation of the AMR effect

the current, the electronic orbits are oriented perpendicular to the current, and the cross-section for scattering is increased, giving a high resistance state.

The net effect (in most materials) is that the electrical resistance has maximum value when the direction of current is parallel to the applied magnetic field (Fig. 1.2). AMR of new materials is being investigated and magnitudes up to 50% have been observed in some ferromagnetic uranium compounds [Wiśniewski, 2007].

The AMR effect is used in a wide array of sensors for measurement of Earth's magnetic field (electronic compass), for electric current measuring (by measuring the magnetic field created around the conductor), for traffic detection and for linear position and angle sensing.

The biggest AMR sensor manufacturers are Honeywell, NXP Semiconductors, and Sensitec GmbH.

1.1.3 Giant, Colossal and Tunnel Magnetoresistance (GMR, CMR and TMR) based sensors

Giant MagnetoResistance

The Giant Magneto Resistive (GMR) effect was first discovered in 1988 by Fert and Grunberg [Grünberg et al., 1986] [Baibich et al., 1988], who were awarded with the Nobel Prize for Physics in 2007 for this achievement. This effect occurs in layer systems with at least two ferromagnetic layers and a single non-magnetic, metallic intermediate layer. If the magnetization in these layers is non-parallel, the resistance is larger than if the magnetization is parallel. The difference may reach up to 50%, thus the name *giant*.

The key structure in GMR materials is a spacer layer of a non-magnetic metal between two magnetic metals (Fig. 1.3). Magnetic materials tend to align their magnetization in the same direction. So if the spacer layer is thin enough, changing the orientation of one of the magnetic layers can cause the next one to align itself in the same direction. But an oscillation in the coupling strength can be observed

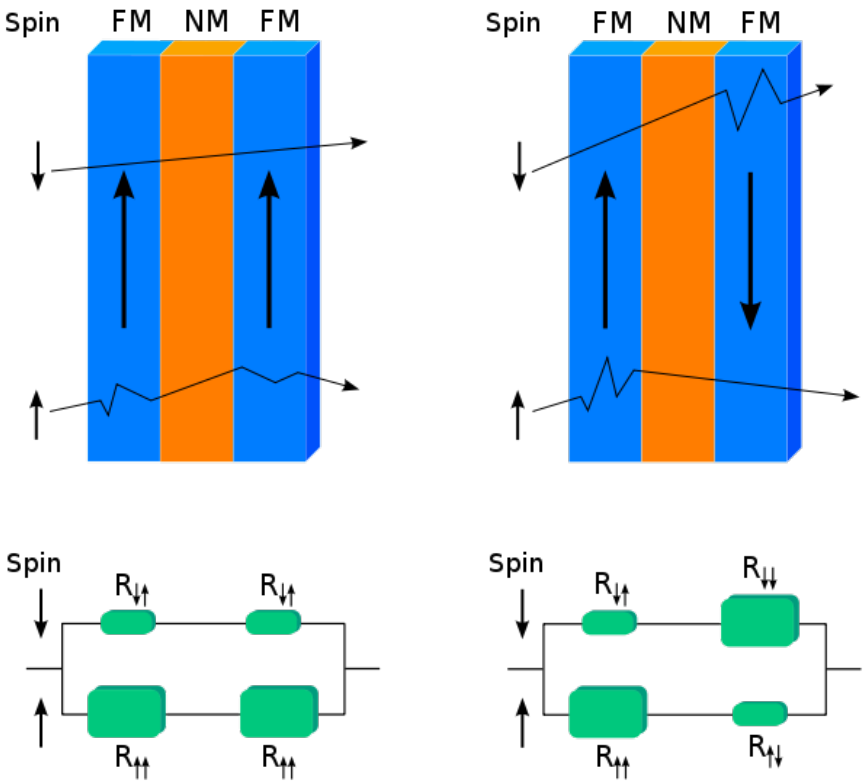

Figure 1.3: Representation of the GMR effect

as a function of the thickness of the non-magnetic layer. The magnetic alignment of the magnetic layers periodically alternate back and forth from being aligned in the same magnetic direction (parallel alignment) to being aligned in opposite magnetic directions (anti-parallel alignment).

The chief source of GMR effect is spin-dependent scattering of electrons. Electrical resistance is due to scattering of electrons within a material. Depending on its magnetic direction, a single-domain magnetic material will scatter electrons with "up" or "down" spin differently (it can be described as in the case of the AMR effect). When the magnetic layers in GMR structures are aligned anti-parallel, the resistance is high because "up" electrons that are not scattered in one layer can be scattered in the other. When the layers are aligned in parallel, all of the "up" electrons will not scatter much, regardless of which layer they pass through, yielding a lower resistance (Fig. 1.3).

GMR sensors offer high sensitivity, wide frequency range, small size, low power consumption and they are compatible with many other state-of-the-art technologies. However, as the linearity range of GMR sensors is narrow compared with other sensors such as Hall sensors and AMR sensors, GMR sensors are not suitable for large current sensing [Jedlicska et al., 2010]. In addition, the output of some of GMR sensors is unipolar, which limits its application in AC measurements [McNeill

et al., 2008].

The main suppliers for GMR sensors are Sensitec GmbH, NVE Corporation and Hitachi.

Colossal MagnetoResistance

In 1993 von Helmholtz et al. discovered the Colossal MagnetoResistive (CMR) effect [von Helmolt et al., 1993]. This effect occurs in perowskitic, manganese based oxides, that change their resistance in the presence of a magnetic field. Of all the known physical effects, by which a solid changes its properties due to magnetism, MR technology has particularly interesting and convincing advantages. However, a fully quantitative understanding of the CMR effect has been elusive and it is still the subject of current research activities. Early prospects of great opportunities for the development of new technologies have not yet come to fruition.

Tunnel MagnetoResistance

The Tunnel MagnetoResistive (TMR) effect [Julliere, 1975], discovered by Julliere in 1975, occurs in layer systems consisting of at least two ferromagnetic layers and a thin insulation layer. The tunnel resistance between both layers depends on the angle of both magnetization directions. If the insulating layer is thin enough (typically a few nanometers), electrons can tunnel from one ferromagnet into the other. Since this process is forbidden in classical physics, the tunnel magnetoresistance is a strictly quantum mechanics phenomenon.

1.1.4 Comparison with other magnetoresistive elements

Figure 1.4 presents a comparison of the sensitivity of various magnetoresistive sensors. It is shown that for large magnetic fields (one Tesla or more) semiconductor magnetoresistors or GMR multilayers are recommended (in this range of magnetic field Hall sensors are used today most widely).

Spin-valve sensors obtain larger output signals than AMR sensors (but for larger magnetic fields). Therefore they are useful for reading information from magnetic tapes or disks (in magnetoresistive heads) where small dimensions of the sensor are the most important parameter. Due to large magnetoresistivity GMR heads allow reading of information with the highest density reported to date. The most frequently used are AMR and GMR/SV sensors - they are also available as commercial products (Philips, Siemens, Honeywell, Nonvolatile Electronics). The semiconductor magnetoresistors are of smaller technical importance due to rather strong temperature dependence and high non-linearity [Popovic et al., 1996].

It is highlighted on Figure 1.4 that for detecting small magnetic fields (for example Earth's magnetic field) the permalloy magnetoresistive sensors are the most suitable. In the following our study is concentrated on the investigation of thin film permalloy AMR sensors.

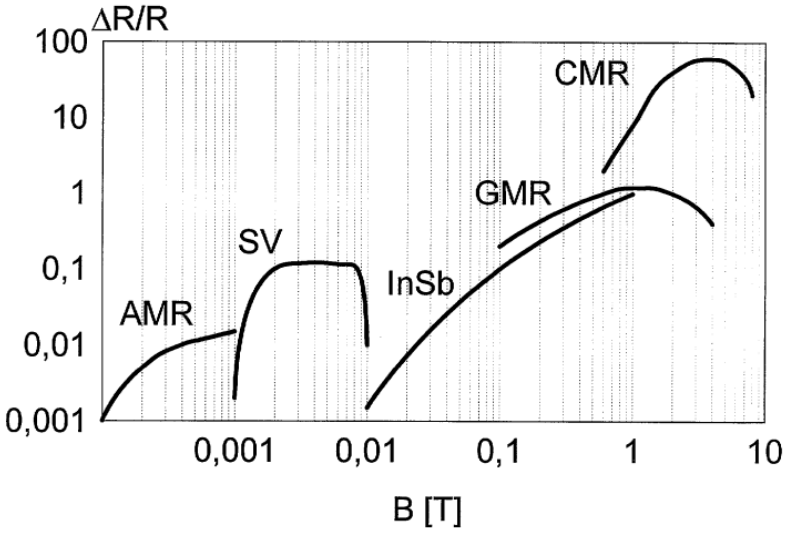

Figure 1.4: The typical field range and resistivity changes of various magnetoresistive sensors - SV : spin valve sensors; InSb : semiconductor magnetoresistors [Heremans, 1993]

1.2 Basic notions of material behavior

AMR effect is closely related to the magnetic behavior of ferromagnetic materials. This work will investigate the role of mechanical stress on this behavior. This section gives a brief overview on the notions of material behavior used in the document.

1.2.1 Different types of magnetic behavior

Materials may be classified by their response to externally applied magnetic fields as diamagnetic, paramagnetic, or ferromagnetic. These magnetic responses differ greatly in strength [Bozorth, 1993]. Diamagnetism is a property of all materials and opposes applied magnetic fields, but is very weak. Paramagnetism, when present, is stronger than diamagnetism and produces magnetization in the direction of the applied field, and proportional to the applied field. Ferromagnetic effects are very large, producing magnetization sometimes orders of magnitude greater than the applied field and as such are much larger than either diamagnetic or paramagnetic effects.

The magnetization of a material is expressed in terms of density of net magnetic dipole moments $\vec{m}$ in the material. We define a vector quantity called the magnetization ($\vec{M}$) by

$$\vec{M} = \vec{\mu_{total}}/V \tag{1.2}$$

where $\vec{\mu_{total}}$ is the sum of magnetic moments over the volume V. Then, the total magnetic field $\vec{B}$ in the material is given by

$$\vec{B} = \mu_0 \vec{H}_0 + \mu_0 \vec{M} \tag{1.3}$$

where μ_0 is the magnetic permeability of vacuum and $\vec{H}$ is the externally applied magnetic field. The relationship between the magnetic induction $\vec{B}$ and the magnetic field $\vec{H}$ in magnetic materials is usually written according to the magnetic permeability μ or relative magnetic permeability μ_r:

$$\vec{B} = \mu \vec{H} = \mu_0 \mu_r \vec{H} \tag{1.4}$$

Another commonly used magnetic quantity is the magnetic susceptibility which relates the magnetization to the magnetic field. From equation 1.3, it can be easily shown that

$$\chi_m = \mu_r - 1 \tag{1.5}$$

For paramagnetic materials $\chi_m > 0$, and for diamagnetic materials $-1 < \chi_m < 0$. For ferromagnetic materials, these quantities may be very large.

1.2.2 Ferromagnetism

Ferromagnets and ferrimagnets are mostly used in the fabrication of magnetic cores. These two types of magnetic materials exhibit a very nonlinear B-H relationship. A typical example is given in Fig.1.5 for an iron-silicon alloy [Hubert et al., 2003]. it is possible to divide the magnetic response into a reversible and irreversible part. The reversible part described by the anhysteretic curve cannot be followed in a continuous manner, because the dissipation mechanisms (mainly linked to magnetic domain wall motion) cannot be avoided. However, this curve can be measured in a discrete manner [Bozorth, 1993].

1.2.3 Mechanical behavior

The mechanical behavior of a material reflects the stress-strain relationship. Important mechanical properties are strength, hardness, ductility, and stiffness [Chikazumi and Graham, 1997]. The degree to which a structure deforms depends on the magnitude of stress. When limited to relatively low stress levels, materials exhibit a linear and reversible mechanical behavior (linear elasticity) described by Hooke's law. In the case of uniaxial tension or compression it is given by :

$$\sigma = E\epsilon \tag{1.6}$$

where σ is the tensile stress and ϵ is the extensional strain. The proportionality constant E (GPa or psi) is the modulus of elasticity, or Young's modulus. For most metallic materials, elastic deformation persists only to strains of about 0.005 [Bozorth, 1993]. As the material is deformed beyond this point, the stress is no longer proportional to strain (Hooke's law ceases to be valid), and permanent, nonrecoverable, or plastic deformation occurs. From an atomic perspective, plastic

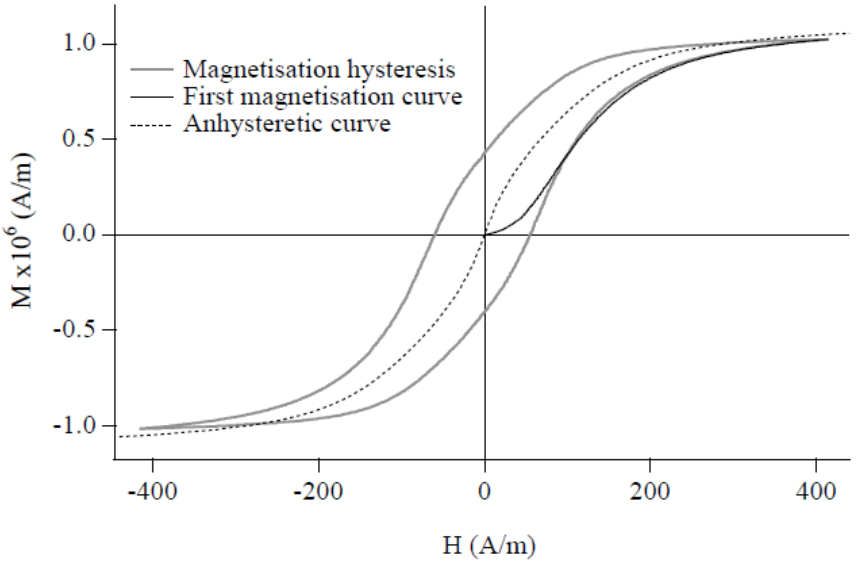

Figure 1.5: First magnetization, hysteresis and anhysteretic curve for a non-oriented silicon iron alloy [Hubert et al., 2003]

deformation corresponds to the breaking of bonds with original atom neighbours and then reforming bonds with new neighbours as large numbers of atoms or molecules move relative to one another; upon removal of the stress they do not return to their original positions.

1.2.4 Magnetoelastic coupling

Magnetostriction is the deformation of a magnetic material due to magnetic interactions. When iron is cooled down from a high temperature through its Curie temperature, an anomalous isotropic expansion is observed near the Curie temperature. This slightly magnetic field-dependent anomaly associated with the magnetism of iron (and other magnetic substances) is called *volume magnetostriction*. This is the isotropic aspect of the spontaneous magnetostriction.

Now, if a magnetic field is applied to the iron sample, an additional anisotropic deformation that stretches or shrinks the sample in the direction of the magnetic field is observed. This field-dependent phenomenon is called *Joule magnetostriction*; it is the anisotropic aspect of the forced magnetostriction.

1.3 AMR models in the literature

Several technologies can be used to ensure an optimal performance of AMR sensors [Tumanski, 2001, Stutzke et al., 2005, Kubik et al., 2006, Zimmermann et al., 2005], but this performance is always related to the intricate relationship between the microstructure and the macroscopic response of the sensor. In the case

of ferromagnetic polycrystalline materials, the microstructure scale is twofold. The material is divided into magnetic domains with different magnetization, and it is also divided into grains with different crystallographic orientations.

From the modeling point of view, a large part of phenomenological models for the AMR effect are based on the hypothesis that the material is at magnetic saturation so that it can be described as a one-domain particle [McGuire and Potter, 1975, Li et al., 2010, Beltran et al., 2007]. This is however a strong simplification given the complex magnetic domain structure of ferromagnetic materials.

Some authors proposed micromagnetic calculations to describe this evolving domain structure in thin film AMR sensors [Koehler et al., 1993, Shiiki et al., 1996]. But these approaches usually lead to dissuasive computation time so that strong simplifying assumptions are needed when describing real systems.

An alternative is the use of a micro-macro approach that incorporates a statistical view of the microstructure to define the effective properties of ferromagnetic materials [Daniel et al., 2008, Daniel and Galopin, 2008]. In this thesis this micro-macro - or multiscale - approach is used to describe the properties of thin film AMR sensors. This model allows us reproducing the main features of AMR magnetic field sensors under typical operating conditions.

Chapter 2

Single crystal behavior

Contents

2.1 Microscopic magneto-elastic model

The first step of our magneto-mechanical modelization is to get an accurate description of the single crystal behavior. A single crystal is seen as an assembly of magnetic domains. The distribution of magnetization (domain configuration) within a single crystal can be very heterogeneous. As its electrical resistance is strongly dependent on the local magnetization (AMR effect), modelization at this microscopic scale (domains or group of atoms) is used in order to investigate the AMR behavior of the whole single crystal.

The external magnetic field or the mechanical stress applied to a magnetic media can change the distribution of domain orientations. As a consequence it modifies the local resistivity, and thus the overall resistivity.

In this chapter a microscopic magneto-elastic model for AMR is proposed based on the magneto-elastic model derived from [Daniel and Galopin, 2008, Daniel et al., 2008]. It can be noticed that the same model can be applied for a grain embedded in a polycrystal (presented in Chapter 3.).

At the scale of a group of atoms, the magnetic equilibrium state can be described by the sum of several energy terms. The free energy W^p of a group of atom can be written [Cullity and Graham, 2011]:

$$W^p = W^{ex} + W^K + W^\sigma + W^H \tag{2.1}$$

where
- W^{ex} denotes the exchange energy,
- W^K denotes the magnetocrystalline anisotropy energy,
- W^H denotes the magneto-static energy and
- W^σ denotes the elastic energy.

In the reminder of this chapter, first, the magnetic energy terms - exchange, anisotropy, magnetostatic and elastic energies - are introduced. Then all these energy terms are presented in the case of a magnetic domain. Then a microscopic magneto-elastic model is presented in order to define in a statistical way the domain configuration of the single crystal. A microscopic AMR model allows us to define the local resistivity depending on the magnetization orientation in the considered domain. Finally a homogenization step allows us retrieving the variation of the resistivity at the single crystal scale. In the last part of the chapter numerical results are compared with experimental results from the literature.

2.1.1 Exchange energy

The phenomenon whereby individual atomic magnetic moments tend to align uniformly within a material is known as the exchange interaction. If the magnetic moments align in a parallel fashion, the material is ferromagnetic, if the magnetic moments align antiparallel, the material is antiferromagnetic.

In ferromagnetic materials the exchange energy can be described in the following form [Hubert and Schäfer, 1998]:

$$W^{ex} = A(grad\boldsymbol{\alpha})^2 \tag{2.2}$$

where A is the exchange constant and $\boldsymbol{\alpha} = {}^t[\alpha_1\ \alpha_2\ \alpha_3]$ the direction cosines of the magnetization ($\mathbf{M}_\alpha = M_s\,\boldsymbol{\alpha}$ with M_s the saturation magnetization of the material).

This energy term is minimal when the spatial variations of the magnetization direction are minimum.

2.1.2 Magnetocrystalline anisotropy energy

Magnetocrystalline anisotropy energy is the energy necessary to deflect the magnetic moment in a single crystal from the easy to the hard direction. The easy and hard directions arise from the interaction of the spin magnetic moment with the crystal lattice (spin-orbit coupling). The magnetocrystalline energy is minimal when the magnetization is aligned with an easy axis and maximal when it is aligned with a hard axis of the single crystal.

The magnetocrystalline anisotropy energy is generally represented as a spherical expansion in powers of the direction cosines of the magnetization. In cubic crystals (like Iron or Nickel) it is sufficient to represent the anisotropy energy in an arbitrary direction by just the first two terms in the series expansion. These two terms each have an empirical constant associated with them called the first- and second order anisotropy constants, K_1 and K_2 respectively.

In the case of cubic crystallographic structure the magnetocrystalline energy can be written [Cullity and Graham, 2011]:

$$W^K = K_1(\alpha_1^2\alpha_2^2 + \alpha_2^2\alpha_3^2 + \alpha_3^2\alpha_1^2) + K_2(\alpha_1^2\alpha_2^2\alpha_3^2) \tag{2.3}$$

If the second term can be neglected, the easy axes are the <100> axes for $K_1 > 0$ (for example Iron) and the <111> directions for $K_1 < 0$ (for example Nickel).

The spatial magnetocrystalline energy distribution of an Iron single crystal is presented in Figure 2.1. As the anisotropy constants of Iron are $K_1 = 42.7\ kJ/m^3$ and $K_2 = 15\ kJ/m^3$ [Bozorth, 1993] its easy magnetization directions (where the energy W^K is minimal) are <100>.

2.1.3 Magnetostatic energy

The magnetostatic energy term comes from the magnetostatic self-energy, which originates from the classical interactions between magnetic dipoles. For a strongly magnetic body, even in the absence of an external magnetic field, magnetostatic energy is generated within the magnetic body by the internal magnetic field generated in the opposite direction from the magnetization (and called the demagnetizing field). So the magnetostatic energy is usually divided into two contributions [Hubert and Schäfer, 1998]. The first part appears when an external magnetic field ($\mathbf{H}_0$) is applied (it is the so-called *Zeeman energy*):

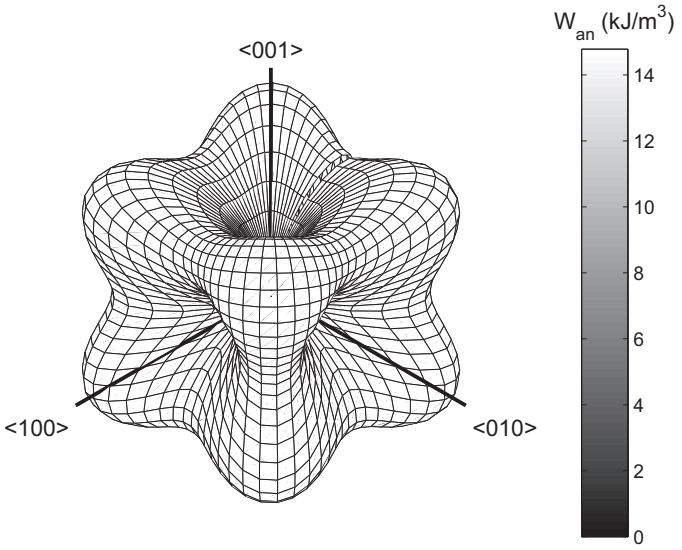

Figure 2.1: Magnetocrystalline energy distribution of an Iron cubic single crystal

$$W^z = -\mu_0 \mathbf{H}_0.\mathbf{M} \tag{2.4}$$

This energy term tends to align the magnetization direction with the applied field as it is minimal when the magnetization $\mathbf{M}$ is parallel to $\mathbf{H}_0$.

The variation of the magnetization in the material creates a demagnetizing field ($\mathbf{H}_d$). This adds a contribution to the magnetostatic energy:

$$W^d = -\mu_0 \mathbf{H}_d.\mathbf{M} \tag{2.5}$$

The demagnetizing field ($\mathbf{H}_d$) opposes the effect of the applied magnetic field ($\mathbf{H}_0$) and it can be calculated from the magnetization:

$$div\mathbf{H}_d = -div\mathbf{M} \tag{2.6}$$

So the total magnetostatic energy is written as:

$$W^H = W^z + W^d = -\mu_0 \mathbf{H}_0.\mathbf{M} - \mu_0 \mathbf{H}_d.\mathbf{M} = -\mu_0 \mathbf{H}_{eff}.\mathbf{M} \tag{2.7}$$

where

$$\mathbf{H}_{eff} = \mathbf{H}_0 + \mathbf{H}_d. \tag{2.8}$$

2.1.4 Elastic energy

In the case of a 3D linear elastic behavior, Hooke's law defines a proportional relation between elastic strain ($\boldsymbol{\varepsilon}^e$) and stress ($\boldsymbol{\sigma}$):

$$\boldsymbol{\sigma} = \mathcal{C} : \varepsilon^e. \tag{2.9}$$

In this model we assume that the deformation has two sources; a mechanical deformation ($\boldsymbol{\varepsilon^e}$) and a magnetostriction strain ($\boldsymbol{\varepsilon^\mu}$). The total deformation is the sum of two:

$$\boldsymbol{\varepsilon} = \boldsymbol{\varepsilon^e} + \boldsymbol{\varepsilon^\mu} \tag{2.10}$$

The elastic energy is written as:

$$W^\sigma = \frac{1}{2}(\boldsymbol{\sigma} : \mathcal{C}^{-1} : \boldsymbol{\sigma}) \tag{2.11}$$

2.2 Calculation at the magnetic domain scale

The lowest calculation scale in our model is the magnetic domain scale. A magnetic domain is a region in which the magnetization vectors are aligned. The magnetization is then uniform in a domain, noted α, and given by $\mathbf{M}_\alpha = M_s\,\boldsymbol{\alpha}$ with M_s the saturation magnetization of the material and $\boldsymbol{\alpha} = {}^t[\alpha_1\ \alpha_2\ \alpha_3]$ the direction cosines of the magnetization. In the following we take the definition of the potential energy given by equation (2.1) and try to make some simplifications associated to the uniformity of the magnetization and the uniformity of elastic coefficients within the domain.

Exchange energy

In a magnetic domain, there is no variation of the magnetization, the exchange energy is zero.

Magnetocrystalline anisotropy energy

At the domain scale equation (2.3) is usable without any modification:

$$W_\alpha^K = K_1(\alpha_1^2\alpha_2^2 + \alpha_2^2\alpha_3^2 + \alpha_3^2\alpha_1^2) + K_2(\alpha_1^2\alpha_2^2\alpha_3^2). \tag{2.12}$$

Magnetostatic energy

To simplify the definition of the magnetostatic energy we introduce the hypothesis that the magnetization in a domain is uniform. The equation (2.7) simplifies for:

$$W_\alpha^H = -\mu_0 \mathbf{M}_\alpha.\mathbf{H}_\alpha. \tag{2.13}$$

Elastic energy

Under uniform strain hypotheses the elastic energy can be written [Daniel et al., 2008]:

$$W_\alpha^\sigma = -\boldsymbol{\sigma_g} : \boldsymbol{\varepsilon_\alpha^\mu} \tag{2.14}$$

In the case of cubic crystallographic symmetry, the magnetostriction strain tensor $\boldsymbol{\varepsilon_\alpha^\mu}$ can be written as

$$\boldsymbol{\varepsilon_\alpha^\mu} = \frac{3}{2}\begin{pmatrix} \lambda_{100}(\alpha_1^2 - \frac{1}{3}) & \lambda_{111}\alpha_1\alpha_2 & \lambda_{111}\alpha_1\alpha_3 \\ \lambda_{111}\alpha_1\alpha_2 & \lambda_{100}(\alpha_2^2 - \frac{1}{3}) & \lambda_{111}\alpha_2\alpha_3 \\ \lambda_{111}\alpha_1\alpha_3 & \lambda_{111}\alpha_2\alpha_3 & \lambda_{100}(\alpha_3^2 - \frac{1}{3}) \end{pmatrix} \tag{2.15}$$

where λ_{100} and λ_{111} are the magnetostrictive constants of the single crystal.

2.2.1 Potential energy of a magnetic domain

As a conclusion the potential energy of a magnetic domain (α) can be written as:

$$W_\alpha = -\mu_0 \mathbf{M}_\alpha.\mathbf{H}_\alpha - \boldsymbol{\sigma_g} : \boldsymbol{\varepsilon_\alpha^\mu} + K_1(\alpha_1^2\alpha_2^2 + \alpha_2^2\alpha_3^2 + \alpha_3^2\alpha_1^2) + K_2(\alpha_1^2\alpha_2^2\alpha_3^2). \tag{2.16}$$

2.2.2 Single domain model of AMR

Let $\boldsymbol{\beta} = {}^t[\beta_1\ \beta_2\ \beta_3]$ be the direction cosines determining the orientation of the current used for measuring the electrical resistance ($\boldsymbol{\alpha} = {}^t[\alpha_1\ \alpha_2\ \alpha_3]$ are still the direction cosines of the magnetization in the considered domain). The general expression for the magnetoresistance in any direction of a cubic crystal can be written in a series form of $\boldsymbol{\alpha}$ and $\boldsymbol{\beta}$ [McGuire and Potter, 1975]. Döring used the following form [Bozorth, 1993] for cubic crystals with negative magnetocrystalline anisotropy constant [1] K_1 (such as nickel and $Fe_{11}Ni_{89}$ permalloy):

$$\begin{aligned} \rho_\alpha = \rho_0 \Big[& 1 + k_1(\alpha_1^2\beta_1^2 + \alpha_2^2\beta_2^2 + \alpha_3^2\beta_3^2 - \tfrac{1}{3}) \\ & + 2k_2(\alpha_1\alpha_2\beta_1\beta_2 + \alpha_2\alpha_3\beta_2\beta_3 + \alpha_3\alpha_1\beta_3\beta_1) \\ & + k_3(s - \tfrac{1}{3}) \\ & + k_4(\alpha_1^4\beta_1^2 + \alpha_2^4\beta_2^2 + \alpha_3^4\beta_3^2 + \tfrac{2s}{3} - \tfrac{1}{3}) \\ & + 2k_5(\alpha_1\alpha_2\beta_1\beta_2\alpha_3^2 + \alpha_2\alpha_3\beta_2\beta_3\alpha_1^2 + \alpha_3\alpha_1\beta_3\beta_1\alpha_2^2)] \end{aligned} \tag{2.17}$$

in wich $s = \alpha_1^2\alpha_2^2 + \alpha_2^2\alpha_3^2 + \alpha_3^2\alpha_1^2$, ρ_0 is the resistivity in the demagnetized state and k_1, k_2, k_3, k_4, k_5 are material constants. For a crystal with positive magnetocrystalline anisotropy constant [2] K_1 (such as iron) the expression is the same except that the term $k_3/3$ is absent.

1. in that case easy magnetization directions are $\langle 111 \rangle$ directions.
2. in that case easy magnetization directions are $\langle 100 \rangle$ directions.

2.3 Calculation at the single crystal scale

The intermediate calculation scale in this model - called mesoscopic scale - is the single crystal or grain, that is seen as a collection of magnetic domains (α) with given magnetization orientation $\boldsymbol{\alpha}$. The microscopic magnetoelastic model allows us defining in a statistical way the domain configuration, introducing as an internal variable the volume fraction f_α of domains with orientation $\boldsymbol{\alpha}$ in a grain g. In each domain, depending on the considered orientation $\boldsymbol{\alpha}$, the magnetization $\mathbf{M}_\alpha$ and magnetostriction strain $\boldsymbol{\varepsilon}^{\boldsymbol{\mu}}_{\boldsymbol{\alpha}}$ are known.

2.3.1 Selection and calculation of state variables

The state variables chosen to describe the magnetization of a single crystal are the volume fraction f_α of the domain family α in the single crystal [Néel, 1944, Chikazumi and Graham, 1997, Buiron, N. et al., 1999, Daniel et al., 2008, Daniel and Galopin, 2008]. The f_α variables are obtained through the numerical integration of the following Boltzmann-type relation [Daniel and Galopin, 2008] over all the possible orientations for the magnetization in the single crystal :

$$f_\alpha = \frac{exp(-A_s.W_\alpha)}{\int_\alpha exp(-A_s.W_\alpha)d\alpha} \tag{2.18}$$

where A_s is an adjustment parameter accounting for the non uniformity of the exchange energy, the magnetic field and the stress tensor within the single crystal. It can be deduced from low field measurement of the anhysteretic magnetization curve ($A_s = \frac{3\chi_0}{\mu_0 M_s^2}$ [Daniel et al., 2008] where χ_0 is the initial anhysteretic susceptibility of the material).

2.3.2 Homogenization

This homogenization step allows us retrieving the overall response of the material at the single crystal scale (magnetization at the grain scale $\mathbf{M}_g$, magnetostriction strain $\boldsymbol{\varepsilon}^{\boldsymbol{\mu}}_{\boldsymbol{g}}$ and the variation of the macroscopic resistivity $\delta\rho_g$) depending on the local values of the response at the domain scale.

Magnetostriction strain and magnetization

The magnetostriction strain and the magnetization within the single crystal are defined by an averaging operation over the single crystal (volume V_g):

$$\boldsymbol{\varepsilon}^{\boldsymbol{\mu}}_{\boldsymbol{g}} = \langle \boldsymbol{\varepsilon}^{\boldsymbol{\mu}} \rangle_g = \frac{1}{V_g} \int_\alpha \boldsymbol{\varepsilon}^{\boldsymbol{\mu}}\, dV = \sum_\alpha f_\alpha\, \boldsymbol{\varepsilon}^{\boldsymbol{\mu}}_{\boldsymbol{\alpha}} \tag{2.19}$$

$$\mathbf{M}_g = \langle \mathbf{M} \rangle_g = \frac{1}{V_g} \int_\alpha \mathbf{M}\, dV = \sum_\alpha f_\alpha\, \vec{M}_\alpha \tag{2.20}$$

where the operation $\langle\ .\ \rangle_g$ is an averaging operation over the whole volume of the single crystal.

If needed, the elastic strain $\boldsymbol{\varepsilon}_g^e$ at the single crystal can be calculated from Hooke's law (equation (2.9)) using the single crystal stiffness tensor $\mathcal{C}_g$. This elastic strain is superimposed to the magnetostriction strain to obtain the total strain of the single crystal ($\boldsymbol{\varepsilon} = \boldsymbol{\varepsilon}^e + \boldsymbol{\varepsilon}^{\boldsymbol{\mu}}$).

$$\boldsymbol{\varepsilon}_g^e = \mathcal{C}_g^{-1} : \boldsymbol{\sigma_g} \tag{2.21}$$

Conductivity

Since the local electric conductivity ς_α in a domain is known ($\varsigma_\alpha = 1/\rho_\alpha$), the effective conductivity of the single crystal ς_g can be obtained through a self-consistent approach, applying the classical Bruggeman relation [Bruggeman, 1935, Stroud, 1975, Daniel and Corcolle, 2007]. ς_g is solution of Equation (2.22) that can be solved easily using a fixed point method.

$$\varsigma_g = \frac{\left\langle \dfrac{\varsigma_\alpha}{2\varsigma_g + \varsigma_\alpha} \right\rangle_g}{\left\langle \dfrac{1}{2\varsigma_g + \varsigma_\alpha} \right\rangle_g} \tag{2.22}$$

The effective resistivity ρ_g is deduced from the effective conductivity ($\rho_g = 1/\varsigma_g$). In the following the variation of the resistivity $\delta\rho_g$ (Equation (2.23)) will be plotted.

$$\delta\rho_g = \frac{\rho_g - \rho_0}{\rho_0} \tag{2.23}$$

It can be noticed from Equations (2.17) and (2.22) that $\delta\rho_g$ does not depend on the value of ρ_0, since ρ_g is proportional to ρ_0.

2.4 Results and comparison to experimental data

Experimental measurements of magnetic properties are available in the literature for pure Iron single crystal with cubic crystallographic symmetry [Webster, 1925].

Low field measurements give the necessary data to identify the parameter A_s. The initial susceptibility of the single crystal is approximatively estimated thanks to the $\langle 100 \rangle$ magnetization curve, where $\chi_{100} \simeq 2000$. It is leading to $A_s = 0.0016 m^3/J$.

This result is obviously approximative since it is based only on the behavior along the $\langle 100 \rangle$ axis. Experimental data indicate that the initial susceptibility in other directions is a little lower, in disaccordance with our initial hypotheses.

For the calculation of the volume fractions f_α, a 10 242 orientation (α) data file was used [Daniel and Galopin, 2008]. All the material constants used for the modelization are defined in Table 2.1 and Table 2.2.

Coefficient	M_S	K_1, K_2	λ_{100}, λ_{111}	A_s	C_{11}, C_{12}, C_{44}
Unit	A/m	kJ/m^3	-	m^3/J	GPa
Iron	1.71x10^6	42.7, 15	21, -21 (x10^{-6})	0.0016	238, 142, 232

Table 2.1: Physical constants of Iron used for the modeling [Bozorth, 1993, Cullity and Graham, 2011]

Coefficient	k_1	k_2	k_3	k_4	k_5
Iron	0.00153	0.00593	0.00194	0.00053	0.00269

Table 2.2: Constants of Döring expression for Iron [Bozorth, 1993]

2.4.1 Magnetoelastic properties

Fig. 2.2 and Fig. 2.3 show the magnetization (resp. the magnetostriction strain) measured in the direction parallel to the magnetic field, when magnetic field is applied along a $\langle 100 \rangle$, $\langle 110 \rangle$ or $\langle 111 \rangle$ axis of the single crystal. We observe a very good agreement between numerical and experimental results, both for magnetic and magnetostrictive behaviors. Strong non-linearity and anisotropy are well reproduced. Such results were already shown in [Daniel et al., 2008].

2.4.2 Magnetoresistive properties

The magnetoresistance in a single crystal is strongly anisotropic. Figure 2.4 shows the change in resistivity in a pure Iron single crystal as a function of the angle between its easy magnetization direction $\langle 100 \rangle$ and the applied magnetic field in the $\{011\}$ crystallographic plane. The change in resistivity (under no applied stress) can vary up to several hundred percent depending on the orientation of the magnetic field with respect to the crystal orientation, both in parallel and perpendicular configurations. As a consequence, the AMR effect can be expected to be very sensitive to the crystallographic texture of materials.

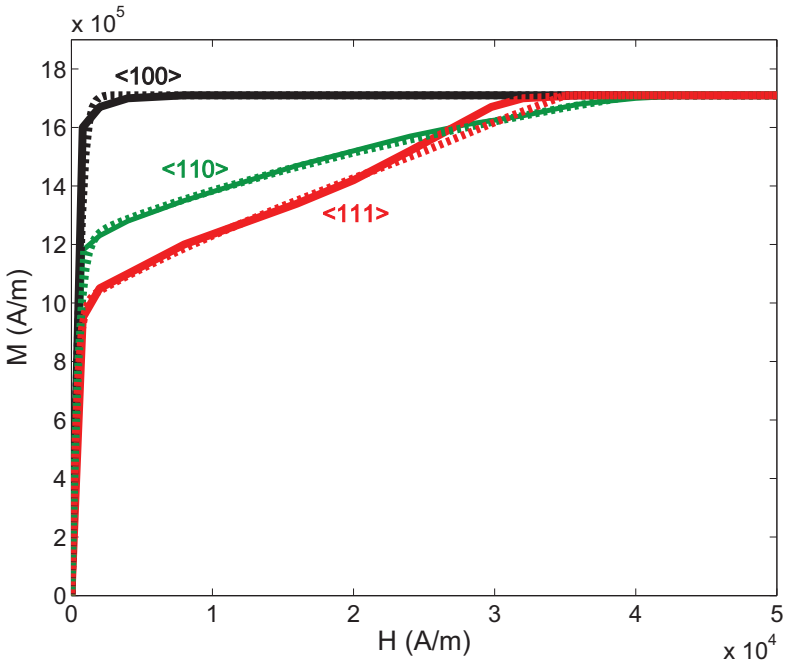

Figure 2.2: Magnetization curves of pure Iron single crystal. Experimental data (line, from [Webster, 1925]) and numerical results (dashed lines).

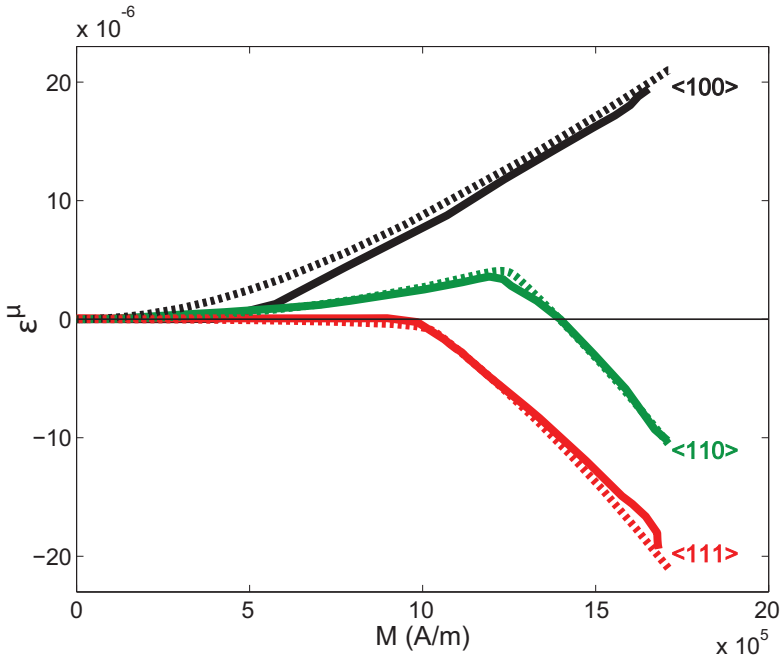

Figure 2.3: Magnetostrictive curves of pure Iron single crystal. Experimental data (line, from [Webster, 1925]) and numerical results (dashed lines).

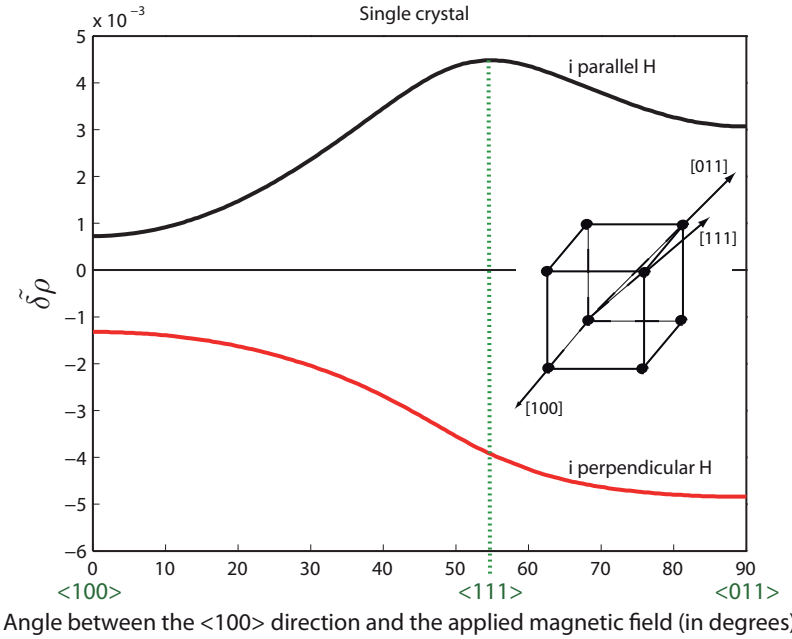

Figure 2.4: Change in resistivity as a function of the angle between the $\langle 100 \rangle$ direction and the applied magnetic field ($10^5 A/m$) in the $\{011\}$ crystallographic plane - pure Iron single crystal in parallel (parallel magnetic field and electrical current) and perpendicular (perpendicular magnetic field and electrical current) configurations.

2.5 Conclusion

In this chapter a microscopic magneto-elastic model has been presented. It is based on a description of the magneto-mechanical coupling at different scales (domain, single crystal) [Daniel and Galopin, 2008, Daniel et al., 2008]. This model allows us determining in a statistical way the domain configuration, introducing the volume fraction f_α of domains α as an internal variable. A phenomenological law for AMR effect has then been used at the domain scale. Finally a homogenization step has been used to retrieve the overall response of the single crystal (magnetization of the single crystal $\mathbf{M}_g$, magnetostriction strain $\boldsymbol{\varepsilon}_g^{\boldsymbol{\mu}}$ and the variation of resistivity $\delta\rho_g$) depending on the local values of the response at the domain scale.

Very good agreement is found between experimental and numerical results, both concerning the magnetization and the magnetostriction for data on Iron single crystal. The model also can predict the variation of the resistivity of single crystals. It has been shown that the change in resistivity can vary up to several hundred percent depending on the orientation of the magnetic field with respect to the crystal orientation. These data are validated in Chapter 3., where the same model will be applied for a grain embedded in a polycrystal.

Chapter 3

Polycrystal behavior

Contents

3.1 Macroscopic model

In the case of polycrystalline media, strain, stress, magnetization and magnetic field are not homogeneous within the material. The local behavior (at the grain scale) has to be written with respect to the local loading. This local loading can be, with specific assumptions concerning the microstructure, deduced from the macroscopic loading.

The uppermost calculation scale in our model - called macroscopic scale - is the polycrystalline Representative Volume Element (RVE) which is seen as an assembly of single crystals or grains (g) with respect to a given orientation function. The crystallographic texture is known through an Orientation Data File (ODF) obtained for example from Electron Back Scattering Diffraction (EBSD) or X-ray measurements.

As the single crystal properties (detailed in Chapter 2.) are known, the objective of this chapter is to link the macroscopic response (mean magnetization $\overline{\mathbf{M}}$, magnetostriction strain $\overline{\boldsymbol{\varepsilon^{\mu}}}$ and variation of macroscopic resistivity $\tilde{\delta\rho}$) of this RVE to the macroscopic loading (external field $\overline{\mathbf{H}}$, stress $\overline{\boldsymbol{\sigma}}$ and current $\overline{\mathbf{I}}$).

3.1.1 Modeling strategy

The general idea of this micro-macro approach is to postulate a localization law, in order to calculate the local loading. The micro-model is then applied at the domains scale and the macro-level is reached through an averaging operation. Since both the local values for the stress and the magnetic field depend on the local magnetization and strain, an iterative process has to be used.

The model proposed in this chapter is based on a three-scale description (polycrystal, single crystal, magnetic domain) and follows the scheme presented in Figure 3.1.

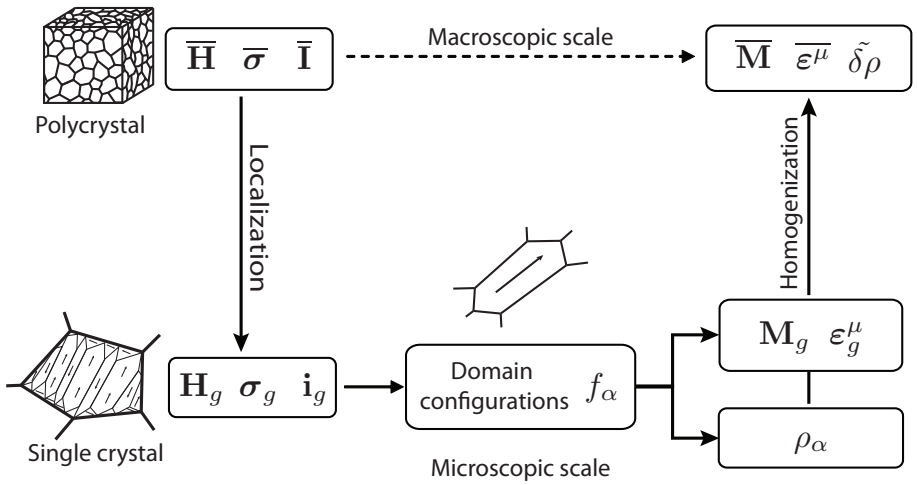

Figure 3.1: Modeling strategy

The intermediate scale - called mesoscopic scale - is the single crystal or grain, that is seen as a collection of magnetic domains (α) with given magnetization orientation ($\boldsymbol{\alpha}$). The lowest scale - called microscopic scale - is the magnetic domain, that is an area with uniform magnetostriction strain and magnetization.

The main steps of this model are divided as follows.

1. The localization steps aim at defining the local loading (magnetic field $\mathbf{H}_\alpha$, stress $\boldsymbol{\sigma}_{\boldsymbol{\alpha}}$ and current $\mathbf{i}_\alpha$) at the microscopic scale as a function of the macroscopic loading (magnetic field $\overline{\mathbf{H}}$, stress $\overline{\boldsymbol{\sigma}}$ and current $\overline{\mathbf{I}}$). The loading at the mesoscopic scale (magnetic field $\mathbf{H}_g$, stress $\boldsymbol{\sigma}_{\boldsymbol{g}}$ and current $\mathbf{i}_g$) is calculated as an intermediate step. These localization steps highly depend on the microstructure of the material.
2. The microscopic magneto-elastic model allows defining in a statistical way the domain configuration, introducing as an internal variable the volume fraction f_α of domains with orientation $\boldsymbol{\alpha}$ in a grain g. In each domain, depending on the considered orientation $\boldsymbol{\alpha}$, the magnetization $\mathbf{M}_\alpha$ and magnetostriction strain $\boldsymbol{\varepsilon}^{\boldsymbol{\mu}}_{\boldsymbol{\alpha}}$ are known.
3. The microscopic AMR model allows to defining the local resistivity (ρ_α) depending on the magnetization orientation $\boldsymbol{\alpha}$ in the considered domain.
4. The homogenization step allows retrieving the overall response of the material at the polycrystal scale (magnetization at the macroscopic scale $\overline{\mathbf{M}}$, macroscopic magnetostriction strain $\overline{\boldsymbol{\varepsilon}^{\boldsymbol{\mu}}}$ and the variation of the macroscopic resistivity $\tilde{\delta\rho}$) depending on the local values of the response at the microscopic scale.

Steps 2. and 3. are detailed in Chapter 2. Steps 1. and 4. are detailed hereafter.

3.1.2 Localization step

The simplest assumption to define the microscopic loading ($\mathbf{H}_\alpha$, $\boldsymbol{\sigma}_{\boldsymbol{\alpha}}$, $\mathbf{i}_\alpha$) as a function of the macroscopic loading ($\overline{\mathbf{H}}$, $\overline{\boldsymbol{\sigma}}$, $\overline{\mathbf{I}}$) would be to consider uniform field hypotheses. Under such hypotheses the localization rules are very simple:

$$\mathbf{H}_\alpha = \overline{\mathbf{H}} \tag{3.1}$$

$$\boldsymbol{\sigma}_{\boldsymbol{\alpha}} = \overline{\boldsymbol{\sigma}} \tag{3.2}$$

and

$$\mathbf{i}_\alpha = \overline{\mathbf{I}} \tag{3.3}$$

However due to the heterogeneity of the materials, these assumptions are often inappropriate.

Macro-meso scale transition

In a polycrystal the susceptibility from one grain to another can vary very significantly. For instance in pure iron the permeability of a grain can vary up to 70% at 400 A/m or 60% at 2000 A/m depending on its relative orientation with respect to the magnetic field [Daniel and Corcolle, 2007]. This heterogeneity results in a significant heterogeneity of the magnetic field within the material. The self-consistent localization scheme is known to provide satisfying estimates for polycrystalline media [Bornert et al., 2001]. The macro-meso localization rule is written as follows:

$$\mathbf{H}_g = \overline{\mathbf{H}} + \frac{1}{3+2\chi^m}(\overline{\mathbf{M}} - \mathbf{M}_g) \tag{3.4}$$

$\overline{\mathbf{M}}$ and $\mathbf{M}_g$ are the magnetization respectively at the macroscopic and mesoscopic scales. In the case of self-consistent hypothesis χ^m is the overall magnetic susceptibility of the material.

The elastic response to a given mechanical loading also significantly differs from one grain to another in a polycrystal. As an example in the case of pure Iron the Young's modulus can vary up to 115% depending on the crystallographic orientation (see the elastic constants in Table 2.1). Here again, the self-consistent localization scheme is used [Hill, 1965]. Under such hypotheses, the macro-meso localization rule can be written in the following form [Daniel et al., 2008]:

$$\boldsymbol{\sigma_g} = \mathcal{B}_\sigma : \overline{\boldsymbol{\sigma}} + \mathcal{L}^{\text{inc}} : (\overline{\boldsymbol{\varepsilon^\mu}} - \boldsymbol{\varepsilon_g^\mu}) \tag{3.5}$$

$\overline{\boldsymbol{\varepsilon^\mu}}$ and $\boldsymbol{\varepsilon_g^\mu}$ are the magnetostriction strain respectively at the macroscopic and mesoscopic scale. $\mathcal{B}_\sigma$ denotes the so-called stress concentration tensor and $\mathcal{L}^{\text{inc}}$ is a tensor accounting for elastic incompatibilities due to magnetostriction. The way to calculate these fourth order tensor can be found in [Daniel et al., 2008] and is briefly re-called hereafter.

$\mathcal{B}_\sigma$ is defined by Equation (3.6) that introduces the single crystal stiffness tensor $\mathcal{C}_g$, the polycrystal effective stiffness tensor $\tilde{\mathcal{C}}$ and the strain localization tensor $\mathcal{A}_\sigma$.

$$\mathcal{B}_\sigma = \mathcal{C}_g : \mathcal{A}_\sigma : \tilde{\mathcal{C}}^{-1} \tag{3.6}$$

$\mathcal{A}_\sigma$ is defined by Equation (3.7) where $\mathcal{C}^*$ is the so-called Hill constraint tensor [Hill, 1965] that can be obtained from the Eshelby tensor $\mathcal{S}^E$ according to Equation (3.8), $\mathcal{I}$ being the fourth order identity tensor.

$$\mathcal{A}_\sigma = (\mathcal{C}_g + \mathcal{C}^*)^{-1} : (\tilde{\mathcal{C}} + \mathcal{C}^*) \tag{3.7}$$

$$\mathcal{C}^* = \tilde{\mathcal{C}} : \left(\mathcal{S}^{E^{-1}} - \mathcal{I}\right) \tag{3.8}$$

$\mathcal{L}^{\text{inc}}$ is defined by Equation (3.9).

$$\mathcal{L}^{\text{inc}} = \mathcal{C}_g : (\mathcal{C}_g + \mathcal{C}^*)^{-1} : \mathcal{C}^* \tag{3.9}$$

In the case of the electrical resistivity, and as will be shown in the following, the heterogeneity is weak. Depending on the orientation of the single crystal, the electrical resistivity does not vary more than a few percent. This is why we apply uniform electric current conditions.

$$\mathbf{i}_g = \overline{\mathbf{I}} \tag{3.10}$$

3.1.3 Calculation of the effective properties

The macroscopic magnetization and strain are obtained through an averaging operation over the whole volume V of the RVE.

$$\overline{\mathbf{M}} = \langle \mathbf{M} \rangle_V = \langle \mathbf{M}_g \rangle_V \tag{3.11}$$

$$\overline{\boldsymbol{\varepsilon}} = \langle \boldsymbol{\varepsilon} \rangle_V = \langle \boldsymbol{\varepsilon}^e + \boldsymbol{\varepsilon}^{\boldsymbol{\mu}} \rangle_V = \langle \boldsymbol{\varepsilon}_{\boldsymbol{g}} \rangle_V \tag{3.12}$$

If needed, the macroscopic magnetostriction strain can be obtained using the following relation [Daniel et al., 2008]:

$$\overline{\boldsymbol{\varepsilon}^{\boldsymbol{\mu}}} = \left\langle {}^t\mathcal{B}_\sigma : \boldsymbol{\varepsilon}^{\boldsymbol{\mu}} \right\rangle_V = \left\langle {}^t\mathcal{B}_\sigma : \boldsymbol{\varepsilon}_{\boldsymbol{g}}^{\boldsymbol{\mu}} \right\rangle_V \tag{3.13}$$

Since the local electric conductivity ς_α in a domain is known ($\varsigma_\alpha = 1/\rho_\alpha$), the effective macroscopic conductivity $\tilde{\varsigma}$ can be obtained through a self-consistent approach, applying the classical Bruggeman relation [Bruggeman, 1935, Stroud, 1975, Daniel and Corcolle, 2007]. $\tilde{\varsigma}$ is solution of Equation (3.14) that can be solved easily using a fixed point method.

$$\tilde{\varsigma} = \frac{\left\langle \dfrac{\varsigma_\alpha}{2\tilde{\varsigma} + \varsigma_\alpha} \right\rangle_V}{\left\langle \dfrac{1}{2\tilde{\varsigma} + \varsigma_\alpha} \right\rangle_V} \tag{3.14}$$

where the operation $\langle \ . \ \rangle_V$ is an averaging operation over the whole volume of the RVE. The effective resistivity $\tilde{\rho}$ is deduced from the effective conductivity ($\tilde{\rho} = 1/\tilde{\varsigma}$). In the following the variation of the macroscopic resistivity $\tilde{\delta\rho}$ (Equation (3.15)) will be plotted. It can be noticed from Equations (2.17) and (2.23) that $\tilde{\delta\rho}$ does not depend on the value of ρ_0.

$$\tilde{\delta\rho} = \frac{\tilde{\rho} - \rho_0}{\rho_0} \tag{3.15}$$

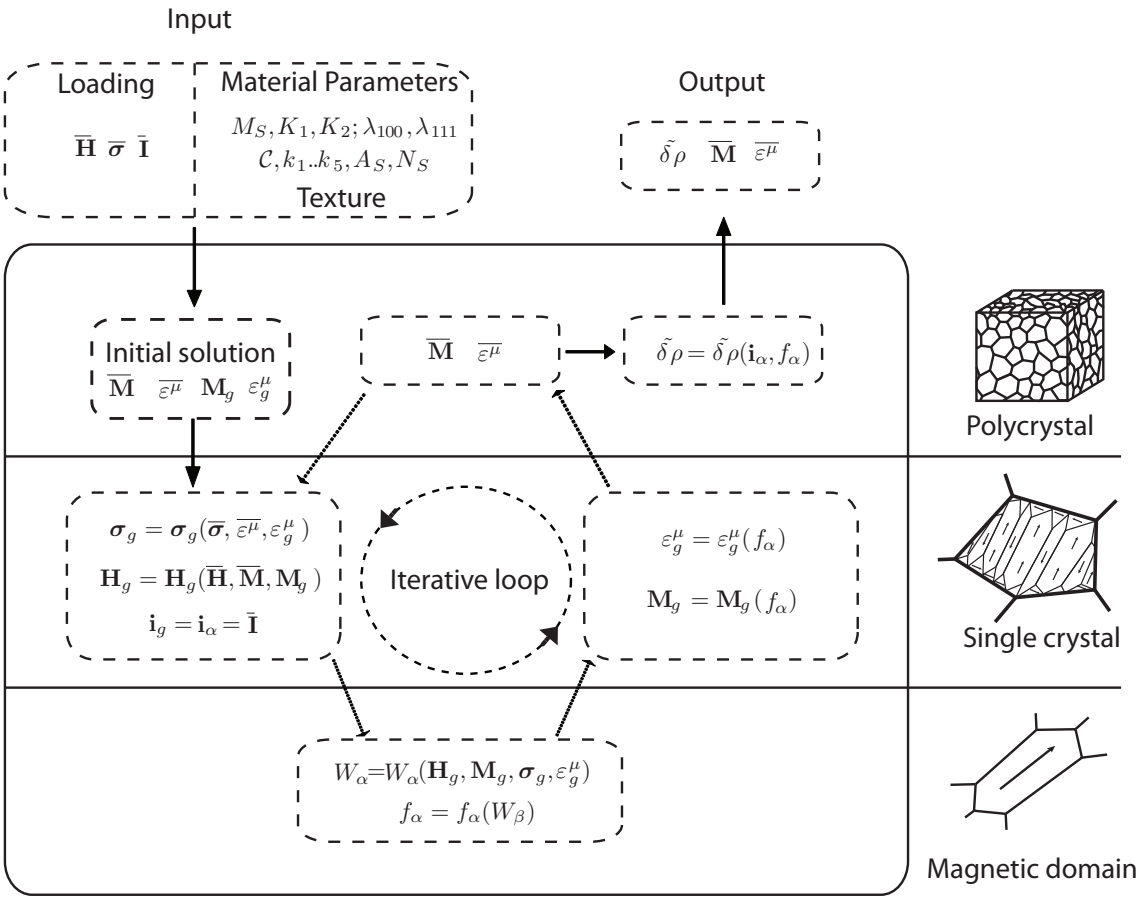

Figure 3.2: Calculation algorithm

3.1.4 Calculation algorithm and model parameters

The generic algorithm for the self-consistent calculation of the AMR response of polycrystalline materials is given in Fig. 3.2.

The input data consist of the applied loading (magnetic field $\overline{\mathbf{H}}$, stress $\overline{\boldsymbol{\sigma}}$ and current $\bar{\mathbf{I}}$) and material parameters. Most of the material parameters are the classical single crystal constants except two adjustment parameters A_s and N_s. The parameter A_s can be readily identified from the initial slope of the anhysteretic magnetization curve (see in Section 2.3.1). The parameter N_s is only used when dealing with thin film structures. It is related to the ratio between the grain size and the film thickness. The determination of the value of N_s is discussed in Section 4.2.1. The crystallographic texture of the material is also needed under the form of an orientation distribution function, for example measured from Electron Back Scattering Diffraction (EBSD).

The calculation being self-consistent, an initial starting point is needed for the macroscopic magnetization and magnetostriction strain. An initial guess is also needed for magnetization and magnetostriction at the grain scale. A uniform strain and magnetization hypothesis is usually chosen at this stage (Eqs. (3.1), (3.2) and

(3.3)). It must be noticed that this initial choice does not affect the final solution but it has an impact on the convergence speed of the process.

From this data, the localization process is started to define the local loading ($\mathbf{H}_g$, $\boldsymbol{\sigma_g}$ and $\mathbf{i}_g$, Eqs. (3.4), (3.5) and (3.10)). The potential energy for each domain family is then computed (Eq. (2.1)), allowing the determination of the volume fractions for each domain family (Eq. (2.18)).

The material response is then computed at the grain scale (Eqs. (2.19) and (2.20)) and at the macroscopic scale (Eqs. (3.11) and (3.12)).

The process is performed iteratively until the convergence on $\overline{\mathbf{M}}$ and $\overline{\boldsymbol{\varepsilon}^{\mu}}$ is reached. The macroscopic resistivity is then obtained with Eq. (3.14).

The material constants of Iron, Nickel and a Permalloy ($Fe_{11}Ni_{89}$) single crystal can be found in the literature. The parameters used for the simulations presented hereafter are defined in Table 2.1, 2.2, 3.1 and 3.2 [1].

Coefficient	M_S	K_1, K_2	λ_{100}, λ_{111}	A_s	C_{11}, C_{12}, C_{44}
Unit	A/m	kJ/m^3	-	m^3/J	GPa
Nickel	4.91x10^5	-5.7, -2.3	-45.9, -24.3 (x10^{-6})	0.016	250, 160, 118
$Fe_{11}Ni_{89}$	7.50x10^5	-1, -2	-15, -10 (x10^{-6})	0.032	243, 148, 122

Table 3.1: Physical constants used for the modeling [Bozorth, 1993, Hausch and Warlimont, 1973, Kanrar and Ghosh, 1983]

Coefficient	k_1	k_2	k_3	k_4	k_5
Nickel	0.0654	0.0266	-0.032	-0.054	0.020
$Fe_{15}Ni_{85}$	0.0518	0.0478	-0.0243	-0.0139	0.0259

Table 3.2: Constants of Döring expression [Bozorth, 1993, Berger and Friedberg, 1968]

The distribution function for crystal orientation (ODF) in the case of isotropic polycrystals has been obtained by simulation. The first possible way to describe the ODF is to choose of a random orientation for each grain, but this choice leads to a great number of grain orientations to reach a reasonable accuracy on the simulated results for instance on the magnetostriction strain [Daniel et al., 2008]. Another choice, already used by [Buiron, N. et al., 1999], is to build a regular zoning in the space of possible orientations. In this case each crystal is defined by three Euler angles (φ_1, ψ, φ_2) following Bunge notation. Each angle takes values regularly distributed in their variation domain. The number of values taken in each space domain gives the precision of the texture isotropy. A good choice, ensuring reasonable computation time and satisfying accuracy, is made of 546 different orientations. The corresponding pole figures are given in Figure 3.3.

1. The accurate data of the constants of Döring expression of $Fe_{11}Ni_{89}$ was not found. The constants of the $Fe_{15}Ni_{85}$ permalloy were used instead.

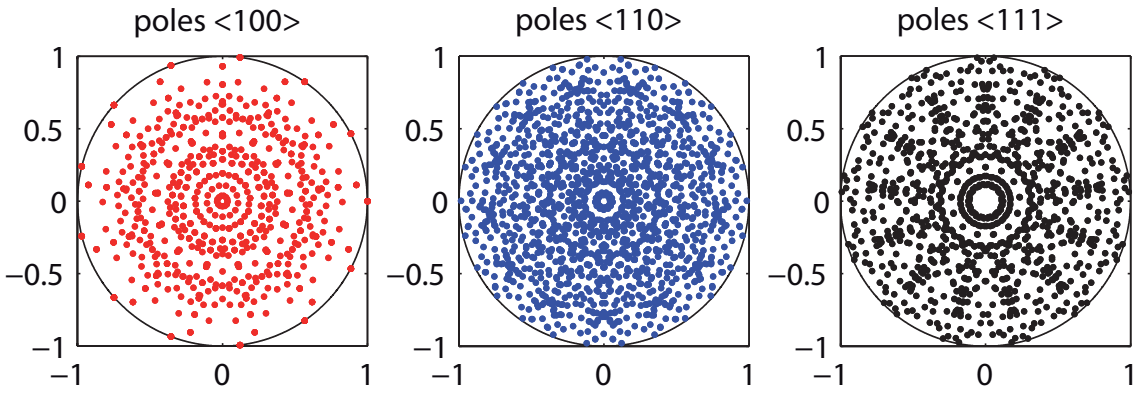

Figure 3.3: Pole figures for an isotropic polycrystal obtained from a regular zoning of the crystallographic space

3.2 Prediction of the AMR effect on ferromagnetic polycrystals

The multiscale approach can be used to predict magnetization and magnetostriction curves as a function of magnetic field for different levels of stress. The results already shown in previous publications [Daniel et al., 2008, Daniel and Galopin, 2008, Hubert and Daniel, 2008]. The novelty of the approach here is to describe magnetoresistance.

The similarity in the phenomena of magnetostriction and magnetoresistance has been known for a long time. This similarity is linked to the strong dependence of both phenomena on the local magnetization state and thus on the magnetic domain configuration. Our model is based on a micro-macro approach of the magneto-elastic behavior of the materials which can give the magnetostriction ($\lambda(H)$) and the magnetoresistive curves ($\delta\rho(H)$). From these results the relation between the change of resistivity and the magnetostriction strain can be easily obtained.

It is illustrated in the case of isotropic Nickel and pure Iron polycrystals without external stress in Figure 3.4 and 3.5. The experimental results are taken from the literature [Bozorth, 1993]. The figures plot the effective magnetostriction strain as a function of the effective change in resistivity for parallel configuration (magnetic field and electrical current are parallel). Experimental observations show that magnetostriction strain first increases with magnetoresistance and then decreases in the case of Iron, and magnetostriction decreases continuously in the case of Nickel. The different behavior of these materials results from the different sign in their material constants (magnetostriction and Döring expression).

The experimental curve is accurately predicted by the model in the case of Nickel. The experimental curve for Iron is qualitatively predicted, but quantitatively overestimated. It is shown by the dot plot in Figure 3.5 that a macroscopic tension of amplitude 25 MPa applied in the direction of the magnetic field provides a numerical

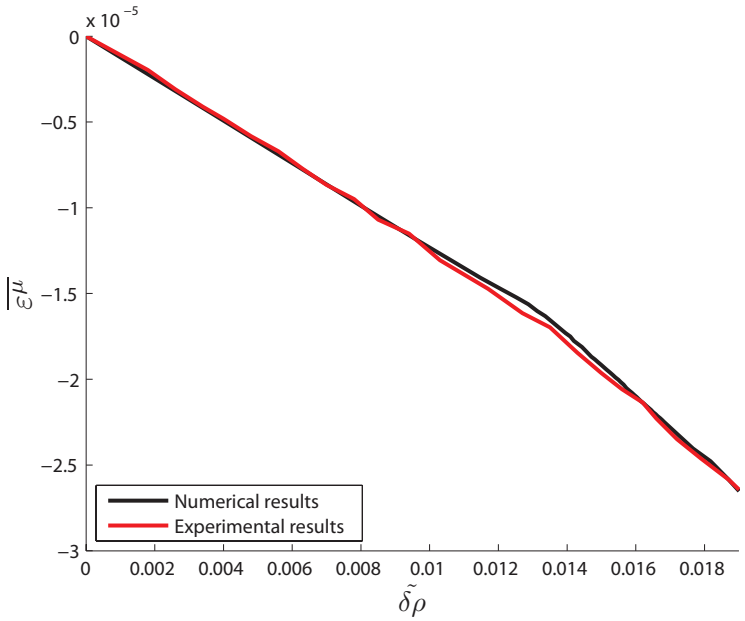

Figure 3.4: Magnetostriction strain of Nickel polycrystal as a function of the change of resistivity (current and applied magnetic field are parallel) - experimental data [Bozorth, 1993] and obtained numerical results

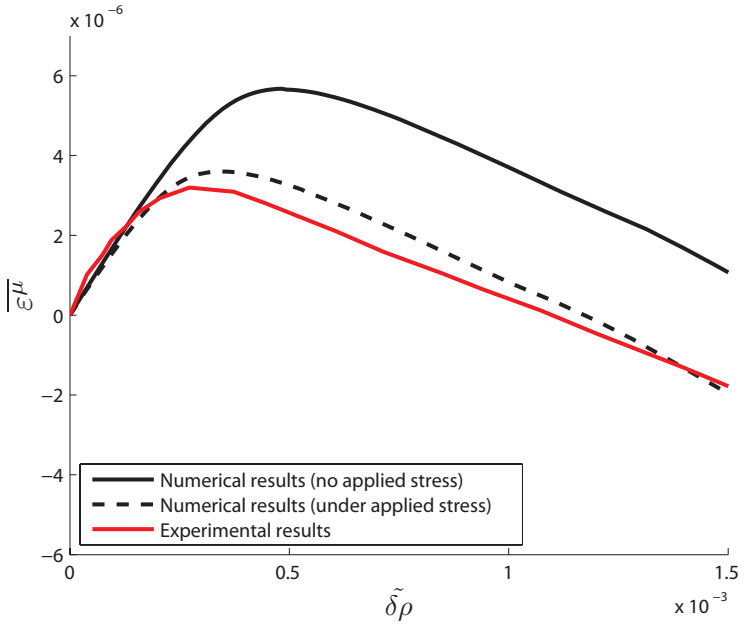

Figure 3.5: Magnetostriction strain of Iron polycrystal as a function of the change of resistivity (current and applied magnetic field are parallel) - experimental data [Bozorth, 1993] and obtained numerical results (dashed line: under 25 MPa tension applied in the direction of magnetic field)

result closer to the experimental observation. This point shows that a residual stress in the material could explain the discrepancies in the case of the Iron specimen.

3.2.1 Effect of stress on the magnetoresistive behavior

In order to study the effect of an applied uniaxial stress on the magnetoresistance, modeling results were compared to experimental results [Bozorth, 1993] on a Permalloy ($Fe_{11}Ni_{89}$) polycrystal. In this case the $\tilde{\delta\rho}(M)$ curves were calculated from the combination of $M(H)$ and $\tilde{\delta\rho}(H)$ modeling results. The results are first plotted in absence of stress (Fig. 3.6) and show a good agreement between numerical results and literature data.

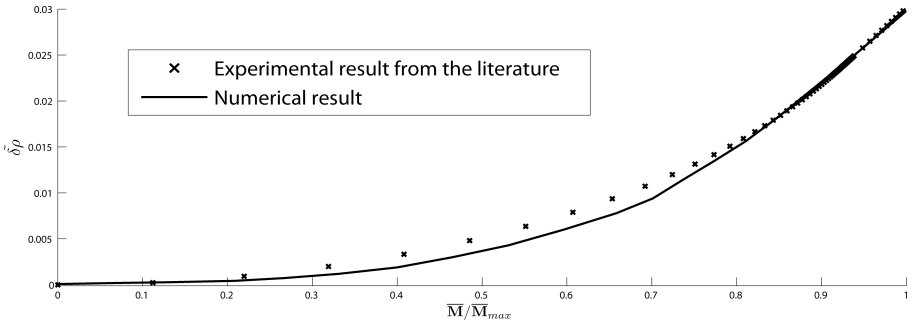

Figure 3.6: Change of resistivity (current and applied magnetic field are parallel) with change of normalized magnetization of a Permalloy polycrystal ($Fe_{11}Ni_{89}$) without applied stress - obtained numerical results (line) and experimental data [Bozorth, 1993] (dots)

This permalloy has negative magnetostriction so that tension stress orients the domains perpendicularly to the direction of tension and this effect decreases the initial resistivity. The comparison between numerical and experimental results (Figure 3.7) gives very satisfying agreement. It shows the nonlinear stress-dependence as well. The stress decreases the initial resistivity and increases the slope of the curves which is an important observation for sensor applications (higher sensitivity at low field measurement).

3.2.2 Effect of crystallographic texture

The mechanical and magnetic properties of a polycrystalline material are highly dependent on the distribution of grain orientations - called crystallographic texture. As the magnetoresistance in a single crystal has been found strongly anisotropic (Fig 2.4), it is important to investigate the effect of crystallographic texture on AMR in polycrystalline samples.

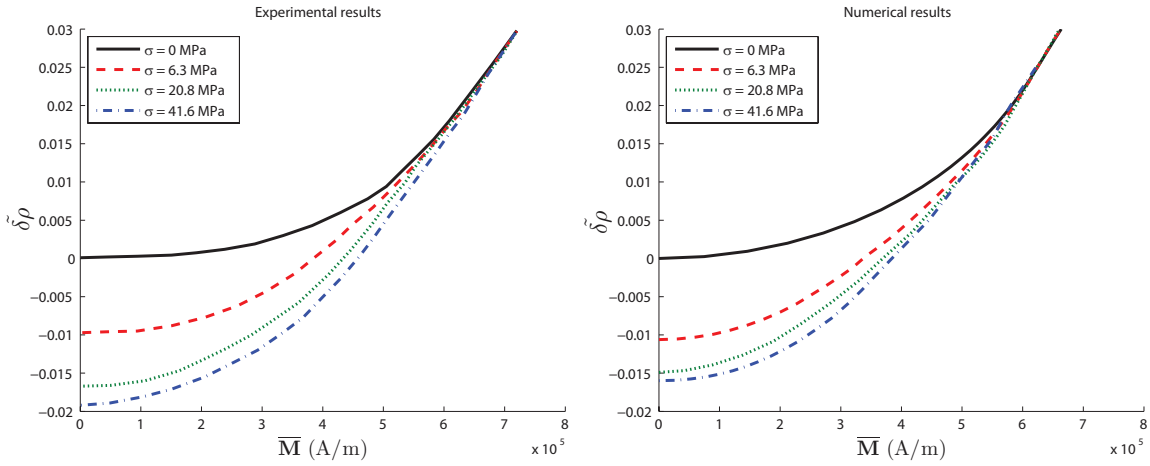

Figure 3.7: Change of resistivity (current and applied magnetic field are parallel) with change of magnetization of Permalloy polycrystals ($Fe_{11}Ni_{89}$), effect of the level of applied uniaxial stress (compression) - obtained numerical results (left) and experimental data [Bozorth, 1993] (right)

Investigation on simulated textures

As a first step, strongly textured specimens have been investigated. The ODF has been determined using simulation on a Cube, a Goss and a Fiber texture. Corresponding pole figures are presented in Fig. 3.10. For each texture, three different field/current configuration have been tested. The value of AMR has been calculated as a difference in values of the resistivity changes between the following states:

- **a.** direction of the current vector is parallel to the applied magnetic field
- **b.** direction of the current vector is perpendicular to the applied magnetic field

For each texture three crystallographic planes have been investigated as follows:

- **Configuration 1**: XY observation plane
- **Configuration 2**: YZ observation plane
- **Configuration 3**: XZ observation plane

The direction of the applied magnetic field and current for each configuration are summarized in Fig. 3.9.

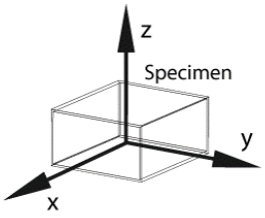

Figure 3.8: Definition of the macroscopic directions

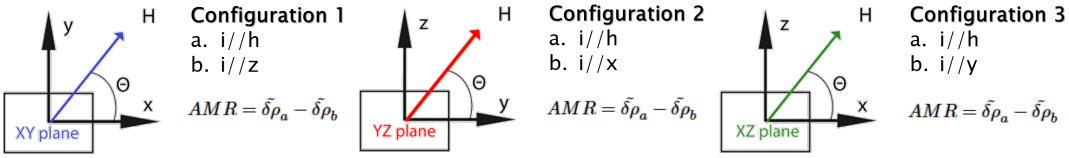

Figure 3.9: Simulation configurations

The simulation results are shown in Fig. 3.10 using the material parameters of pure Iron, and an applied magnetic field of $10^5 A/m$. The green dotted line represents the results on the discrete isotropic texture presented in Fig. 3.3. The strong influence of crystallographic texture on AMR effect is highlighted. In the case of cubic symmetry no difference were observed between the three configurations. In the case of Goss and Fiber texture the observation plane plays an important role.

Investigation on measured texture

In order to investigate the effect of crystallographic texture on a real AMR specimen, the crystallographic texture of an Armco sample (pure Iron), known as isotropic, has been obtained from electron back-scattered diffraction (EBSD) measurement. The corresponding pole figures are given in Fig. 3.11. It shows a weak texture compared with the calculated isotropic crystal orientation distribution used previously and showed in Fig. 3.3.

The prediction of the AMR effect for pure Iron using this latter crystallographic texture has been compared with the prediction using the isotropic orientation data file. Fig 3.12 shows the change in resistivity in the parallel current/applied magnetic field configuration as a function of current orientation in the polycrystal. In the case of Armco specimen two planes (XY and YZ) have been investigated.

It is shown that even for this very weakly textured material the magnetoresistance can vary up to 10% depending on the orientation of the solicitation (parallel configuration). The magnetoresistance is confirmed to be strongly dependent on crystallographic texture.

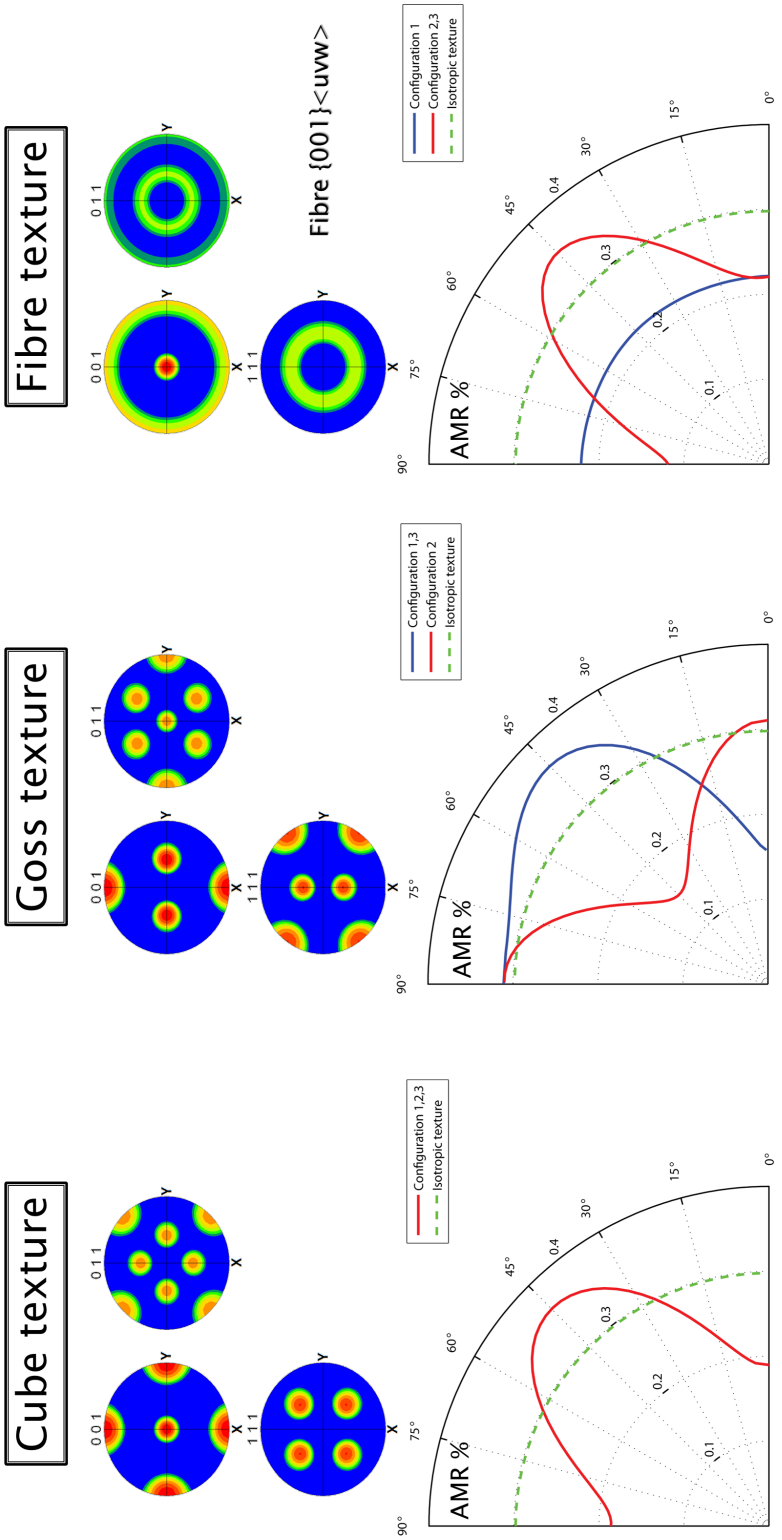

Figure 3.10: Calculated AMR values using different crystallographic texture and corresponding pole figures

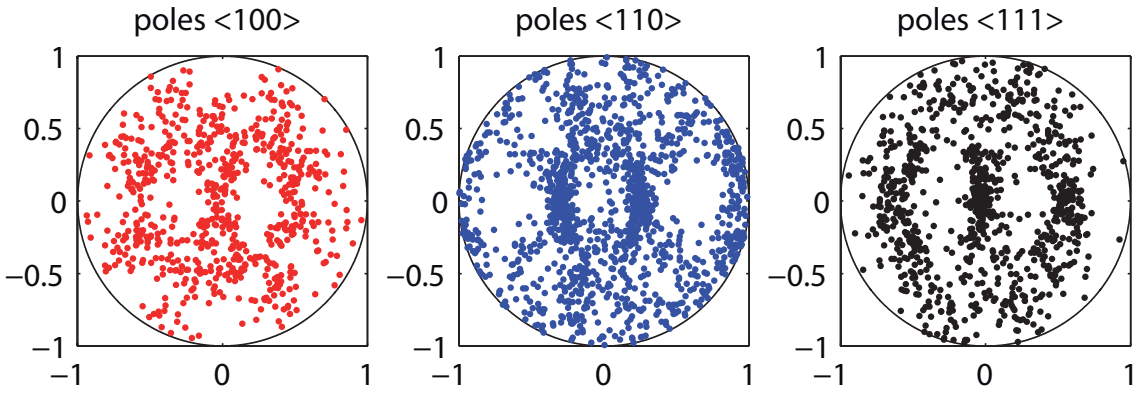

Figure 3.11: Pole figures of an Armco steel obtained from EBSD measurement.

3.3 Conclusion

In this Chapter a micro-macro model for the magnetoresistive behavior of polycristalline materials has been presented. This model includes the effect of stress on anisotropic magnetoresistance. It is based on a description of the magneto-mechanical coupling at several scales (domain, single crystal, polycrystal). The magnetic, magnetoelastic and magnetoresistive properties of Iron, Nickel and a Permalloy ($Fe_{11}Ni_{89}$) polycrystal have been calculated using a simulated isotropic distribution function for crystallographic orientations. Numerical results have been compared with experimental results from the literature with very satisfying agreement. This model enables us also to investigate the effect of crystallographic texture on AMR effect. The strong influence of crystallographic textures on the variation of resistivity of the specimen has been showed. the model could also be used to investigate the effect of stress, and notably multiaxial stress, on magnetoresistance. The model has been used so far to describe magnetoresistive effects from a material perspective, and considering bulk samples. In practice, the effect is used mostly in the design of magnetic field sensors which are usually thin film structures. In the next section, the modeling approach is extended so as to simulate the behavior of typical AMR sensors.

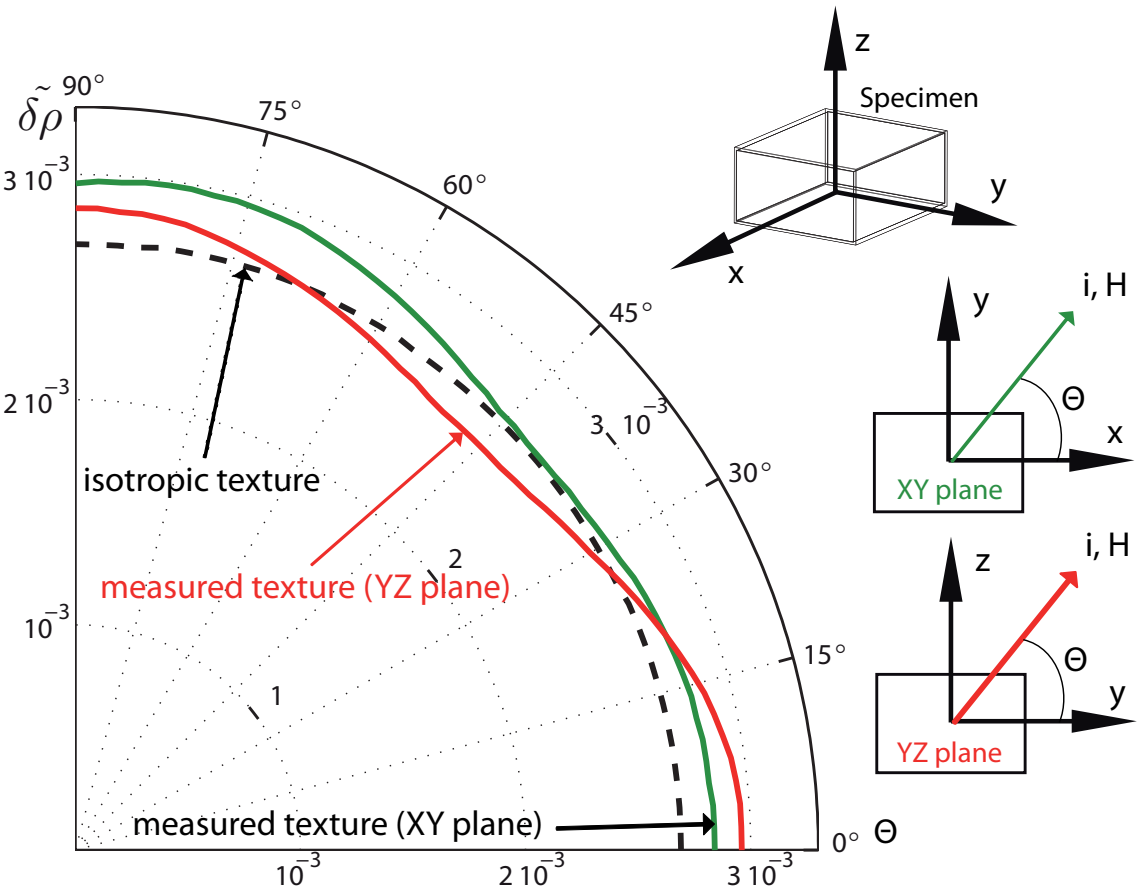

Figure 3.12: Change in resistivity (current and applied magnetic field are parallel) with change in the orientation of the applied magnetic field (10^5 Am^{-1}) for pure Iron polycrystal using an isotropic texture (dotted line) and texture data from EBSD measurement in different planes (lines).

Chapter 4

Modeling of thin film AMR sensor properties

Contents

AMR sensors are among the most widely deployed magnetic field sensors. In contrast to other technologies it has a simple structure and a low production cost. In this Chapter the previously presented multiscale modeling strategy is implemented to describe the performance of these sensors taking their specific features into account. The prediction of the behavior of a typical AMR thin film sensor is studied and the results are compared to experimental measurements from the literature.

4.1 Design and contruction of AMR sensors

AMR sensors are mostly made of ferromagnetic thin films. The application of a magnetic field changes the magnetization of the film, and the corresponding change in resistivity is measured through an electronic circuit. These devices can be used as magnetic field detectors according to the *all-or-nothing* operation method. They can then be part of displacement, position or rotation speed sensors in electromechanical machines [Adelerhof and Geven, 2000, Honeywell, 2010]. AMR devices can also be used for the quantitative measurement of magnetic field. This type of AMR sensors is used in electronic compasses (measurement of Earth's magnetic field) [Vcelak et al., 2005] and for non-contact detection of electrical currents (by measuring the magnetic field created around the conductor) [Mlejnek et al., 2008].

An AMR sensor has two main parts, a magnetoresistive sensor element and a comparator circuit prepared on one chip. The sensor elements are typically made of highly textured thin permalloy films deposited on a silicon wafer and patterned as a resistive strip [Tumanski, 2001]. Thanks to the thin film structure the magnetization remains mostly in the film plane so that the film behavior is insensitive to the perpendicular component of the external field. As the electrical resistivity depends on the angle between the direction of the electrical current and the magnetization, a close-saturation magnetization state can ensure the ideal sensing properties. The permalloy film element (xy plane) is deposited in a strong magnetic field that sets the preferred orientation (macroscopic easy axis, x). It results in a strong orientation of crystallographic easy magnetic axes along the x direction. In the absence of external magnetic field the macroscopic magnetization vector is set parallel to the length of the resistor and can be set to point in either direction, left or right in the film. The component of the external magnetic field measured by the sensor will then be the y component (Fig. 4.1).

As a first step before the real field measurement, an external magnetic field can be used to align the magnetic domains in the preferred direction (reset procedure). During the measurement, a bias magnetic field (created by additional hard magnets or coils) is applied in direction x so that the magnetization aligns with the x axis. The sensor is then unidirectional : it is only sensitive to the y component of the external field. This y component tends to rotate the magnetization in the film plane which results in a detectable change in the electrical resistivity of the sensor element. Nevertheless, the x component of the external field must remain low enough to avoid a change in the sign of the original magnetization (*flipping-effect*). The bias field has an effect on the measurement range and the sensitivity of the sensor, and its

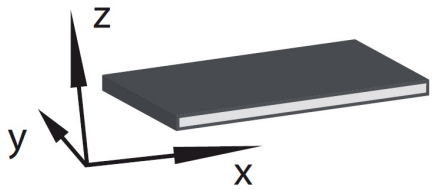

Figure 4.1: Magnetic field sensor. x: Macroscopic easy magnetization axis and y: measurement direction.

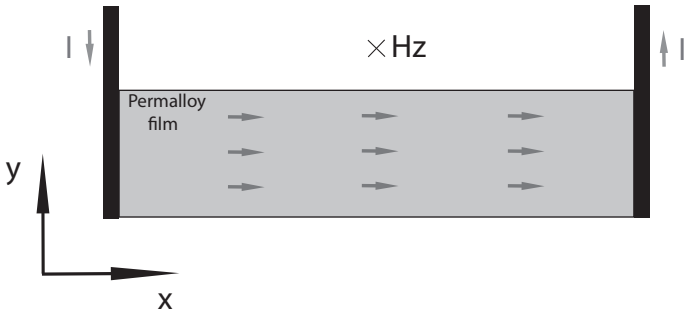

Figure 4.2: *Single-path* sensor element

value must be carefully set depending on the application.

The first generation of AMR thin film sensors was used in the read head of hard disk drives. The sensor elements had single-path structure as it is presented in Fig. 4.2. Here the electrical current (dark lines) flows in the easy direction (x) of the film. A perturbation field in the z direction (diffused magnetic field of a magnetic bit on the hard disk for example) changes the resistivity. This device has been used in the *all-or-nothing* operation method.

If a quantitative measurement of the magnetic field is necessary, then a linear response of the sensor is preferred. An electrical current oriented 45° from the x axis can ensure this linearity. These sensors use a layout technique that places low-resistance shorting bars (so called barber-pole) oriented 45° from the x axis, as presented in Fig. 4.3. The current, following the shortest path, flows from one bar to the next at a 45° angle.

In the magnetoresistive sensor elements, four of these resistors are connected in a Wheatstone bridge to compensate the temperature-dependence effects. The comparator circuit adds a linear amplification to the sensor element's signal. So finally the change in the output voltage of the sensor is proportional to the change in resistivity of the AMR thin film. If the sensor is used in the linear range, then this change in resistivity is itself proportional to the y component of the external magnetic field.

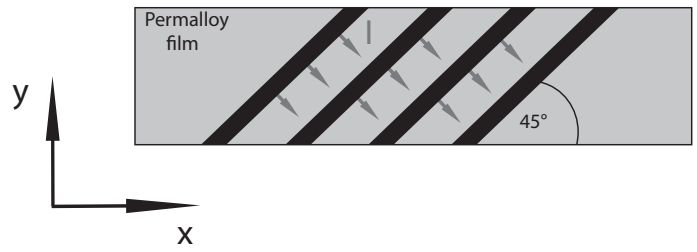

Figure 4.3: *Barber-pole* sensor element

4.2 Modeling thin film properties

The model proposed in this Chapter is an extension of the model for bulk magnetoresistive materials. The main change is the introduction of a demagnetizing surface term in the potential energy of a domain - to describe thin film behavior - and the introduction of a sharp texture representative for standard thin film AMR sensors.

4.2.1 Introduction of surface effect

Compared to the initial model presented before, an additional contribution is introduced in the potential energy of a domain. Instead of the initial equation 2.1, an additional term (W^s) will be added:

$$W^p = W^{ex} + W^K + W^\sigma + W^H + W^s \tag{4.1}$$

where W^s is the surface energy, accounting for the strong demagnetizing effects due to the small thickness of the films. Such a demagnetizing term was proposed in [Hubert and Daniel, 2008] to describe the magnetoelastic behavior of Iron-Silicon Grain Oriented sheets. For a domain family $\boldsymbol{\alpha}$ it can be written as:

$$W^s_\alpha = N_s(\boldsymbol{\alpha}.\mathbf{z})^2 \tag{4.2}$$

where z is the direction normal to the film and N_s is the demagnetizing factor.

4.2.2 Textured AMR thin film sensor properties

In the following, we investigate the properties of a $Fe_{11}Ni_{89}$ polycrystal. This type of permalloy is often used in AMR sensors due to its significant AMR effect (2%). The parameters used in the present simulation are defined in Tables 3.1 and 3.2. The adjustment parameter, N_s has been assigned the value 800 J/m^3.

In order to describe the possible orientation $\boldsymbol{\alpha}$ for the magnetization in the domain families, $\boldsymbol{\alpha}$ are described through the mesh of a unit radius sphere in space. We used a 10242 point mesh for each crystallographic orientation.

The sharp crystallographic texture of AMR thin films resulting from the fabrication process is approximated by a perfect $\{hkl\}\langle 111\rangle$ Fiber texture. Each grain

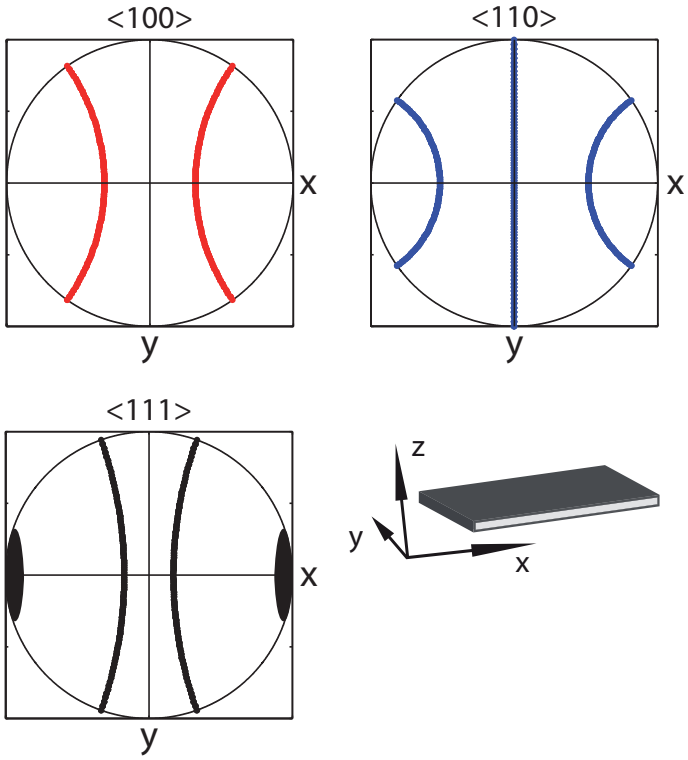

Figure 4.4: ⟨100⟩, ⟨110⟩ and ⟨111⟩ pole figures for the AMR thin film (perfect $\{hkl\}\langle 111\rangle$ Fiber texture, 180 orientations)

of the polycrystalline film is assumed to have ⟨111⟩ direction aligned along the x direction. The plane normal to this ⟨111⟩ direction is then obtained from uniformly distributed rotation around the ⟨111⟩ direction. The corresponding pole figures are given in Fig. 4.4. A distribution of 180 grain orientations has been used. The use of a thin film with such a crystallographic texture makes the x direction an easy magnetization axis (due to the negative magnetocrystalline anisotropy constants, easy axis are ⟨111⟩ directions for $Fe_{11}Ni_{89}$ single crystal).

4.3 Effect of biasing magnetic field

As it is usually done in such devices, a bias magnetic field has been applied along the x direction. Due to the barber-pole configuration, the electric current is assumed to be oriented at 45° in the plane xy (see Fig. 4.3).

The change in resistivity as a function of the applied field in the measurement direction (y) is plotted in Fig. 4.5 for several bias fields (applied in the x direction). This result can be compared to measurements performed on a Philips commercial AMR sensor [Philips, 2000] (Fig. 4.6). The output voltage of the sensor is expected to be proportional to the change in resistivity (Fig. 4.5), the ratio depending on the specific electronic circuit used in the device.

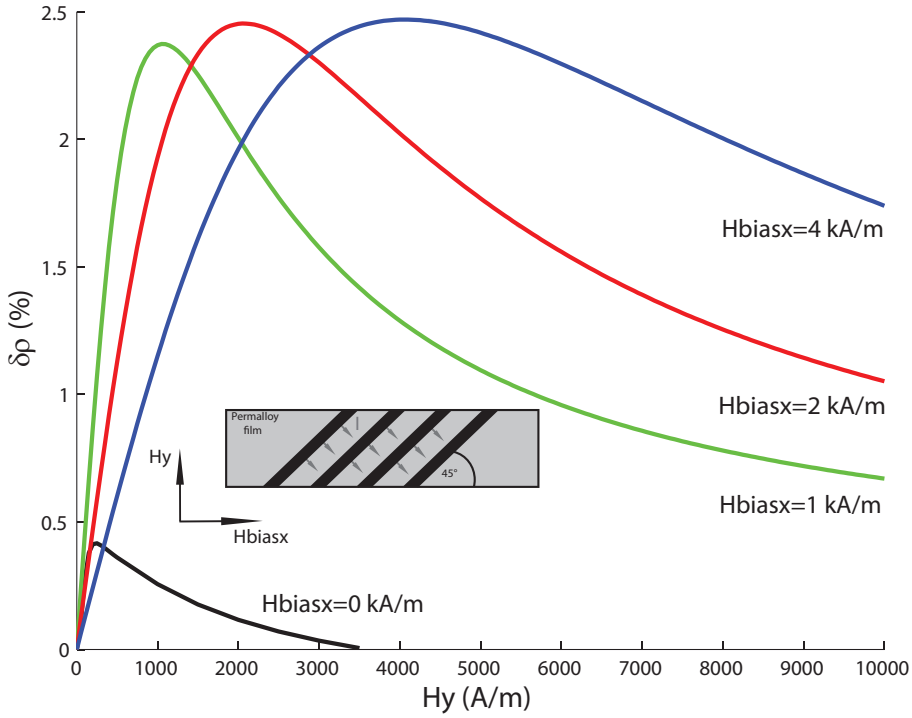

Figure 4.5: Change in resistivity versus applied field for several bias field levels - modeling results.

Although the particular composition and crystallographic texture of the permalloy used in the Philips AMR sensor are unknown, a good qualitative agreement is obtained between modeling and measurement. The increase in resistivity is approximately linear with respect to the applied field up to a point corresponding to a configuration in which a large number of magnetic domains are parallel to the electric current (leading to the maximum resistivity). The resistivity then decreases while the magnetic domains tend to align along the direction of the applied magnetic field, closer and closer to the y direction. The initial linear stage of these curves defines the range of measurement of the sensor. High bias fields provide higher variations of resistivity and wider linear range but the slope - representative for the sensitivity of the sensor - is then lower. These effects are well captured by the model. The predicted level for the change in resistivity is much lower when no bias field is applied compared to the 1 kA/m bias field. This is not in accordance with the experimental observation. It probably means that the anisotropy of the thin film has been underestimated in the calculation. An other reason can be that our model is anhysteretic and experimental results can be modified by a domain pre-orientation (biaising reset) step. However as soon as a significant bias field is applied, it dominates the behavior of the sensor, and the model gets consistent with the experimental observation. The range of linearity of the AMR thin film is also underestimated by the model. The peak value of the curves is obtained for lower values of the applied magnetic field Hy. This is related to the fact that

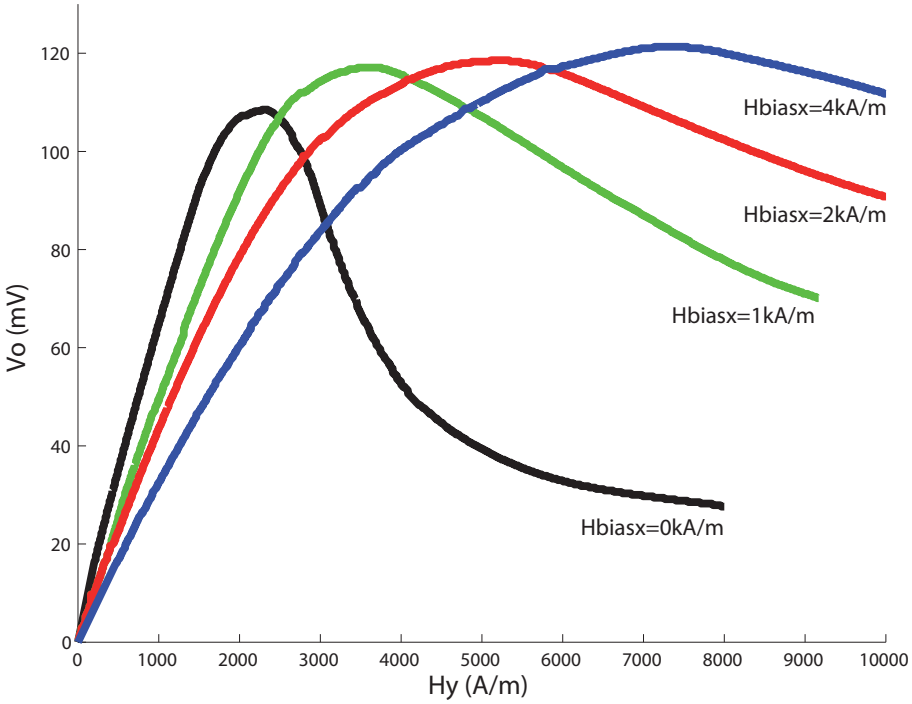

Figure 4.6: Change in output voltage versus applied field for several bias field levels - experimental results from [Philips, 2000]

hysteresis effects have not been introduced in the modeling. The predicted curves are reversible whereas the resistivity versus total magnetic field experimental curves exhibit a hysteresis cycle - not shown in Fig. 4.6. The anhysteretic representation stands inside this hysteresis cycle. This discrepancy should not affect the accuracy of the prediction of the sensitivity of the sensor, but will only allow relative comparisons concerning the range of measurement.

4.3.1 Definition of the sensitivity of an AMR sensor element

For the purpose of the discussion, we first define the sensitivity S and range of measurement H_{max} of an AMR sensor (see Fig. 4.7). The sensitivity S is defined as the slope of the linear part of the curve. The range of measurement is the applied field value from which the resistivity change becomes non linear with the applied field. The loss of linearity is defined by a switch of δH with respect to the linear response (see Fig. 4.7). In the following, we will use the arbitrary value of $\delta H = 5A/m$. The minimum detectable level of magnetic field results in a combination of the magnetic field sensitivity and the device noise (sensor + electronic conditioner). The latter on results in the combination of the sensor intrinsic noise and electronic noise which is out of the scope of this work focused on the material AMB behavoir.

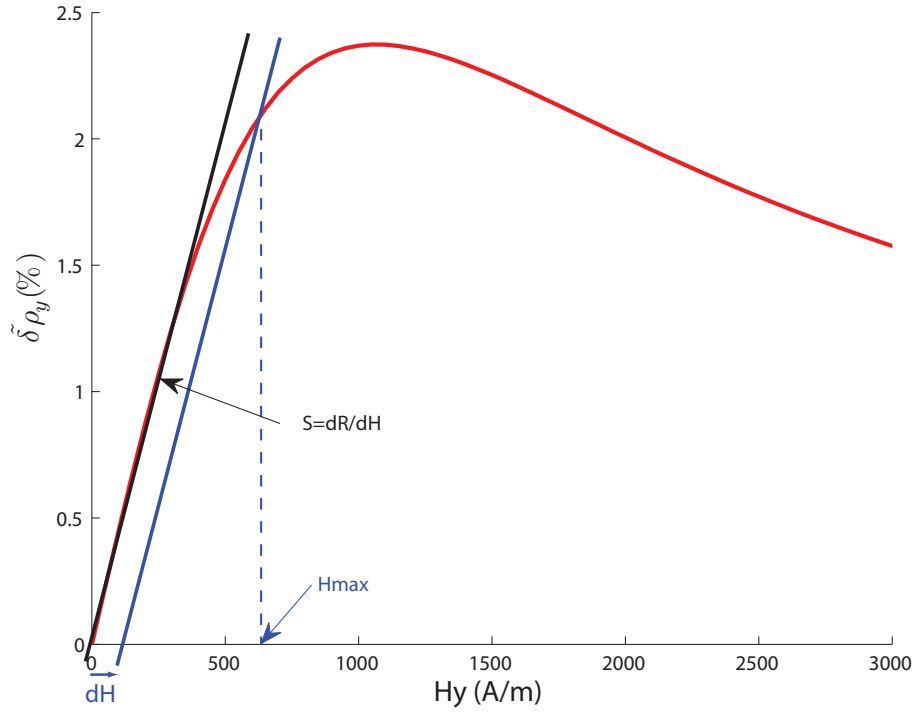

Figure 4.7: Definition of the sensitivity S and range of measurement H_{max} on a magnetoresistive curve.

As seen in Fig. 4.5, the application of a bias field significantly increases the range of measurement of the sensor. This effect is illustrated in Fig. 4.8. But the main role of the bias field (along the direction x) is to ensure that the sensor is unidirectional, meaning that it is sensitive only in the direction y of the film. This effect can be captured by the model. Fig. 4.8 shows the sensitivity of the permalloy thin film sensor in directions x and y as a function of the bias field H_{biasx}. The sensitivity in direction z has not been plotted. Due to the surface effect - resulting from the thin film geometry - the material is very hard to magnetise in direction z, the sensitivity in that direction is then very low, almost zero.

As soon as the bias field level reaches a yield value (approximately 250 A/m in that case, in accordance with standard bias field levels in AMR sensors), the sensitivity along direction x vanishes. This is due to the saturation of the material with a magnetization along direction x. On the other hand, the sensitivity in the direction y first increases with the bias field and then decreases, so that an optimal value for the bias field can be obtained. In the case illustrated in Fig. 4.8, a minimum bias field of 250 A/m is required but the intensity of the bias field can be adjusted depending on the desired compromise between sensitivity and range of measurement. The proposed model is then a tool to optimize this choice.

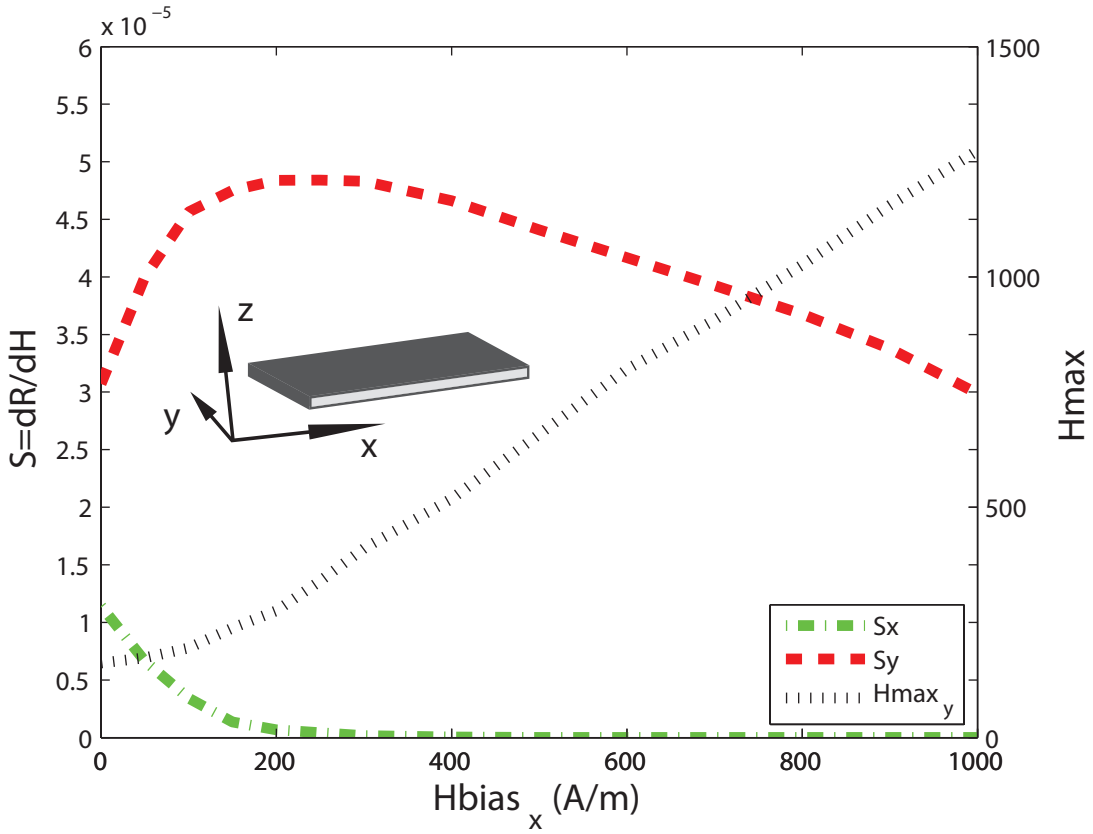

Figure 4.8: Sensor sensitivity along x-axis S_x and y-axis S_y, and maximum measurement range H_{maxy} as a function of the bias field applied in the x direction.

4.4 Influence of the film thickness

The influence of the film thickness w can also be investigated through the variation of the parameter N_s. For a given grain size of the material, N_s is inversely proportional to the film thickness [Hubert and Daniel, 2008]. In the case of the sensor configuration studied above with a strong in plane ⟨111⟩ Fiber and an in-plane magnetic field, the role of the thickness is weak since the magnetization spontaneously remains in-plane. On the other hand, if the magnetic field is normal to the thin film plane, then the thickness plays a significant role. To study this role, we focus now on a *single-path* AMR sensor.

The influence of the film thickness on the sensing properties of single-path AMR sensors has been studied experimentally by Tumanski [Tumanski, 2001]. The structure of this type of sensors has been previously presented (Fig. 4.2). The main difference from the *barber-pole* sensors is the direction of the current as it aligns here in the direction of the macroscopic easy axis, x, in the film plane. The magnetic field is applied perpendicular to the film plane (z direction). Fig. 4.9 shows the modeling results compared to the experimental observations. The parameter N_s has

been fitted using the experimental curve with 50 μm thickness as a reference and the same model parameters as before. Assuming that N_s is inversely proportional to the film thickness, its values can be determined from this first fitting in order to predict the curves with 25 and 75 μm thicknesses. The comparison between numerical and experimental results gives satisfying agreement. The model can predict the influence of the film thickness on the sensing properties.

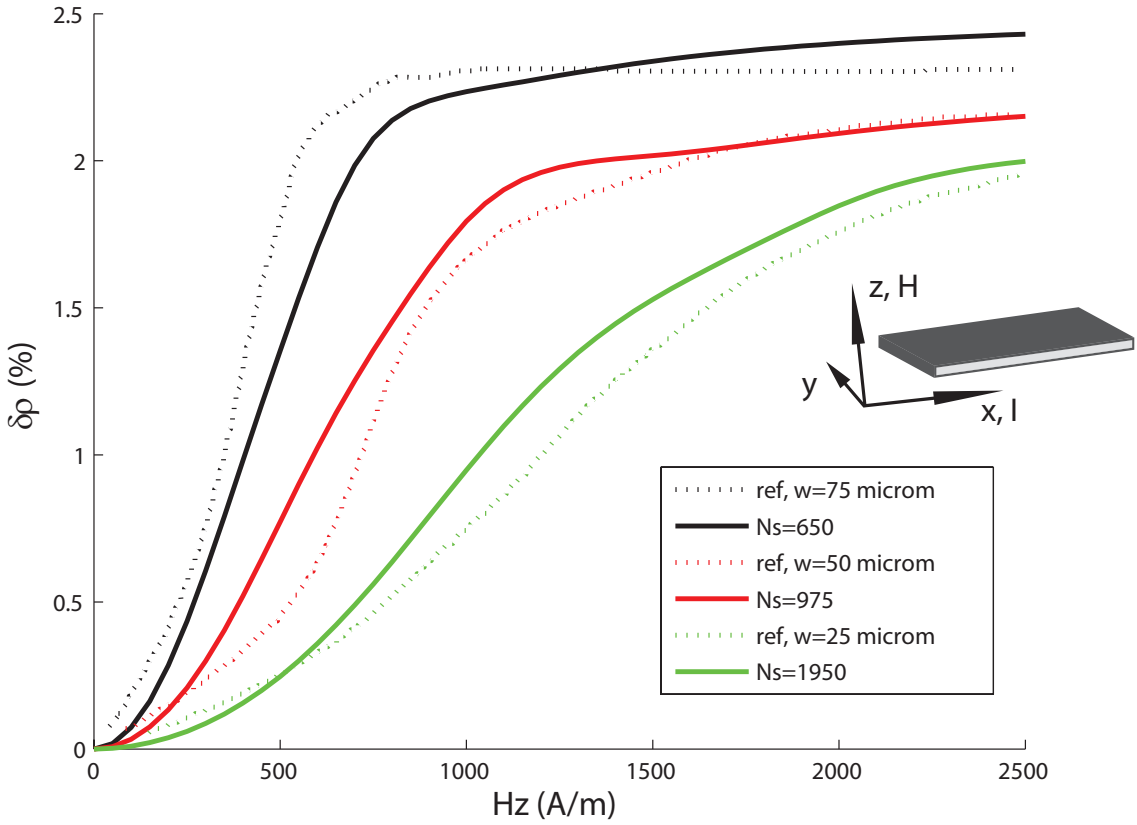

Figure 4.9: Change in resistivity versus applied field for several film thicknesses of a *single-path* AMR sensor element - modeling (lines) and experimental results [Tumanski, 2001] (dotted lines).

4.5 Effect of stress on the properties of AMR thin film sensors

Apart from the application of an external magnetic field, mechanical stress can also change magnetic domains configuration and thus the macroscopic resistivity. We propose hereafter a method to investigate from a modeling point of view the effect of stress on AMR effect and its consequences on the sensitivity of AMR thin film sensors.

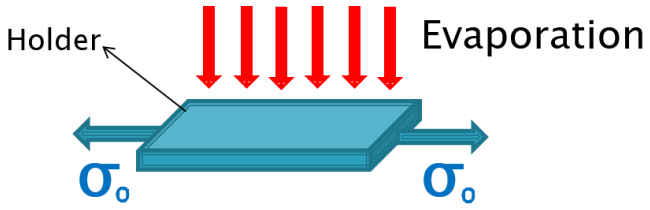

Figure 4.10: An example how to introduce residual stress during vacuum evaporation of thin film sensor

A possible way to introduce stress during the preparation of a thin film is to apply a tensile stress on the sample holder during the vacuum evaporation process (Fig. 4.10). If this applied stress is pure tension (uniform stress hypothesis), after the let-off, the residual stress in the thin film (using the orientations defined in Fig. 4.1) can be considered in the form :

$$\overline{\boldsymbol{\sigma}} = \begin{pmatrix} \sigma & 0 & 0 \\ 0 & -3\sigma & 0 \\ 0 & 0 & 0 \end{pmatrix} \tag{4.3}$$

Using this residual stress configuration, the sensitivity and the range of measurement (as defined in Fig. 4.7) of a permalloy thin film has been calculated as a function of the value of σ, using $H_{biasx} = 400A/m$. Results are shown in Fig. 4.11.

It is highlighted that this type of residual stress can significantly increase the sensitivity of the sensor (red curve). Nevertheless the measurement range (the range where the sensor response is supposed to be linear, black dotted line) decreases at the same time. As it has been shown previously, the bias field plays an important role on the sensitivity of the sensor, as a next step, the effect of the bias field has been investigated on the sensor's properties with residual stress.

An arbitrary value of σ has been chosen (σ=10 MPa) and the sensor parameters have been calculated as a function of the bias field (4.12).

Results show that a minimum value of $H_{biasx} = 200A/m$ is needed to have a high sensitivity, but in this case (compared with results obtained without applied stress in Fig. 4.8) the maximum value of sensitivity is higher. Choosing for example a lower bias field (300 A/m) the sensitivity can increase by 60% if a residual stress has been introduced. On the other hand the measurement range (H_{maxy}) decreases by 30%.

The development of the multiscale model has allowed an investigation on the promising potentialities of tailored residual stresses in AMR sensors. Proposals for the introduction of these residual stresses has been patented during the course of this work [Daniel et al., 2013]. The model is then a useful optimization tool for higher precision AMR devices.

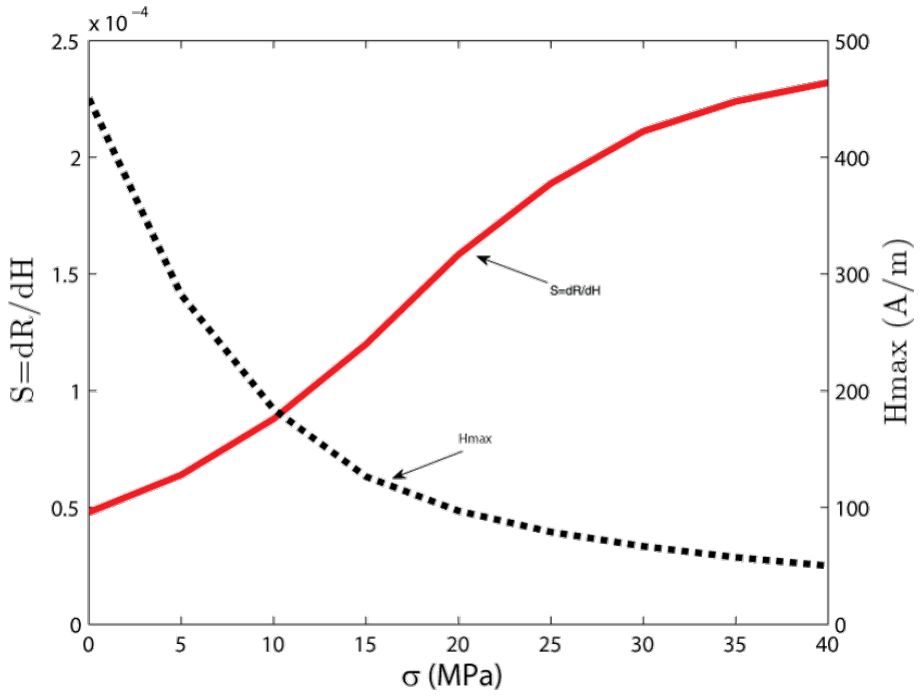

Figure 4.11: Effect of stress on the sensitivity of an AMR thin film sensor

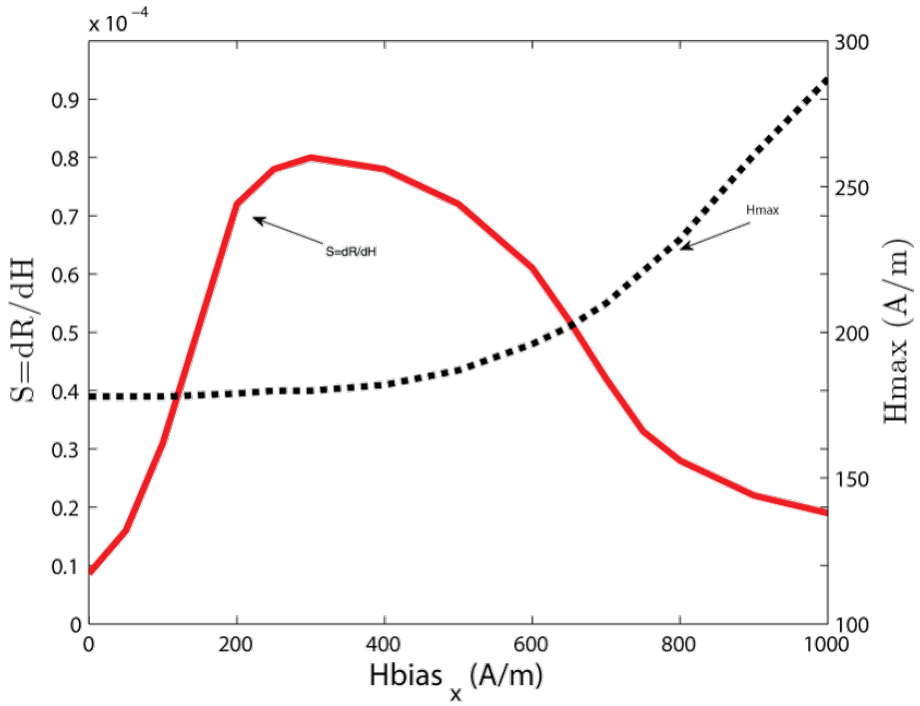

Figure 4.12: Effect of the bias field on sensor element prepared with introduced residual stress

4.6 Conclusion

In this Chapter the multiscale approach has been extended to the case of AMR thin film sensors. The thin film structure has been taken into account through a surface effect coefficient and strongly textured material has been considered. The particular architecture of AMR sensors (barber-pole configuration) has been described. The approach could also be easily extended to amorphous or nanocrystalline alloys by introducing appropriate anisotropy terms.

The model has been applied to the modeling of a polycrystalline permalloy thin film sensor. The nonlinear magnetoresistive behavior of this type of structures in 3D has been investigated. It can be used for optimization purpose to define optimal material composition, crystallographic texture, film thickness, bias field level and applied stress for specific applications. It has been shown that a well-chosen applied residual stress configuration can significantly modify the sensitivity and range of measurement of AMR sensors allowing the design of optimal precision devices.

General conclusion

In this thesis a multiscale model for anisotropic magnetoresistance has been presented. It is based on a description of the magneto-mechanical coupling at several scales (domain, single crystal, polycrystal) combined with a local model for material resistivity (Döring model). The model has been applied to single crystals and polycrystals. Satisfying results have been obtained in the description of the magnetization, magnetostriction and magneto-resistance of bulk materials. For single crystals, it has been shown that the change in resistivity can vary up to several hundred percent depending on the orientation of the magnetic field with respect to crystal orientation. For polycrystals, the model enabled the investigation of crystallographic texture effects on the AMR response. These results have been published in [Bartók et al., 2011]. Finally, the model has been extended to describe the response of AMR thin film sensors. For that purpose, the approach has been complemented with the specific features of AMR sensors such as thin film structure, barber-pole configuration and sharp crystallographic texture. The model has been applied to the modeling of a polycrystalline permalloy thin film sensor. These results have been published in [Bartók et al., 2013]. The numerical tool allowed the investigation of nonlinear magnetoresistive behavior of this type of structures in 3D. It can be used for as an optimization tool to define optimal material composition, crystallographic texture, film thickness or bias field level. Finally it was shown that stress can be used as an adjustment variable to tune AMR sensing properties for specific applications. This result has been patented and is now the object of a paper in preparation.

The main perspective of this project would be to process AMR sensors with stress-tunable properties. This step has to be based on a collaboration with research laboratories or sensor producers so has to have access to thin films processing and characterisation techniques. The combination of an analysis of the possible residual stress tensors applicable to thin films with an optimisation performed with the proposed multiscale approach could create the conditions for the emergence of a new generation of tunable magnetic field sensors.

From the modeling perspective, it would be interesting to see how hysteresis affects the properties of AMR sensors. This could be made by introducing hysteresis effects in the model along the lines recently proposed for magneto-mechanical behavior [Daniel et al., 2014]. Another interesting extension of the multiscale approach would be to consider multilayer systems so as to describe other type of sensors such as Giant Magneto-Resistive sensors.

Bibliography

[Adelerhof and Geven, 2000] Adelerhof, D. J. and Geven, W. (2000). New position detectors based on amr sensors. *Sensors and Actuators A: Physical*, 85(1-3):48 – 53.

[Baibich et al., 1988] Baibich, M. N., Broto, J. M., Fert, A., Van Dau, F. N., Petroff, F., Etienne, P., Creuzet, G., Friederich, A., and Chazelas, J. (1988). Giant magnetoresistance of (001)fe/(001)cr magnetic superlattices. *Phys. Rev. Lett.*, 61:2472–2475.

[Bartók et al., 2011] Bartók, A., Daniel, L., and Razek, A. (2011). Micro-macro modelling of stress-dependent anisotropic magnetoresistance. *Journal of Physics D: Applied Physics*, 44(13):135001.

[Bartók et al., 2013] Bartók, A., Daniel, L., and Razek, A. (2013). A multiscale model for thin film amr sensors. *Journal of Magnetism and Magnetic Materials*, 326:116–122.

[Beltran et al., 2007] Beltran, H., Reig, C., Fuster, V., Ramirez, D., and Cubells-Beltran, M. (2007). Modeling of magnetoresistive-based electrical current sensors: A technological approach. *Sensors Journal, IEEE*, 7(11):1532–1537.

[Berger and Friedberg, 1968] Berger, L. and Friedberg, S. (1968). Magnetoresistance of a permalloy single crystal and effect of 3 d orbital degeneracies. *Physical Review*, 165(2):670.

[Bornert et al., 2001] Bornert, M., Bretheau, T., and Gilormini, P. (2001). *Homogénéisation en mécanique des matériaux*. Hermes Science Publications.

[Bouchaud, 2012] Bouchaud, J. (2012). Magnetic sensors market tracker. IHS-iSuppli Market Report 2012, iSuppli Corporation, USA. See http://www.isuppli.com/.

[Bozorth, 1993] Bozorth, R. (1993). *Ferromagnetism*. IEEE Press Classic Reissue. Wiley.

[Bruggeman, 1935] Bruggeman, D. A. G. (1935). Berechnung verschiedener physikalischer konstanten von heterogenen substanzen. *Annalen der Physik*, 416(8):665–679.

[Buiron, N. et al., 1999] Buiron, N., Hirsinger, L., and Billardon, R. (1999). A multiscale model for magneto-elastic couplings. *J. Phys. IV France*, 09:Pr9–187–Pr9–196.

[Chikazumi and Graham, 1997] Chikazumi, S. and Graham, C. (1997). *Physics of Ferromagnetism*. International Series of Monographs on Physics. Clarendon Press.

[Cullity and Graham, 2011] Cullity, B. and Graham, C. (2011). *Introduction to Magnetic Materials*. Wiley.

[Daniel et al., 2013] Daniel, L., Bartok, A., and Razek, A. (2013). Method for realizing film in anisotropic magnetoresistance sensor for measurement or detection of magnetic anomaly, involves introducing non-zero residual mechanical stress in anisotropy direction parallel to surface of film. *French patent*, -(FR 2991780 A1).

[Daniel and Corcolle, 2007] Daniel, L. and Corcolle, R. (2007). A note on the effective magnetic permeability of polycrystals. *Magnetics, IEEE Transactions on*, 43(7):3153–3158.

[Daniel and Galopin, 2008] Daniel, L. and Galopin, N. (2008). A constitutive law for magnetostrictive materials and its application to Terfenol-d single and polycrystals. *Eur. Phys. J. Appl. Phys.*, 42:153.

[Daniel et al., 2008] Daniel, L., O., Buiron, N., and Billardon, R. (2008). Reversible magneto-elastic behavior: A multiscale approach. *J. Mech. Phys. Solids*, 56:1018.

[Daniel et al., 2014] Daniel, L., Rekik, M., and Hubert, O. (2014). A multiscale model for magneto-elastic behaviour including hysteresis effects. *Archive of Applied Mechanics*, 84(9-11):1307–1323.

[Dixon, 2011] Dixon, R. (2011). Magnetic sensors in automotive motors to enjoy brisk growth. IHS-iSuppli Market Report 2011, iSuppli Corporation, USA. See http://www.isuppli.com/.

[Grünberg et al., 1986] Grünberg, P., Schreiber, R., Pang, Y., Brodsky, M. B., and Sowers, H. (1986). Layered magnetic structures: Evidence for antiferromagnetic coupling of fe layers across cr interlayers. *Phys. Rev. Lett.*, 57:2442–2445.

[Hausch and Warlimont, 1973] Hausch, G. and Warlimont, H. (1973). Single crystalline elastic constants of ferromagnetic face centered cubic fe-ni invar alloys. *Acta Metallurgica*, 21(4):401 – 414.

[Heremans, 1993] Heremans, J. (1993). Solid state magnetic field sensors and applications. *Journal of Physics D: Applied Physics*, 26(8):1149.

[Hill, 1965] Hill, R. (1965). Continuum micro-mechanics of elastoplastic polycrystals. *Journal of the Mechanics and Physics of Solids*, 13(2):89 – 101.

[Honeywell, 2010] Honeywell (2010). Linear / angular / rotary displacement sensors. Technical Report HMC1501-1512, Honeywell, www.ssec.honeywell.com.

[Hubert and Schäfer, 1998] Hubert, A. and Schäfer, R. (1998). *Magnetic Domains: The Analysis of Magnetic Microstructures*. Springer.

[Hubert and Daniel, 2008] Hubert, O. and Daniel, L. (2008). Multiscale modeling of the magneto-mechanical behavior of grain-oriented silicon steels. *Journal of Magnetism and Magnetic Materials*, 320(7):1412 – 1422.

[Hubert et al., 2003] Hubert, O., Daniel, L., and Billardon, R. (2003). Experimental analysis of the magnetoelastic anisotropy of a non-oriented silicon iron alloy.

Journal of Magnetism and Magnetic Materials, 254-255:352–354. Proceedings of the 15th International Conference on Soft Magnetic Materials (SMM15).

[Jedlicska et al., 2010] Jedlicska, I., Weiss, R., and Weigel, R. (2010). Linearizing the output characteristic of gmr current sensors through hysteresis modeling. *Industrial Electronics, IEEE Transactions on*, 57(5):1728–1734.

[Julliere, 1975] Julliere, M. (1975). Tunneling between ferromagnetic films. *Physics Letters A*, 54(3):225 – 226.

[Kanrar and Ghosh, 1983] Kanrar, A. and Ghosh, U. (1983). The variation of elastic constants of nickel-iron single crystal alloys from 78 to 300 k. *Journal of Physics and Chemistry of Solids*, 44(5):457 – 462.

[Koehler et al., 1993] Koehler, T. R., Yang, B., Chen, W., and Fredkin, D. R. (1993). Simulation of magnetoresistive response in a small permalloy strip. *Journal of Applied Physics*, 73(10):6504–6506.

[Kubik et al., 2006] Kubik, J., Vcelak, J., and Ripka, P. (2006). On cross-axis effect of the anisotropic magnetoresistive sensors. *Sensors and Actuators A: Physical*, 129(1-2):15–19. EMSA 2004 Selected Papers from the 5th European Magnetic Sensors Actuators Conference - 2004, Cardiff, UK, 4-6 July 2004.

[Li et al., 2010] Li, J., Li, S. L., Wu, Z. W., Li, S., Chu, H. F., Wang, J., Zhang, Y., Tian, H. Y., and Zheng, D. N. (2010). A phenomenological approach to the anisotropic magnetoresistance and planar hall effect in tetragonal $La_{2/3}Ca_{1/3}Mno_3$ thin films. *J. Phys.: Condens. Matter*, page 146006.

[McGuire and Potter, 1975] McGuire, T. and Potter, R. (1975). Anisotropic magnetoresistance in ferromagnetic 3d alloys. *IEEE Trans. Magn.*, 11:1018.

[McNeill et al., 2008] McNeill, N., Gupta, N., Burrow, S., Holliday, D., and Mellor, P. (2008). Application of reset voltage feedback for droop minimization in the unidirectional current pulse transformer. *Power Electronics, IEEE Transactions on*, 23(2):591–599.

[Mlejnek et al., 2008] Mlejnek, P., Vopalensky, M., and Ripka, P. (2008). Amr current measurement device. *Sensors and Actuators A*, 141:649.

[NDT-Inc., 2015] NDT-Inc. (2015). Hall-effect representation. Technical report, NDT INC., https://www.nde-ed.org/EducationResources/CommunityCollege/MagParticle/Physics/Measuring.htm.

[Néel, 1944] Néel, L. (1944). Les lois de l'aimantation et de la subdivision en domaines élémentaires d'un monocristal de fer. *J. Phys. Radium*, 5(11):241–251.

[Philips, 2000] Philips (2000). Application note, general magnetoresistive sensors for magnetic field measurement. Technical Report KMZ10, Philips, www.philips.com.

[Popovic et al., 1996] Popovic, R., Flanagan, J., and Besse, P. (1996). The future of magnetic sensors. *Sensors and actuators A: Physical*, 56(1):39–55.

[Shiiki et al., 1996] Shiiki, K., Mitsui, Y., and Hirata, Y. (1996). Effect of anisotropy dispersion on magnetization process in magnetoresistive sensor films. *Journal of Applied Physics*, 79(5):2590–2593.

[Stroud, 1975] Stroud, D. (1975). Generalized effective-medium approach to the conductivity of an inhomogeneous material. *Phys. Rev. B*, 12:3368–3373.

[Stutzke et al., 2005] Stutzke, N. A., Russek, S. E., Pappas, D. P., and Tondra, M. (2005). Low-frequency noise measurements on commercial magnetoresistive magnetic field sensors. *Journal of Applied Physics*, 97(10):10Q107.

[Tumanski, 2001] Tumanski, S. (2001). *Thin Film Magnotoresistive Sensors*. Taylor and Francis Press.

[Vcelak et al., 2005] Vcelak, J., Ripka, P., Kubik, J., Platil, A., and Kaspar, P. (2005). Amr navigation systems and methods of their calibration. *Sensors and Actuators A*, 123-124:122.

[von Helmolt et al., 1993] von Helmolt, R., Wecker, J., Holzapfel, B., Schultz, L., and Samwer, K. (1993). Giant negative magnetoresistance in perovskitelike. *Phys. Rev. Lett.*, 71:2331–2333.

[Webster, 1925] Webster, W. L. (1925). The magnetic properties of iron crystals. *Proceedings of the Royal Society of London A: Mathematical, Physical and Engineering Sciences*, 107(743):496–509.

[Wiśniewski, 2007] Wiśniewski, P. (2007). Giant anisotropic magnetoresistance and magnetothermopower in cubic 3:4 uranium pnictides. *Applied Physics Letters*, 90(19):192106.

[Zimmermann et al., 2005] Zimmermann, E., Verweerd, A., Glaas, W., Tillmann, A., and Kemna, A. (2005). An amr sensor-based measurement system for magnetoelectrical resistivity tomography. *Sensors Journal, IEEE*, 5(2):233–241.

List of publications

Publications related to the work presented in this thesis:

– Peer reviewed journals

- ▷ **Andras BARTOK**, Laurent DANIEL and Adel RAZEK
  A multiscale model for thin film AMR sensors
  Journal of Magnetism and Magnetic Materials **326**, 116-122 (2013)

- ▷ **Andras BARTOK**, Laurent DANIEL and Adel RAZEK
  Micro−macro modelling of stress-dependent anisotropic magnetoresistance
  Journal of Physics D: Applied Physics **44**, 135001 (2011)

– Patent

- ▷ Laurent DANIEL, **Andras BARTOK** et Adel RAZEK
  Procédé de réalisation de films á magnétorésistance anisotrope et procédé et dispositifs de détection et/ou de mesure comprenant de tels films
  Brevet CNRS, numéro FR2991780.

– Conference communications

- ▷ **Andras BARTOK**, Laurent DANIEL and Adel RAZEK
  Effect of stress on the sensitivity of AMR sensors
  SMM21 (21st International Conference on Soft Magnetic Materials), Budapest, Hungary (2013)

- ▷ **Andras BARTOK**, Laurent DANIEL, Thierry BAUDIN and Adel RAZEK
  Investigation of the role of crystallographic texture on the sensitivity of AMR thin film sensors
  EMSA (The European Magnetic Sensors and Actuators Conference), Prague, Czech Republic (2012)

- ▷ **Andras BARTOK**, Laurent DANIEL, Thierry BAUDIN and Adel RAZEK
  Investigation of the effect of crystallographic texture on AMR
  EUROMAT (European Congress on Advenced Materials and Processes), Montpellier, France (2011)

Other publications:

– Peer reviewed journals

▷ **Andras BARTOK**, Mikhail KUSTOV, Lesley F. KOHEN, Alexander PASKO, Karim ZEHANI, Lotfi BESSAIS, Frederic MAZALEYRAT and Martino LOBUE
Study of the first paramagnetic to ferromagnetic transition in as prepared samples of Mn-Fe-P-Si magnetocaloric compounds prepared by different synthesis routes
Journal of Magnetism and Magnetic Materials - accepted paper in press (2015)

▷ Frederic MAZALEYRAT, Alexander PASKO, **Andras BARTOK** and Martino LOBUE
Giant coercivity of dense nanostructured spark plasma sintered barium hexaferrite
Journal of Applied Physics **109**, 07A708 (2011)

▷ Katalin NEUROHR, Attila CSIK, Kalman VAD, **Andras BARTOK**, Gyorgy MOLNAR and Laszlo PETER
Composition depth profile analysis of electrodeposited alloys and metal multilayers: the reverse approach
Journal of Solid State Electrochemistry **15**, 2523-2544 (2011)

▷ **Andras BARTOK**, Attila CSIK, Kalman VAD, Gyorgy MOLNAR, Eniko TOTH-KADAR and Laszlo PETER
Application of Surface Roughness Data for the evaluation of depth profile measurements of nanoscale multilayers
Journal of The Electrochemical Society **156**, D253-D260 (2009)

– Conference communications

▷ **Andras BARTOK**, Mikhail KUSTOV, Lesley F. KOHEN, Alexander PASKO, Karim ZEHANI, Lotfi BESSAIS, Frederic MAZALEYRAT and Martino LOBUE
Study of the first paramagnetic to ferromagnetic transition in as prepared samples of Mn-Fe-P-Si magnetocaloric compounds prepared by different synthesis routes
ICM2015 (20th International Conference on Magnetism), Barcelona, Spain (2015)

- **Andras BARTOK**, Alexander PASKO, Karim ZEHANI, Lotfi BESSAIS, Frederic MAZALEYRAT and Martino LOBUE
  Comparison of conventional and spark plasma sintering routes for the fabrication of room temperature magnetocaloric Mn-Fe-P-Si
  Thermag VI. (6th International Conference on Magnetic Refrigeration at Room Temperature), Victoria, Canada (2014)

- Frederic MAZALEYRAT, Alexander PASKO, **Andras BARTOK** and Martino LOBUE
  Giant Hc of SPS sintered barium hexaferrite
  55th MMM Conference (Magnetism and Magnetic Materials), Atlanta, USA (2010)

- Laszlo PETER, Attila CSIK, Kalman VAD, **Andras BARTOK**, Eniko TOTH-KADAR and Gyorgy MOLNAR
  Reverse depth profile analysis of electrodeposited Fe-Co-Ni alloys and Co/Cu multilayers
  216th Meeting of The Electrochemical Society, Wien, Austria (2009)

- **Andras BARTOK**, Imre BAKONYI, Kalman VAD, Daniel MERKEL and Laszlo PETER
  Study of surface roughness evolution with thickness in electrodeposited Co/Cu multilayers
  EAST (European Academy of Surface Technology Forum), Trento, Italy (2008)

- **Andras BARTOK**, Attila CSIK, Kalman VAD, Gyorgy MOLNAR, Eniko TOTH-KADAR and Laszlo PETER
  Calculation of reverse depth profile analysis results from surface roughness data of electrodeposited multilayers
  6th EDNANO (International Workshop On Electrodeposited Nanostructures), Bendorf, Austria (2008)

- Laszlo PETER, **Andras BARTOK**, Eniko TOTH-KADAR and Jozsef PADAR
  Electrodeposition of Pd-Cu alloys and nanoporous Pd formation by anodic dealloying
  59th ISE (Annual Meeting of the International Society of Electrochemistry), Sevilla, Spain (2008)

(19) RÉPUBLIQUE FRANÇAISE

INSTITUT NATIONAL DE LA PROPRIÉTÉ INDUSTRIELLE

PARIS

(11) **N° de publication :** ***2 991 780***

(à n'utiliser que pour les commandes de reproduction)

(21) **N° d'enregistrement national :** **12 55287**

(51) Int Cl[8] : ***G 01 R 33/09*** *(2013.01)*

(12) DEMANDE DE BREVET D'INVENTION A1

(22) **Date de dépôt :** 06.06.12.

(30) **Priorité :**

(43) **Date de mise à la disposition du public de la demande :** 13.12.13 Bulletin 13/50.

(56) **Liste des documents cités dans le rapport de recherche préliminaire :** *Se reporter à la fin du présent fascicule*

(60) **Références à d'autres documents nationaux apparentés :**

(71) **Demandeur(s) :** *CENTRE NATIONAL DE LA RECHERCHE SCIENTIFIQUE Etablissement public* — FR.

(72) **Inventeur(s) :** DANIEL LAURENT, BARTOK ANDRAS et RAZEK ADEL.

(73) **Titulaire(s) :** CENTRE NATIONAL DE LA RECHERCHE SCIENTIFIQUE Etablissement public.

(74) **Mandataire(s) :** CABINET PONTET ALLANO & ASSOCIES SELARL.

(54) PROCEDE DE REALISATION DE FILMS A MAGNETORESISTANCE ANISOTROPE ET PROCEDE ET DISPOSITIFS DE DETECTION ET/OU DE MESURE COMPRENANT DE TELS FILMS.

(57) L'invention concerne un procédé de réalisation d'un film comprenant au moins un matériau à magnétorésistance anisotrope, prévu pour être utilisé dans un dispositif (700) de mesure ou de détection d'un champ magnétique, ledit procédé comprenant une étape de réalisation dudit film sur au moins un support, caractérisé en ce qu'il comprend en outre une étape d'introduction d'une contrainte mécanique rémanente non nulle selon au moins une direction, dite d'anisotropie, parallèle à la surface dudit film par traitement dudit matériau et/ou dudit film et/ou dudit support.

Elle concerne également un film AMR comportant une contrainte mécanique rémanente au moins selon une direction d'anisotropie et un dispositif de détection et/ou de mesure d'un champ magnétique permettant d'appliquer une contrainte mécanique selon au moins une direction d'anisotropie.

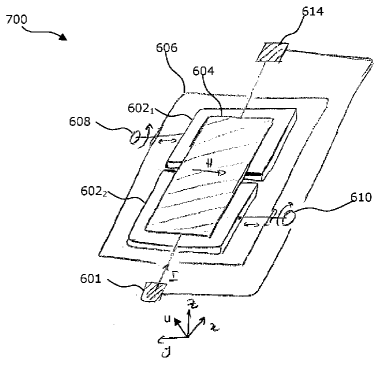

FR 2 991 780 - A1

« Procédé de réalisation de films à magnétorésistance anisotrope et procédé et dispositifs de détection et/ou de mesure comprenant de tels films »

La présente invention concerne un procédé pour la réalisation de films à magnétorésistance anisotrope utilisé dans des dispositifs de mesure ou de détection d'un champ magnétique, tels que les capteurs AMR. Elle concerne également un dispositif de mesure ou de détection d'un champ magnétique, tel qu'un capteur AMR, comprenant un film à magnétorésistance anisotrope.

Le domaine de l'invention est le domaine des dispositifs de mesure ou de détection d'un champ électromagnétique en exploitant des matériaux à magnétorésistance anisotrope, tels que des capteurs AMR.

Etat de la technique

Il existe actuellement de nombreux capteurs AMR comprenant chacun un film présentant une magnétorésistance anisotrope.

La magnétorésistance est la propriété qu'ont certains matériaux de présenter une résistance électrique qui évolue lorsqu'ils sont soumis à un champ magnétique. La magnétorésistance anisotrope (aussi appelé AMR pour « Anisotropic magnetoresistance » en anglais) est la propriété de certains matériaux à présenter une résistance électrique dépendant de l'angle formé entre le flux de courant dans ce matériau et l'orientation de l'aimantation dans ce matériau. Ainsi, une résistance électrique maximale est obtenue lorsque la direction du courant est parallèle à l'aimantation. L'aimantation dépend elle-même d'un champ magnétique appliqué au matériau.

Les matériaux présentant une propriété AMR sont utilisés dans des capteurs, appelés capteurs AMR, pour détecter et mesurer le champ magnétique dans une direction donnée. Un capteur AMR comprend un film d'épaisseur faible ou négligeable, aussi appelé film AMR, réalisé en ou comprenant un matériau présentant une propriété AMR. Un courant électrique traverse le film dans une direction souvent orientée à 45° par rapport à la direction, dite de mesure, dans laquelle on souhaite détecter ou

mesurer le champ magnétique. En fonction du courant traversant le film dans la direction de mesure et la tension appliquée, la résistance du film est déterminée, puis le champ magnétique.

Un film AMR présente une propriété AMR selon une direction donnée, dite de mesure, se trouvant dans le plan du film. Pour mesurer la valeur du champ magnétique ou détecter un champ magnétique dans une direction cible, le film AMR est positionné de sorte que la direction de mesure soit parallèle à la direction cible. La sensibilité d'un film AMR, et donc d'un capteur AMR, est définie par la variation de la résistivité $\Delta\delta\rho$ du film dans la direction de mesure en fonction de la variation ΔH du champ magnétique dans cette direction, c'est-à-dire la valeur de la pente de la courbe répondant à la fonction $\delta\rho = f(H)$. La gamme de mesure d'un film AMR, et donc d'un capteur AMR est définie comme étant le champ magnétique maximum H_{max} détectable par le film AMR.

Les films AMR actuels, et donc les capteurs AMR actuels, ne permettent pas d'adapter ou de choisir la sensibilité de mesure ou la gamme de mesure d'un capteur AMR. Plus particulièrement, les films et les capteurs AMR actuels ne permettent pas une méthode de réglage simple de manière à avoir une sensibilité maximale pour une gamme de mesure envisagée.

Un but de la présente invention est de remédier à ces inconvénients.

Un autre but de l'invention est de proposer un procédé de réalisation d'un film AMR et un capteur AMR plus personnalisables en fonction des applications envisagées.

Un autre but de l'invention est de proposer un procédé de réalisation d'un film AMR et un capteur AMR dont la sensibilité de mesure est réglable en fonction des applications envisagées.

Un autre but de l'invention est de proposer un procédé de réalisation d'un film AMR et un capteur AMR dont la gamme de mesure est réglable en fonction des applications envisagées.

Enfin, un autre but de l'invention est de proposer un procédé de réalisation d'un film AMR et un capteur AMR dont la sensibilité de mesure est réglable pour une gamme de mesure donnée de sorte à obtenir une sensibilité maximale pour la gamme de mesure donnée.

Exposé de l'invention

L'invention permet d'atteindre au moins l'un de ces buts par un procédé de réalisation d'un film comprenant au moins un matériau à magnétorésistance anisotrope, prévu pour être utilisé dans un dispositif de mesure ou de détection d'un champ magnétique, ledit procédé comprenant une étape de réalisation dudit film sur au moins un support, caractérisé en ce qu'il comprend en outre une étape d'introduction d'une contrainte mécanique rémanente non nulle selon au moins une direction, dite d'anisotropie, parallèle à la surface dudit film, et plus particulièrement une contrainte mécanique non nulle dans le plan formé par le film, par traitement dudit matériau et/ou dudit film et/ou dudit support.

Un tel procédé permet d'obtenir un film AMR présentant une contrainte mécanique rémanente dans une direction d'anisotropie, dans le plan défini par le film AMR.

Les inventeurs de la présente invention ont découvert que la présence d'une contrainte mécanique non nulle dans une direction donnée parallèle à la surface du film permet d'une part de modifier la sensibilité de mesure du film AMR et d'autre part la gamme de mesure du film AMR pour mesurer et/ou détecter un champ magnétique suivant une direction, dite de mesure, parallèle à la surface du film et plus particulièrement dans la direction d'anisotropie.

Il est donc possible en réglant la contrainte mécanique rémanente dans le film AMR de modifier et d'ajuster la sensibilité et/ou la gamme de mesure du film AMR, et par conséquent du capteur AMR, en fonction des applications envisagées. Par exemple, il est possible d'augmenter la sensibilité de mesure d'un capteur AMR lorsque l'application envisagée requiert une grande sensibilité de mesure pour une petite gamme de mesure. Il est également possible d'élargir la gamme de mesure si l'application envisagée nécessite de pouvoir mesurer des valeurs de champ magnétiques dans une large gamme de mesure avec une faible sensibilité.

Dans un premier mode de réalisation, l'étape d'introduction d'une contrainte mécanique rémanente peut comprendre :

- une introduction d'une précontrainte par application temporaire, pendant l'étape de réalisation du film, d'une charge mécanique créant au moins selon la direction d'anisotropie, et plus particulièrement dans le plan du film, une déformation élastique temporaire du support, et/ou
- une introduction d'une post-contrainte par application temporaire, après la réalisation du film, d'une charge mécanique entraînant au moins selon la direction d'anisotropie, et plus particulièrement dans le plan du film, une déformation plastique durable du support.

L'application d'une charge mécanique directement sur le support, et non sur le film, permet de ne pas manipuler directement le film, ce qui est plus simple à réaliser, et présente moins de risque d'abimer le film AMR qui est fragile.

Dans un deuxième mode de réalisation, l'étape d'introduction d'une contrainte mécanique rémanente peut comprendre :

- une introduction d'une précontrainte par application temporaire, pendant la réalisation du film, d'un traitement thermique créant au moins selon la direction d'anisotropie, plus particulièrement dans le plan du film, une déformation élastique temporaire du support, et/ou
- une introduction d'une post-contrainte par application temporaire, après la réalisation, d'un traitement thermique entraînant au moins selon la direction d'anisotropie, plus particulièrement dans le plan du film, une déformation plastique durable du support.

Dans cette version, ni le support, ni le film n'est soumis à une manipulation mécanique, ce qui permet d'éviter tout risque de mauvaise manipulation pouvant abimer le support ou le film AMR.

Dans le cas d'une précontrainte, la déformation du support étant élastique pendant la réalisation du film, la suppression de la charge mécanique ou du traitement thermique va entrainer une contrainte

mécanique rémanente dans le film dans le sens contraire à la direction d'application de la charge mécanique ou du traitement thermique, toujours au moins dans la direction d'anisotropie, et plus particulièrement dans le plan du film.

Dans le cas d'une post-contrainte, la déformation du support étant plastique après la réalisation du film, une contrainte mécanique rémanente est introduite dans le film dans le même sens que la charge mécanique ou l'application thermique.

Dans un troisième mode de réalisation, l'introduction de la contrainte mécanique rémanente peut être obtenue par un choix d'un support présentant un paramètre de maille différent du paramètre de maille du ou des matériaux composant le film de sorte à créer dans ledit film une contrainte au moins selon la direction d'anisotropie, et plus particulièrement dans le plan du film.

Dans un quatrième mode de réalisation, l'étape d'introduction de la contrainte mécanique rémanente peut comprendre les étapes suivantes :

- avant ou pendant la réalisation du film, ajout d'au moins un composé, dit cible, dans la composition dudit film, et
- après la réalisation dudit film, application d'un traitement, par exemple optique, thermique, chimique ou électrique, modifiant le volume ou la présence dudit composé dans ledit film de sorte à créer dans ledit film une contrainte au moins selon la direction d'anisotropie, plus particulièrement dans le plan du film.

Ce mode de réalisation permet d'éviter d'intervenir sur le support mais directement sur le film, tout en évitant une déformation du support.

Un tel composé cible peut par exemple comprendre/consister en de Hélium ou de l'Hydrogène éliminé après la réalisation du film par exemple sur un support.

Dans un cinquième mode de réalisation, l'étape d'introduction de la contrainte mécanique rémanente peut comprendre, après la réalisation dudit

film, une étape d'irradiation du film et/ou du support par ions légers modifiant l'état de certains éléments/molécules présent(e)s dans le film et/ou le support et créant ainsi une contrainte mécanique rémanente au moins selon la direction d'anisotropie, et plus particulièrement dans le plan du film.

Au moins deux des quatre modes de réalisation décrits ci-dessus peuvent être combinés entre eux pour augmenter ou faciliter l'introduction de la contrainte mécanique rémanente dans le film.

Dans une version préférée de l'invention, le matériau à magnétorésistance anisotrope peut être ou peut comprendre un permalloy de formule $Fe_{11}Ni_{89}$.

Le film AMR peut être réalisé selon l'une quelconque des techniques suivantes :

- dépôt du matériau à magnétorésistance anisotrope, éventuellement mélangé à au moins un autre matériau, sur le support,
- évaporation sous vide,
- méthode de pulvérisation (cathodique, par faisceau d'ions, …)
- épithaxie par jet moléculaire, et
- électrodéposition.

Selon un autre aspect de l'invention il est proposé un dispositif de mesure ou de détection d'un champ magnétique, par exemple un capteur AMR, comprenant au moins un film réalisé suivant le procédé selon l'invention.

Selon encore un autre aspect de l'invention il est proposé un dispositif de mesure ou de détection d'un champ magnétique comprenant au moins un film réalisé au moins en partie en un matériau magnétorésistif anisotrope, caractérisé en ce qu'il comprend en outre au moins un moyen, dit de

contrainte, pour appliquer une contrainte mécanique audit film au moins dans une direction, dite d'anisotropie, parallèle à la surface dudit film, et plus particulièrement dans le plan du film.

Ainsi, un tel dispositif permet de régler la sensibilité de mesure et/ou la gamme de mesure qui lui est associée(s) pour mesurer et/ou détecter un champ magnétique suivant une direction, dite de mesure, parallèle à la surface du film. Un tel dispositif est donc personnalisable selon l'application envisagée.

Avantageusement, le film peut aussi être un film présentant une contrainte rémanente au moins dans la direction d'anisotropie, tel qu'un film obtenu par le procédé décrit précédemment. Dans ce cas l'effet obtenu est amplifié.

Dans un exemple de réalisation particulier, l'au moins un moyen de contrainte peut comprendre :

- au moins deux supports, indépendants l'un de l'autre, et chacun solidaire du film,
- des moyens pour déplacer au moins l'un desdits supports, par rapport à l'autre au moins dans une direction parallèle à la surface dudit film.

Dans un autre mode de réalisation, l'au moins un moyen de contrainte peut comprendre :

- au moins un support solidaire dudit film,
- des moyens pour déformer, par exemple par compression ou par étirement, ledit au moins un support déformable au moins dans une direction parallèle à la surface dudit film, et plus particulièrement dans la direction d'anisotropie.

Avantageusement, l'au moins un moyen de contrainte peut être agencé pour appliquer une contrainte mécanique ajustable, au moins en intensité.

Dans ce cas, le dispositif selon l'invention peut en outre comprendre au moins un moyen pour ajuster l'intensité de la contrainte mécanique, au moins dans la direction d'anisotropie.

L'au moins un moyen pour ajuster l'intensité de la contrainte mécanique peut permettre un ajustement manuel de la contrainte mécanique, par exemple une ou plusieurs vis micrométriques.

L'au moins un moyen pour ajuster l'intensité de la contrainte mécanique peut permettre un ajustement électrique de la contrainte mécanique, par exemple un ou plusieurs moyens piézoélectriques contrôlables par une source électrique.

Avantageusement, l'au moins un moyen de contrainte peut être agencé pour appliquer une contrainte mécanique ajustable, au moins en direction ou en sens.

Dans ce cas, le dispositif selon l'invention peut en outre comprendre au moins un moyen pour ajuster la direction, le sens ou la forme de la contrainte mécanique.

L'au moins un moyen pour ajuster la direction, le sens ou la forme de la contrainte mécanique peut permettre un ajustement manuel, par exemple une ou plusieurs vis micrométriques modifiant le sens, la direction ou la forme de la contrainte mécanique.

L'au moins un moyen pour ajuster l'intensité de la contrainte mécanique peut permettre un ajustement électrique de la contrainte mécanique, par exemple un ou plusieurs moyens piézoélectriques contrôlables par une source électrique.

Un tel dispositif de mesure ou de détection d'un champ magnétique, dans lequel l'intensité, la direction, le sens ou la forme de la contrainte mécanique est ajustable, est réutilisable pour différentes applications …

Le dispositif selon l'invention peut en outre comprendre plusieurs films et, pour chacun desdits films, au moins un moyen de contrainte pour appliquer une contrainte mécanique audit film au moins dans une direction parallèle à la surface dudit film.

Le moyen de contrainte associé à chaque film peut être agencé pour appliquer une contrainte indépendamment des autres films.

Le dispositif selon l'invention peut en outre comprendre plusieurs films disposés dans des plans non parallèles, et plus particulièrement perpendiculaires entre eux.

Dans un mode de réalisation particulier, le dispositif selon l'invention peut comprendre 2 ou 3 films disposés chacun dans un plan non parallèle, en particulier perpendiculaire, au(x) plan(s) dans le(s)quel(s) sont disposés l'autre ou les autres film(s).

Le dispositif de mesure et de détection selon l'invention peut être utilisé pour la mesure ou la détection d'une anomalie magnétique, d'un courant électrique, d'une position ou d'une vitesse de rotation d'un élément ou d'un ensemble d'éléments comprenant une partie magnétique.

Selon encore un autre aspect de l'invention il est proposé un procédé de mesure ou de détection d'un champ magnétique avec au moins un dispositif selon l'invention, caractérisé en ce qu'il comprend une étape de modification ou d'ajustement d'une sensibilité et/ou d'une gamme de mesure par modification de la contrainte mécanique appliquée au film.

Selon l'invention, la contrainte mécanique rémanente ou la contrainte mécanique appliquée peut être uniaxiale ou multiaxiale, préférentiellement dans le plan du film.

Selon un mode de réalisation préféré, la contrainte mécanique rémanente ou la contrainte mécanique appliquée comprend une contrainte de cisaillement, préférentiellement dans le plan du film. Les inventeurs ont découvert qu'une telle contrainte de cisaillement produit les meilleurs résultats.

D'autres avantages et caractéristiques apparaîtront à l'examen de la description détaillée d'un mode de réalisation nullement limitatif, et des dessins annexés sur lesquels

- la FIGURE 1 est une représentation schématique d'un film AMR ;
- la FIGURE 2 est un tableau récapitulant les caractéristiques d'un matériau AMR utilisé pour réaliser le film AMR de la figure 1 ;
- la FIGURE 3 est une courbe de caractérisation d'un film AMR en l'absence de toute contrainte mécanique ;
- la FIGURE 4 est une représentation schématique des étapes d'un exemple d'un procédé selon l'invention dans le cas d'un support élastique ;
- la FIGURE 5 est une représentation schématique des étapes d'un exemple d'un procédé selon l'invention dans le cas d'un support plastique ;
- la FIGURE 6 est une représentation schématique d'un premier exemple d'un dispositif selon l'invention ;
- la FIGURE 7 est une représentation schématique d'un deuxième exemple d'un dispositif selon l'invention ; et
- les FIGURES 8a, 8b et 9 sont des courbes de caractérisation d'un film AMR soumis à une contrainte mécanique selon l'invention.

Il est bien entendu que les modes de réalisation qui seront décrits dans la suite ne sont nullement limitatifs. On pourra notamment imaginer des variantes de l'invention ne comprenant qu'une sélection de caractéristiques décrites par la suite isolées des autres caractéristiques décrites, si cette sélection de caractéristiques est suffisante pour conférer un avantage technique ou pour différencier l'invention par rapport à de l'état de la technique antérieur. Cette sélection comprend au moins une caractéristique de préférence fonctionnelle sans détails structurels, ou avec seulement une partie des détails structurels si c'est cette partie qui est uniquement suffisante pour conférer un avantage technique ou pour différencier l'invention par rapport à l'état de la technique antérieur.

Sur les figures les éléments communs à plusieurs figures conservent la même référence.

La FIGURE 1 est une représentation schématique d'un film AMR 100.

Le film AMR 100 se présente sous la forme d'une couche rectangulaire comprenant ou consistant en un matériau à magnétorésistance anisotrope.

L'épaisseur de la couche, dans la direction z, est négligeable. Le film AMR 100 présente une plus grande dimension dans la direction x par rapport à sa dimension dans la direction y.

Dans un exemple de réalisation particulier, le film est réalisé uniquement en un matériau à magnétorésistance anisotrope qui est un permalloy répondant à la formule $Fe_{11}Ni_{89}$.

La FIGURE 2 donne les caractéristiques de ce matériau. Bien entendu l'invention n'est pas limitée à cet exemple particulier de réalisation et d'autre(s) matériau(x) peuvent être utilisés pour réaliser le film AMR.

Dans la suite de la description, le film AMR 100 est utilisé pour mesurer un champ magnétique H dans la direction y. Pour cela, un champ magnétique de polarisation $^{x}H_{bias}$ est appliqué dans la direction x pour s'assurer que la résistivité du film AMR ne varie pas ou très peu à un champ magnétique selon la direction x. L'épaisseur du film AMR 100 étant négligeable dans la direction z, le film AMR reste sensible à un champ magnétique uniquement dans la direction y.

La FIGURE 3 est une courbe représentant l'évolution du champ magnétique H mesuré dans la direction y, c'est-à-dire dans la direction de la largeur du film AMR 100, en A/m en fonction de la variation de la résistivité dR en %, dans le cas suivant :

- le matériau utilisé est du $Fe_{11}Ni_{89}$,
- le champ de polarisation dans la direction x est de $^{x}H_{bias}$=500 A/m, et
- en l'absence de toute contrainte mécanique extérieure sur le film ou rémanente dans le film.

Sur la figure 3, l'axe horizontal 202 correspond à la valeur du champ magnétique et l'axe vertical 204 correspond à la valeur de la résistivité.

Ainsi, on remarque que la courbe 206 comporte une zone linéaire 208 présentant une bonne sensibilité, la sensibilité correspondant à la pente de la courbe 206. Avant cette zone linéaire 208, la courbe présente une zone non linéaire 210 dont l'intersection avec la zone linéaire 206 donne la valeur minimale du champ extérieur mesurable ${}^{y}H_{min}$ qui est de 200A/m.

Après la zone linéaire 208, la courbe 206 comporte une zone de saturation 212 dans laquelle la sensibilité diminue, devient nulle, voire négative. L'intersection de la zone linéaire 208 avec la zone de saturation 212 donne la valeur maximale du champ extérieur mesurable ${}^{y}H_{max}$ qui est de 500A/m.

La gamme de mesure du film dans ces conditions est donc de 200-500 A/m.

En pratique, la valeur minimale ${}^{y}H_{min}$ du champ magnétique mesurable dépend principalement de l'électronique utilisée et ne sera donc pas prise en compte dans la suite de la description.

La présente invention a pour but de modifier la gamme de mesure et la sensibilité de mesure du film AMR par application d'une contrainte mécanique sur le film :

- sous la forme d'une contrainte mécanique rémanente introduite dans le film avant une mesure, et/ou
- sous la forme d'une contrainte mécanique appliquée sur le film pendant la mesure.

La FIGURE 4 est une représentation schématique d'un exemple de procédé pour introduire une contrainte rémanente non nulle dans un film AMR dans le cas où le film AMR est réalisé sur un support élastique.

Le procédé 400 comprend une étape 402 dans laquelle une contrainte mécanique est appliquée sur le support élastique dans au moins une direction donnée, dite direction d'anisotropie, qui dans le présent exemple

est la direction y, et parallèle au support. Dans une version préférée, la contrainte appliquée est une contrainte de cisaillement dans le plan du film.

La contrainte mécanique appliquée peut être une contrainte en compression du support, en étirement du support ou une contrainte de cisaillement comprenant une composante non nulle dans la direction d'anisotropie.

La contrainte mécanique peut également être appliquée par d'autres procédés qu'un procédé purement mécanique. Par exemple la contrainte peut être appliquée par un procédé thermique, comprenant un chauffage (respectivement un refroidissement) du support, provoquant ainsi une expansion (respectivement un rétrécissement) du support au moins dans la direction d'anisotropie.

L'étape 402 permet d'obtenir un support élastique « déformé » au moins dans la direction d'anisotropie, à savoir la direction y, préférentiellement dans le plan xy.

Le procédé 400 comprend ensuite une étape 404 pendant laquelle le film AMR est réalisé sur le support « déformé ». Le film AMR peut être réalisé par dépôt d'une couche fine de matériau AMR sur le support « déformé ». Cette étape 404 peut être réalisée par toute technique connue de réalisation d'un film AMR (évaporation sous vide, méthode de pulvérisation (cathodique, par faisceau d'ions, …), épitaxie par jet moléculaire, électrodéposition, etc.

Une fois le film AMR réalisé sur le support « déformé », la contrainte mécanique et/ou le traitement thermique appliqué lors de l'étape 402 est supprimé(e) lors de l'étape 406. Le support étant élastique, la suppression de la contrainte mécanique et/ou du traitement thermique a pour conséquence une suppression de la déformation obtenue lors de l'étape 402, et donc une contrainte mécanique dans le film AMR au moins dans la direction d'anisotropie.

La FIGURE 5 est une représentation schématique d'un exemple de procédé pour introduire une contrainte rémanente non nulle dans un film AMR dans le cas où le film AMR est réalisé sur un support plastique.

Le procédé 500 comprend tout d'abord une étape 502 pendant laquelle le film AMR est réalisé sur le support plastique. Le film AMR peut être réalisé par dépôt d'une couche fine de matériau AMR sur le support plastique. Cette étape 452 peut être réalisée par toute technique connue de réalisation d'un film AMR,(évaporation sous vide, méthode de pulvérisation (cathodique, par faisceau d'ions, …), épitaxie par jet moléculaire, électrodéposition, etc.

Le procédé 500 comprend ensuite une étape 504 pendant laquelle une contrainte mécanique est appliquée sur le support plastique dans au moins une direction donnée, correspondant à la direction d'anisotropie, qui dans le présent exemple est la direction y, et parallèle au support. La contrainte appliquée peut être une contrainte en compression, en étirement du support ou une contrainte de cisaillement comprenant une composante non nulle dans la direction d'anisotropie, et préférentiellement dans le plan défini par le film.

La contrainte mécanique peut également être appliquée par d'autres procédés qu'un procédé purement mécanique. Par exemple la contrainte peut être appliquée par un procédé thermique, comprenant un chauffage (respectivement un refroidissement) du support plastique, provoquant ainsi une expansion (respectivement un rétrécissement) du support plastique au moins dans la direction d'anisotropie.

L'étape 504 permet d'obtenir un support plastique « déformé » au moins dans la direction d'anisotropie, à savoir la direction y, et donc une contrainte mécanique dans le film AMR au moins dans la direction y, et préférentiellement dans le plan du film c'est-à-dire dans le plan xy.

Lors de l'étape 506, la contrainte mécanique et/ou le traitement thermique appliqué lors de l'étape 504 est supprimé(e). Le support étant plastique, la suppression de la contrainte mécanique et/ou du traitement thermique n'a aucune conséquence ou très peu de conséquence et le support « déformé », obtenu après l'étape 504, reste déformé, et donc une contrainte mécanique rémanente est introduite dans le film AMR présent sur le support plastique au moins dans la direction d'anisotropie : la direction y.

La FIGURE 6 est une représentation schématique d'un premier exemple d'un dispositif de mesure et/ou de détection d'un champ magnétique selon l'invention.

Le dispositif 600 représenté sur la figure 6 comprend un support 602 élastique et/ou plastique, par exemple en silicium, sur lequel est disposé solidairement un film AMR 604, tel que le film AMR 100 de la figure 1.

Le support 602 est fixé à un boîtier ou châssis 606 par l'intermédiaire de deux vis micrométriques 608 et 610 libres en rotation. Chacune des vis micrométriques 608 et 610 peut être utilisée pour exercer une contrainte mécanique en compression ou en étirement sur le support 602 selon la direction y.

Le dispositif 600 comprend en outre des moyens (non représentés) pour appliquer un champ de polarisation selon la direction x, de tels moyens pouvant comprendre des bobines inductrices couplées à une source électrique alimentant ces bobines. Ce champ de polarisation permet de rendre le film AMR peu sensible, voir insensible au champ magnétique dans la direction x.

Le dispositif 600 comprend en outre une source électrique 612 appliquant un courant I dans le film AMR 604 selon une direction u, se trouvant dans le plan x-y à 45° par rapport à la direction x et par rapport à la direction y.

Le dispositif 600 comprend en outre un ampèremètre 614 mesurant le courant traversant le film AMR 604.

Dans l'exemple particulier représenté sur la figure 6, le film AMR présente une structure en « Barber pole » de manière à orienter le courant I à 45° par rapport à la surface du film AMR 604, c'est-à-dire par rapport au plan x-y.

Les vis micrométriques 608 et 610 permettent d'appliquer une contrainte mécanique ajustable et modifiable sur le support 602, soit en compression, soit en étirement, au moins selon la direction y et permettent ainsi de modifier la sensibilité de mesure et/ou la gamme de mesure dans la direction y. Le dispositif 600 permet de mesurer ou détecter un champ magnétique H selon la direction y.

La FIGURE 7 est une représentation schématique d'un deuxième exemple d'un dispositif de mesure et/ou de détection d'un champ magnétique selon l'invention.

Le dispositif 700 représenté à la figure 7 diffère du dispositif 600 représenté sur la figure 6 en ce qu'il comprend deux supports 602_1 et 602_2 coplanaires indépendants entre eux. La vis micrométrique 608 est fixée au support 602_1 et permet de déplacer le support 602_1 dans le plan x-y par rapport au châssis 606 et au support 602_2 et la vis micrométrique 610 est fixée au support 602_2 et permet de déplacer le support 602_2 dans le plan x-y par rapport au châssis 606 et au support 602_1.

La ou les vis micrométriques 608 et 610 permet(tent) de déplacer au moins l'un des supports 602_1 et 602_2 dans un sens ou dans l'autre, et permet(tent) ainsi d'appliquer une contrainte mécanique de cisaillement non nulle dans le film AMR dans le plan x-y. Ainsi, les vis micrométriques permettent de modifier la sensibilité de mesure et/ou la gamme de mesure dans la direction y. Le dispositif 700 permet de mesurer ou détecter un champ magnétique H selon la direction y.

Les vis micrométriques peuvent être déplacées manuellement ou de manière automatisée.

Les vis micrométriques peuvent être remplacées par d'autres moyens motorisés ou piézoélectriques.

Chacun des dispositifs 600 et 700 peut comprendre plusieurs films 604, chacun agencé pour mesurer ou détecter un champ magnétique suivant une direction différente. Par exemple, chacun des dispositifs de mesure peut comprendre un premier film 604 pour mesurer un champ magnétique selon la direction y, un deuxième film 604 pour mesurer un champ magnétique selon la direction x, un troisième film 604 pour mesurer un champ magnétique selon la direction z. Chacun des dispositifs peut comprendre également, pour chacun des films AMR :

- des moyens pour appliquer, indépendamment des autres films AMR, une contrainte mécanique non nulle selon la direction de mesure, et plus particulièrement dans le plan défini par le film, et

- des moyens pour appliquer un champ de polarisation selon une direction perpendiculaire à la direction de mesure et la direction de l'épaisseur du film AMR.

Les FIGURES 8a et 8b sont des courbes montrant l'évolution de la gamme de mesure « H_{max} » en A/m et de la sensibilité « ^{y}S » en % suivant la direction y en fonction de la contrainte mécanique « Sigma »multiaxiale (rémanente dans le film AMR ou appliquée sur le film AMR) en Mpa comprenant une composante non-nulle suivant la direction y, respectivement pour un champ de polarisation $^{x}H_{bias}$ de 500 A/m et de 800 A/m suivant la direction x. Le tenseur de contraintes Sigma est le suivant :

$$\bar{\sigma} = \begin{pmatrix} \sigma & 0 & 0 \\ 0 & -3\sigma & 0 \\ 0 & 0 & 0 \end{pmatrix}$$

Ainsi, on constate clairement que, lorsque la contrainte mécanique augmente, la gamme de mesure H_{max} diminue et la sensibilité de mesure dans la direction y ^{y}S augmente.

On constate également que plus le champ de polarisation $^{x}H_{bias}$ est grand plus la gamme de mesure est grande pour des faibles contraintes mécaniques et plus la sensibilité de mesure est petite pour de fortes contraintes mécaniques.

La FIGURE 9 est une courbe montrant l'évolution de la gamme de mesure « H_{max} » en A/m et de la sensibilité « ^{y}S » en % suivant la direction y, en fonction du champ de polarisation $^{x}H_{bias}$ suivant la direction x, pour une contrainte mécanique de cisaillement dans le plan x-y (rémanente ou appliquée) de 10MPa suivant la direction y.

On constate ainsi que la sensibilité de mesure augmente avec le champ de polarisation jusqu'à 500A/m de champ de polarisation puis

diminue et que la gamme de mesure augmente avec le champ de polarisation.

Selon l'invention il est donc possible de modifier et d'ajuster la gamme de mesure et/ou la sensibilité de mesure selon une direction donnée, dite de mesure, d'une part en fonction de la contrainte mécanique appliquée sur/rémanente dans le film AMR selon cette direction de mesure et d'autre part en fonction du champ de polarisation appliquée selon une direction perpendiculaire à la direction de mesure et parallèle à la surface du film AMR.

Bien entendu, l'invention n'est pas limitée aux exemples détaillés ci-dessus.

REVENDICATIONS

1. Procédé (400 ;500) de réalisation d'un film (100) comprenant au moins un matériau à magnétorésistance anisotrope, prévu pour être utilisé dans un dispositif (600,700) de mesure ou de détection d'un champ magnétique, ledit procédé comprenant une étape (404 ;502) de réalisation dudit film (100) sur au moins un support, caractérisé en ce qu'il comprend en outre une étape (402,406 ;504,506) d'introduction d'une contrainte mécanique rémanente non nulle selon au moins une direction, dite d'anisotropie, parallèle à la surface dudit film (100) par traitement dudit matériau et/ou dudit film et/ou dudit support.

2. Procédé (400 ;500) selon la revendication 1, caractérisé en ce que l'étape d'introduction d'une contrainte mécanique rémanente comprend :

- une introduction (402) d'une précontrainte par application temporaire, pendant l'étape (404) de réalisation du film, d'une charge mécanique créant selon la direction d'anisotropie une déformation élastique temporaire du support, et/ou
- une introduction (504) d'une post-contrainte par application temporaire, après la réalisation du film, d'une charge mécanique entraînant selon la direction d'anisotropie une déformation plastique durable du support.

3. Procédé (400 ;500) selon l'une quelconque des revendications précédentes, caractérisé en ce que l'étape d'introduction d'une contrainte mécanique rémanente comprend :

- une introduction (402) d'une précontrainte par application temporaire, pendant la réalisation du film, d'un traitement thermique créant selon la direction d'anisotropie une déformation élastique temporaire du support, et/ou
- une introduction (404) d'une post-contrainte par application temporaire, après la réalisation, d'un traitement thermique

entraînant selon la direction d'anisotropie une déformation plastique durable du support.

4. Procédé selon l'une quelconque des revendications précédentes, caractérisé en ce que l'introduction de la contrainte mécanique rémanente est obtenue par un choix d'un support présentant un paramètre de maille différent du paramètre de maille du ou des matériaux composant le film de sorte à créer dans ledit film une contrainte selon la direction d'anisotropie.

5. Procédé selon l'une quelconque des revendications précédentes, caractérisé en ce que l'étape d'introduction de la contrainte mécanique rémanente comprend les étapes suivantes :

- avant ou pendant la réalisation du film, ajout d'au moins un composé, dit cible, dans la composition dudit film, et
- après la réalisation dudit film, application d'un traitement modifiant le volume ou la présence dudit composé dans ledit film de sorte à créer dans ledit film une contrainte selon la direction d'anisotropie.

6. Procédé (400,500) selon l'une quelconque des revendications précédentes, caractérisé en ce que le matériau à magnétorésistance anisotrope est un permalloy de formule $Fe_{11}Ni_{89}$.

7. Procédé (400,500) selon l'une quelconque des revendications précédentes, caractérisé en ce que le film est réalisé par :

- dépôt du matériau à magnétorésistance isotopique, éventuellement mélangé à d'au moins un autre matériau sur le support,
- évaporation sous vide,
- méthode de pulvérisation (cathodique, par faisceau d'ions, …),
- épithaxie par jet moléculaire, et/ou
- électrodéposition.

8. Dispositif (600,700) de mesure ou de détection d'un champ magnétique comprenant au moins un film (604) réalisé suivant le procédé l'une quelconque des revendications précédentes.

9. Dispositif (600 ;700) de mesure ou de détection d'un champ magnétique comprenant au moins un film (604) réalisé au moins en partie en un matériau magnétorésistif anisotrope, caractérisé en ce qu'il comprend en outre au moins un moyen (608,610), dit de contrainte, pour appliquer une contrainte mécanique audit film (604) au moins dans une direction, dite d'anisotropie, parallèle à la surface dudit film (604).

10. Dispositif (700) selon la revendication 9, caractérisé en ce que l'au moins un moyen de contrainte comprend :

- au moins deux supports (602_1, 602_2), indépendants l'un de l'autre, et chacun solidaire du film (604),
- des moyens (608,610) pour déplacer au moins l'un desdits supports (602_1, 602_2), par rapport à l'autre au moins dans une direction parallèle à la surface dudit film (604).

11. Dispositif (600) selon l'une quelconque des revendications 9 ou 10, caractérisé en ce que les moyens de contrainte comprennent :

- au moins un support (602) solidaire dudit film (604),
- des moyens (608,610) pour déformer ledit au moins un support (602) déformable au moins dans une direction parallèle à la surface dudit film (604).

12. Dispositif (600 ;700) selon l'une quelconque des revendications 9 à 11, caractérisé en ce que les moyens de contrainte (608,610) sont agencés pour appliquer une contrainte mécanique ajustable.

13. Dispositif selon l'une quelconque des revendications 9 à 12, caractérisé en ce qu'il comprend plusieurs films et, pour chacun desdits films, au moins

un moyen de contrainte pour appliquer une contrainte mécanique audit film au moins dans une direction parallèle à la surface dudit film.

14. Dispositif selon l'une quelconque des revendications 8 à 13, caractérisé en ce qu'il comprend plusieurs films disposés dans des plans non parallèles entre eux.

15. Utilisation d'un dispositif selon l'une quelconque des revendications 8 à 14 pour la mesure ou la détection d'une anomalie magnétique, d'un courant électrique, d'une position ou d'une vitesse de rotation.

16. Procédé de mesure ou de détection d'un champ magnétique avec au moins un dispositif selon l'une quelconque des revendications 9 à 14, caractérisé en ce qu'il comprend une étape de modification ou d'ajustement d'une sensibilité et/ou d'une gamme de mesure par modification de la contrainte mécanique appliquée au film.

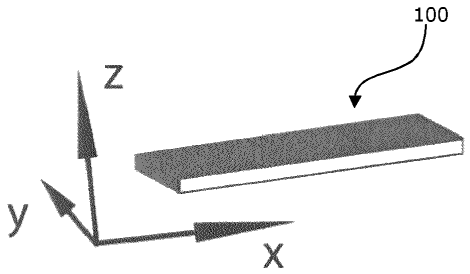

FIG. 1

Grandeur	Aimantation à saturation	Constantes d'anisotropie	Coefficients de magnétostriction	Constantes élastiques	Coefficients magnétorésistifs (modèle de Döring)
Notation	M_s	K_1 ; K_2	λ_{100} ; λ_{111}	C_{11} ; C_{12} ; C_{44}	k1 ; k2 ; k3 ; k4 ; k5
Unité	A/m	kJ/m3	-	GPa	-
Valeur	$7{,}50.10^5$	-1.0 ; -2.0	$-1{,}5.10^{-5}$; $-1{,}0.10^{-5}$	243 ; 148 ; 122	0,0518 ; 0,0478 ; -0,0243 ; -0,0139 ; 0,0259

FIG. 2

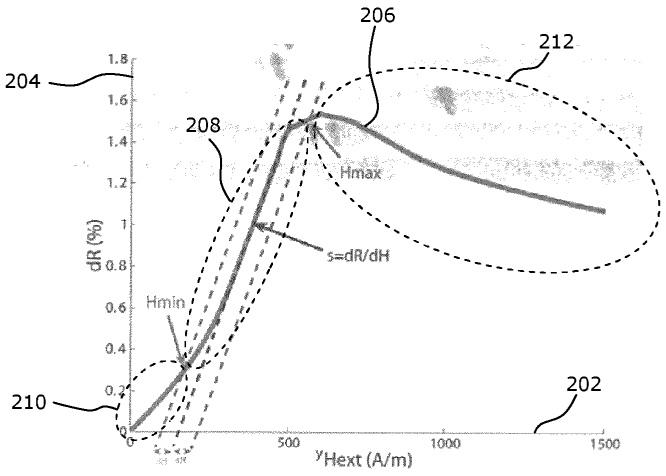

FIG. 3

2/4

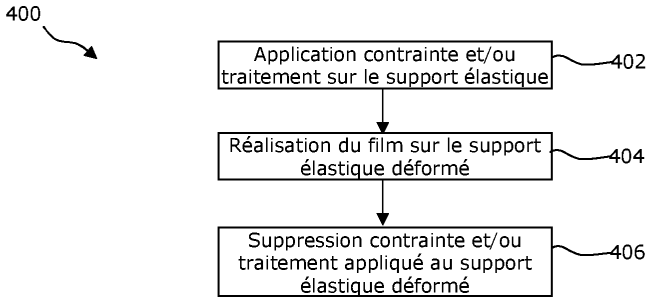
400
Application contrainte et/ou traitement sur le support élastique
402
Réalisation du film sur le support élastique déformé
404
Suppression contrainte et/ou traitement appliqué au support élastique déformé
406

FIG. 4

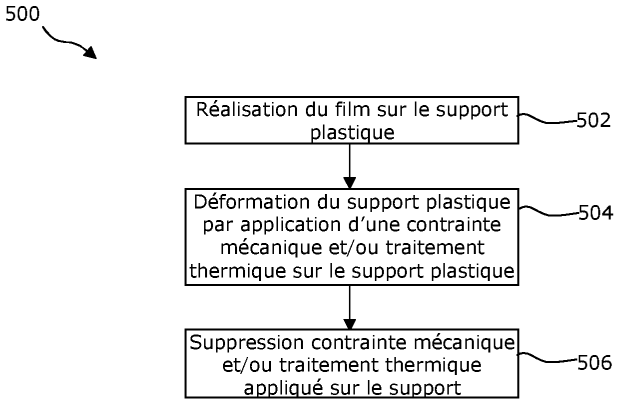
500
Réalisation du film sur le support plastique
502
Déformation du support plastique par application d'une contrainte mécanique et/ou traitement thermique sur le support plastique
504
Suppression contrainte mécanique et/ou traitement thermique appliqué sur le support
506

FIG. 5

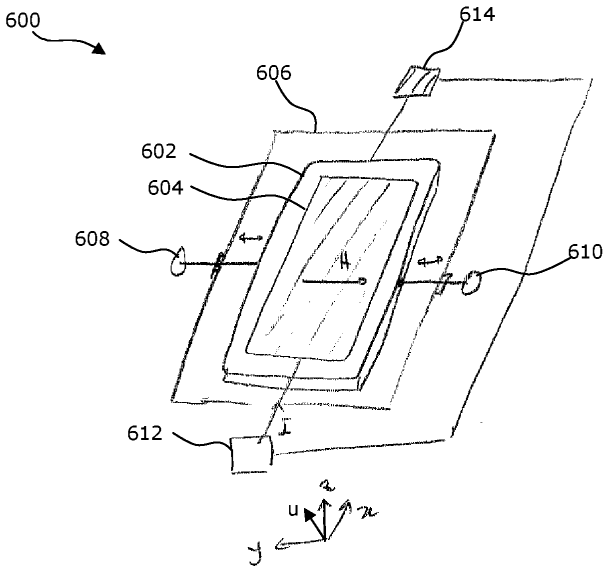
600
614
606
602
604
608
610
612
I
H
u
z
x
y

FIG. 6

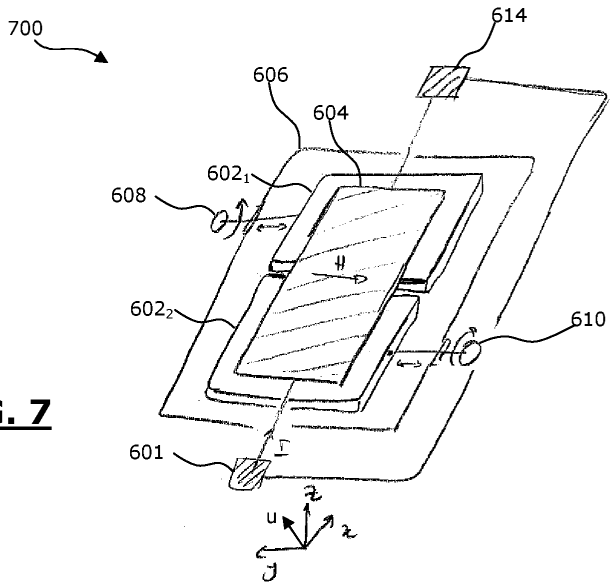
700
614
606
604
602₁
608
H
602₂
610
601
I
u
z
x
y

FIG. 7

4/4

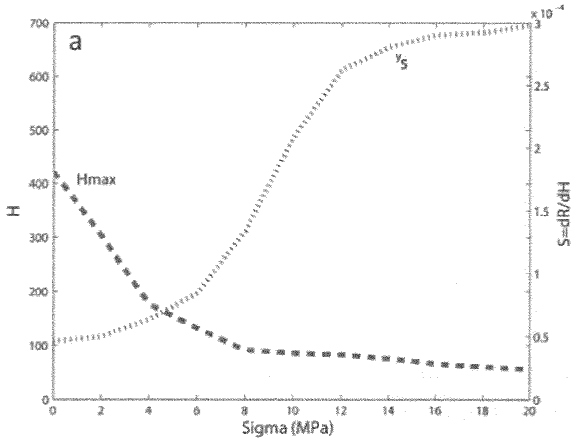

FIG. 8a

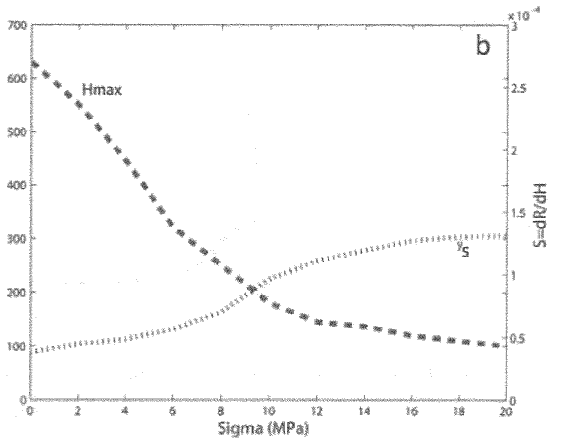

FIG. 8b

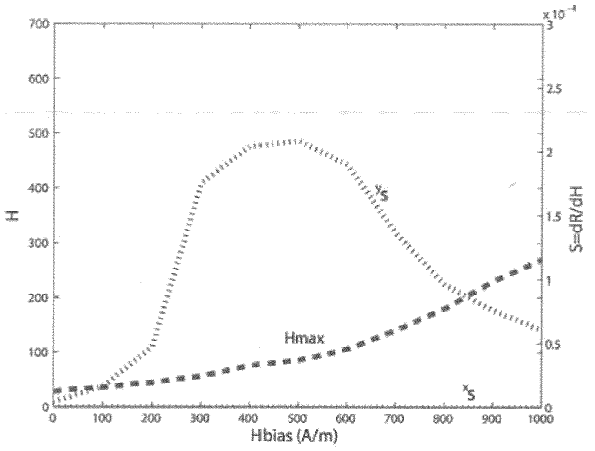

FIG. 9

université PARIS-SACLAY
ÉCOLE DOCTORALE
Physique et ingénierie : électrons, photons, sciences du vivant (EOBE)

Title : A multiscale model for anisotropic magnetoresistance

Keywords : multiscale model, anisotropic magnetoresistance, magnetic field sensor

Abstract : The anisotropic magnetoresistance (AMR) of ferromagnetic materials is widely used as the basic phenomenon for measuring or detecting magnetic field. Owing to the relationship between magnetic domain configuration and macroscopic resistivity, the application of an external magnetic field changes the resistivity of ferromagnetic materials. Although this effect is widely used in industrial applications, some basic aspects of AMR behavior are still unsufficiently understood. For example, the role of crystallographic texture is not accurately described by conventional modeling tools. As a consequence of the direct relationship between microstructure and AMR, models for AMR effect are generally based on micromagnetic calculations. For these calculations, the number of degrees of freedom and interactions can grow exponentially when investigating macroscopic behavior (case of polycrystals for example).

The thesis deals with the numerical modeling of AMR effect in ferromagnetic materials. This new 3D modeling tool can overcome this major drawback of micromagnetic approaches. A model to describe the effects of magneto-elastic coupling using a micro-macro approach is available at the laboratory GeePs. Based on the same principles of micro-macro modeling, an AMR effect simulation tool has been developed including the effect of mechanical stress and the role of crystallographic texture of materials.

The modeling strategy is as follows:

Three scales of description of the behavior are introduced: the Representative Volume Element (RVE) of polycrystals (macro scale), the single crystal or grain, and finally the magnetic domain (micro scale).

A first step, named localization, determines the magneto-mechanical loading (magnetic field and mechanical stress) within a grain depending on the external applied load. The introduction of internal variables and corresponding evolution laws allow describing in a statistical way the evolution of the magnetic domain microstructure under the influence of the local load. Also at this scale, the use of the phenomenological Doring model allows for each area, to calculate the resistivity as a function of the relative orientation between local magnetization and electric current. Once this local resistivity is known, a so-called homogenization step based on the Bruggeman model is used to determine the macroscopic resistivity of the RVE. It is thus possible to predict the variation in resistivity between an initial demagnetized state and a state under any magneto-mechanical loading.

The results obtained by this approach were successfully compared to experimental results from literature on polycrystalline nickel, pure iron or Permalloy.

Then simulations reproducing AMR sensors operating conditions were carried out. These simulations lead to the conclusion that it is possible to improve the sensitivity of AMR sensors by introducing an appropriate biaxial residual stress.

Université Paris-Saclay
Espace Technologique / Immeuble Discovery
Route de l'Orme aux Merisiers RD 128 / 91190 Saint-Aubin, France

université PARIS-SACLAY
ÉCOLE DOCTORALE
Physique et ingénierie : électrons, photons, sciences du vivant (EOBE)

Titre : Un modèle multi-échelle de la magnétorésistance anisotrope

Mots clés : modèle multi-échelle, magnétorésistance anisotrope, capteur de champ magnétique

Résumé : La magnétorésistance anisotrope (AMR) des matériaux ferromagnétiques est largement utilisée comme le phénomène de base pour la mesure ou la détection de champ magnétique. En raison de la relation entre la configuration en domaines magnétiques et la résistivité macroscopique, l'application d'un champ magnétique externe modifie la résistivité des matériaux ferromagnétiques. Bien que cet effet soit largement utilisé dans des applications industrielles, certains aspects fondamentaux du comportement AMR sont encore assez mal compris. Par exemple, le rôle de la texture cristallographique dans le comportement effectif n'est pas décrit avec précision par les outils classiques de modélisation. En raison de ce lien direct entre la microstructure en domaines et l'effet AMR, les modèles de description de l'effet AMR reposent généralement sur des calculs micromagnétiques. Pour ces calculs, le nombre de degrés de liberté et d'interactions peuvent se multiplier rapidement si on recherche à décrire un comportement macroscopique (cas des polycristaux par exemple).
La thèse porte sur la modélisation numérique de l'effet de magnétorésistance anisotrope des matériaux ferromagnétiques. Ce nouvel outil de modélisation 3D peut remédier à cet inconvénient majeur des approches micromagnétiques. Un modèle permettant de décrire les effets de couplage magnéto-élastique en utilisant une approche micro-macro est disponible au laboratoire GeePs. Sur la base des mêmes principes de la modélisation micro-macro, un outil de simulation de l'effet AMR en fonction de la contrainte mécanique et de la texture cristallographique des matériaux a été développé.
La stratégie de modélisation est la suivante:
Trois échelles de description du comportement sont introduites: le Volume Elémentaire Représentatif (VER) polycristallin (échelle macro), le monocristal ou grain, et enfin le domaine magnétique (échelle micro).
Une première étape dite de localisation permet de déterminer le chargement magnéto-mécanique (champ magnétique et contrainte mécanique) à l'échelle d'un grain en fonction du chargement extérieur appliqué. L'introduction de variables internes et des lois d'évolution correspondantes permet de décrire de façon statistique l'évolution de la microstructure en domaines magnétiques sous l'influence de ce chargement local. Toujours à cette échelle, l'utilisation du modèle phénoménologique de Doring permet, pour chaque domaine, de calculer la résistivité en fonction de l'orientation relative entre aimantation locale et courant électrique. Une fois cette résistivité locale connue, une étape dite d'homogénéisation s'appuyant sur le modèle de Bruggeman permet de déterminer la résistivité macroscopique du VER polycristallin. Il est ainsi possible de prédire la variation de la résistivité entre un état initial désaimanté et un état sous chargement magnéto-mécanique quelconque.
Les résultats obtenus par cette démarche ont été comparés avec succès à des résultats expérimentaux extraits de la littérature portant sur des polycristaux de Nickel, de Fer pur ou encore de Permalloy.
Ensuite des simulations reproduisant les conditions de fonctionnement des capteurs AMR ont été effectuées. Ces simulations permettent de conclure qu'il est possible d'améliorer la sensibilité des capteurs AMR en générant une contrainte résiduelle biaxiale.

Université Paris-Saclay
Espace Technologique / Immeuble Discovery
Route de l'Orme aux Merisiers RD 128 / 91190 Saint-Aubin, France